

# Analysis of Contrail Formation Regions and Changes due to Climate Impact

MSc Thesis

J. Xu



# Analysis of Contrail Formation Regions and Changes due to Climate Impact

MSc Thesis

by

J. Xu

to obtain the degree of Master of Science

at the Delft University of Technology,

to be defended publicly on Tuesday October 30, 2018 at 10:00 AM.

Student number: 4405668  
Project duration: June 5, 2017 – October 30, 2018  
Thesis committee: Prof. dr. ir. V. Grewe, TU Delft(C&O-ANCE),DLR, supervisor  
Dr. ir. M. Snellen, TU Delft(C&O-ANCE)  
Ir. P. C. Roling, TU Delft(C&O-ATO)

An electronic version of this thesis is available at <http://repository.tudelft.nl/>.



# Preface

This master thesis marks the completion of my study at Delft University of Technology as well as my almost 20 years of life as a student. This thesis mainly focuses on analyzing the regions where contrails can form, in order to help reduce the number of contrails being formed in the future. I feel this is a timely topic with global warming has always been in a serious situation, especially lately news about global temperature getting out of the control of mankind is everywhere. Every little bit helps.

At this point, I would like to thank Prof. Dr. Volker Grewe for his supervision and support throughout this thesis. I would like to thank Feijia for answering all my stupid questions. My thank also goes to Co for being my shrink. Last but not least, I would like to thank my parents and friends who have always been there to support me no matter what and thanks to everyone walk along with me through the past year.

*Jinghua Xu*  
*Delft, October, 2018*



# Abstract

As global warming has become a prominent issue for mankind, scientists are working on every possible aspects to slow down its pace. With the booming aviation activities, aviation emission contribute more and more to the anthropogenic climate impact. Therefore, many researches focused on finding ways to mitigate the impact of aviation on the global climate have been performed. The emission of aviation include:  $CO$ ,  $NO_x$ ,  $SO_x$ ,  $H_2O$ ,  $CO_2$ , soot and contrails, where contrails contributes to about 30% of the aviation induced RF (Lee, Fahey, et al. 2009). Among the options that are proposed to mitigate the contrail formation, one of it is to re-route the aircraft in a way to avoid flying through the contrail formation regions (CFRs). To carry out this option, it is necessary to have a better understanding of the distribution of the CFRs as well as their seasonal variation and future trend.

The CFRs analyzed in this thesis are simulated by EMAC model and the data are verified by both MOZAIK and MLS. The CFRs are the regions where contrails can both form and persist. In this thesis, two 30 years time spans are selected, 1984-2013 and 2070-2099, to analyze the past and future trend of the CFRs. Furthermore, the CFRs for four different seasons within both NH mid-latitude regions and tropics are analyzed separately.

In this thesis, the CFRs' characterisations studied including their zonal and meridional coverage length, stretch factor, direction in the vertical and horizontal plane as well as their seasonal variations and future trend. Generally, CFRs are located around the tropopause. In the NH mid-latitude, CFRs are mostly scattered between the layer from 400 hPa to 200 hPa. In the tropics, CFRs are mostly between the layer from 110 hPa to 90 hPa. Overall, the coverage ratio of CFRs in the tropics is about two times of that in the NH mid-latitude regions.

At both NH mid-latitude and tropics, in the horizontal plane, apart from the none stretched single grid CFRs, most of the CFRs have a stretch factor of 1.4 which their length is about six times their width. Due to the Earth's rotation, around 20% of the CFRs have a west-east direction, and the tilted CFRs are generally following the atmospheric circulation. Within the vertical plane, the CFRs are way more stretched than those in the horizontal plane, typically they have a stretch factor around 11. And most of the CFRs have a horizontal direction, make the CFRs more easier to avoid by changing the one flight level up or down.

coverage ratio of CFRs in the tropics is about two times of that in the NH mid-latitude regions. to the global warming as the temperature in some regions might just be too high for contrails to form and persist. Furthermore, an uplifting trend of the CFRs distribution is also discovered which might lead to more contrails being formed at a higher altitude that will contribute more to the global warming compared to a contrail persists at a lower level.



# Contents

<b>Abstract</b>	<b>v</b>
<b>Nomenclature</b>	<b>xi</b>
<b>List of Figures</b>	<b>xiii</b>
<b>List of Tables</b>	<b>xix</b>
<b>1 Introduction</b>	<b>1</b>
1.1 Thesis Background . . . . .	1
1.2 Research Objective . . . . .	2
1.3 Thesis Structure . . . . .	2
<b>2 Contrail Formation Region</b>	<b>5</b>
2.1 Contrail . . . . .	5
2.2 Ice Supersaturated Regions (ISSRs) . . . . .	7
2.3 Schmidt-Appleman criterion (SAC) . . . . .	8
2.4 Contrail Formation Regions (CFR) . . . . .	9
<b>3 EMAC Model Description</b>	<b>13</b>
3.1 Hindcast with specified dynamics of the past (RC1SD) . . . . .	13
3.2 Free running hindcast and projection simulations of the future (RC2) . . . . .	13
3.3 Temperature and humidity differences between RC1SD and RC2 . . . . .	14
<b>4 Methodology</b>	<b>17</b>
4.1 General Approach . . . . .	17
4.2 Selection of time spans . . . . .	17
4.3 CFR's Characterisation . . . . .	18
4.3.1 Zonal mean of CFRs' coverage . . . . .	18
4.3.2 Meridional mean of CFRs' coverage . . . . .	18
4.3.3 Conditional mean of meridional CFRs' coverage length . . . . .	19
4.3.4 Vertical Extension of CFRs . . . . .	19
4.3.5 Stretch factor of CFRs . . . . .	19
4.3.6 Direction of CFRs . . . . .	19

4.4	Regions of Interest . . . . .	21
4.5	RC1SD and RC2. . . . .	21
4.6	Definition of connected region . . . . .	21
4.7	Potential Coverage Threshold (PT) . . . . .	22
4.7.1	Sensitivity of PT. . . . .	23
4.7.2	Selection of PT . . . . .	25
4.8	Data Analyzing and Presenting Methods . . . . .	25
4.8.1	Boxplot . . . . .	25
4.8.2	Kernel Density Estimation . . . . .	25
4.8.3	Welch's Two Sample T-test . . . . .	26
<b>5</b>	<b>Model Validation</b>	<b>27</b>
5.1	ISSRs Measurement by in Service Aircraft: MOZAIC. . . . .	27
5.2	ISSRs Observation by Satellite: MLS . . . . .	27
5.3	Validation of EMAC . . . . .	28
5.3.1	EMAC and MLS . . . . .	28
5.3.2	EMAC and MOZAIC . . . . .	33
<b>6</b>	<b>Characterizations and Seasonality of CFRs: Coverage Length</b>	<b>39</b>
6.1	Meridional mean of CFRs' coverage. . . . .	39
6.1.1	NH Mid-latitude Regions . . . . .	39
6.1.2	Tropics. . . . .	43
6.2	Conditional Mean of Meridional CFRs' Coverage Length . . . . .	46
6.2.1	NH Mid-latitude Regions . . . . .	46
6.2.2	Tropics. . . . .	49
6.3	Zonal Mean of CFRs' Coverage . . . . .	49
6.3.1	Discussions . . . . .	50
<b>7</b>	<b>Characterisation of CFR: Stretch Factor and Direction</b>	<b>55</b>
7.1	Stretch factor of CFRs . . . . .	55
7.1.1	Stretch Factor of CFRs in Horizontal Plane . . . . .	55
7.1.2	Stretch Factor of CFRs in Vertical Plane. . . . .	58
7.2	Direction of CFRs. . . . .	60
7.2.1	Direction of CFRs in the Horizontal Plane . . . . .	62
7.2.2	Direction of CFRs in the Vertical Plane . . . . .	66
7.2.3	Discussion . . . . .	69

<b>8</b>	<b>Trends of Contrail Formation Regions (CFRs) and Climate Impact</b>	<b>71</b>
8.1	Trend of Zonal and Meridional Mean of CFRs . . . . .	71
8.1.1	Meridional Mean of CFRs Coverage Trend . . . . .	71
8.1.2	Zonal Mean CFRs Coverage Length Trend . . . . .	74
8.2	Climate Impact on the Trend of CFRs. . . . .	78
8.2.1	Trend of the Global CFRs' Vertical Extension . . . . .	78
8.2.2	Trend of the CFRs' Meridional Mean Coverage Length . . . . .	80
8.3	Discussion . . . . .	84
<b>9</b>	<b>Conclusions and Recommendations</b>	<b>85</b>
9.1	Conclusions. . . . .	85
9.2	Recommendations . . . . .	86
<b>A</b>	<b>Appendix</b>	<b>89</b>
<b>B</b>	<b>Appendix</b>	<b>93</b>
<b>C</b>	<b>Appendix</b>	<b>115</b>



# Nomenclature

## Acronyms

CFR	Contrail Formation Region
EMAC	ECHAM/MESSy Atmospheric Chemistry
FL	Flight Level
GPCP	Global Precipitation Climatology Project
HadGEM2-ES	Hadley Centre Global Environment Model version 2-Earth System Model
IPO	Interdecadal Pacific Oscillation
ISS	Ice Super Saturation
ISSR	Ice Super Saturated Region
ITCZ	Intertropical Convergence Zone
KDE	Kernel Density Estimation
LQR	Likely Range of Variation
MLS	Microwave Limb Sounder
MOZAIC	Measurements of OZone by Airbus In-service airCRAFT
NH	Northern Hemisphere
PDF	Probability Density Function
POTCOV	POTential contrail COVerage
PT	Potential coverage Threshold
RCP	Representative Concentration Pathway
RF	Radiative Forcing
RHi	Relative Humidity with respect to ice
SAC	Schmidt-Appleman criterion
SH	Southern Hemisphere
SIC	Sea Ice Concentrations
SST	Sea Surface Temperatures
UARS	Upper Atmosphere Research Satellite



# List of Figures

2.1	Contrails . . . . .	5
2.2	Global mean diurnal cycle of (top) air traffic density, contrail cirrus coverage, and (bottom) long wave, short wave, and net RF vs local time (Figure obtained from Schumann et al. (2017)) . . . . .	6
2.3	Radiative forcing (RF) components from global aviation as evaluated from preindustrial times until 2005. With the total aviation induced RF including and excluding induced cirrus (Figure obtained from Lee et al. (2009)) . . . . .	7
2.4	Relative Humidity and Temperature of ISSRs . . . . .	8
2.5	ISSR and mixing lines with same slope . . . . .	9
2.6	ISSR and Mixing Lines with Different Physical Conditions of Aircraft Exhaust Air . . . . .	10
2.7	Cirrus coverage, potential contrail coverage, potential contrail cirrus coverage and potential contrail coverage according to Ponater et al. (2002)(Figure obtained from Burkhardt et al. (2008)) . . . . .	11
2.8	Annual Mean Potential Contrail Coverage [%] at 300hPa (Figure obtained from Burkhardt et al. (2008)) . . . . .	11
2.9	Potential Contrail Cirrus Coverage [%] at 300hPa (Figure obtained from Burkhardt et al. (2008)) . . . . .	12
3.1	Temperature biases . . . . .	15
4.1	Demonstration of how the CFR grids are numbered . . . . .	22
4.2	CFR Frequency 200hPa RC1SD . . . . .	23
4.3	RC1SD PT10 and PT90 Comparison of Two Different Months in 1996 . . . . .	24
5.1	CFRs' Frequency at 147 hPa Simulate by RC1SD with Four Different PTs . . . . .	29
5.2	CFRs' Frequency by MLS and EMAC Simulations at 147 hPa . . . . .	30
5.3	CFRs Frequency 215hPa RC1SD and RC2 . . . . .	32
5.4	Frequency of occurrence of ISSRs at 200 hPa by MOZAIC (Marenco et al. 1998) . . . . .	34
5.5	ISSR Frequency 200 hPa RC1SD and RC2 . . . . .	35
5.6	Frequency of Occurrence of ISSRs at 250hPa by MOZAIC (Marenco et al. 1998) . . . . .	36
5.7	ISSR Frequency 250hPa RC1SD and RC2 . . . . .	37
6.1	Meridional Mean of CFRs' Coverage in Spring NH Mid-latitude . . . . .	40
6.2	Meridional Mean of CFRs' Coverage in Summer NH Mid-latitude . . . . .	41

6.3	Meridional Mean of CFRs' Coverage in Autumn NH Mid-latitude . . . . .	41
6.4	Meridional Mean of CFRs' Coverage in Winter NH Mid-latitude . . . . .	42
6.5	Meridional Mean of CFRs' Coverage in Spring Tropics . . . . .	44
6.6	Meridional Mean of CFRs' Coverage in Summer Tropics . . . . .	44
6.7	Meridional Mean of CFRs' Coverage in Autumn Tropics . . . . .	45
6.8	Meridional Mean of CFRs' Coverage in Winter Tropics . . . . .	45
6.9	Conditional Mean of Meridional CFRs' Coverage Length in Spring . . . . .	47
6.10	Conditional Mean of Meridional CFRs' Coverage Length in Summer . . . . .	47
6.11	Conditional Mean of Meridional CFRs' Coverage Length in Autumn . . . . .	48
6.12	Conditional Mean of Meridional CFRs' Coverage Length in Winter . . . . .	48
6.13	Effective Meridional Coverage Length in Spring . . . . .	49
6.14	Seasonal variation of the meridional profile of the zonally averaged TRG tropopause (1979–93; 1200 UTC): annual mean (full line), DJF (dotted), and JJA (broken). The outermost lines represent the envelope lines for all monthly mean values (Figure obtained from (Hoinka 1998)) . . . . .	51
6.15	Zonal Mean Coverage Length in Spring . . . . .	51
6.16	Zonal Mean Coverage Length in Summer . . . . .	52
6.17	Zonal mean coverage length in autumn . . . . .	52
6.18	Zonal Mean Coverage Length in Winter . . . . .	53
7.1	PDF of CFRs' Stretch factor in horizontal plane NH mid-latitude spring . . . . .	56
7.2	PDF of CFRs' Stretch factor in horizontal plane Tropics spring . . . . .	57
7.3	Vertical Stretch factor at Different Pressure altitude . . . . .	58
7.4	PDF of CFRs' Stretch factor in vertical plane NH mid-latitude spring . . . . .	59
7.5	PDF of CFRs' Stretch factor in vertical plane Tropics spring . . . . .	60
7.6	Example of the CFR direction definition . . . . .	60
7.7	CFR direction in horizontal plane . . . . .	61
7.8	CFR direction in vertical plane . . . . .	61
7.9	Atmospheric Circulation Pattern (Figure obtained on July 16, 2018 from: <a href="https://commons.wikimedia.org/wiki/User:Kaidor">https://commons.wikimedia.org/wiki/User:Kaidor</a> ) . . . . .	62
7.10	PDF of CFRs' Direction in horizontal plane NH mid-latitude spring . . . . .	63
7.11	PDF of CFRs' Direction in horizontal plane NH mid-latitude summer . . . . .	64
7.12	PDF of CFRs' Direction in horizontal plane Tropics spring . . . . .	65
7.13	CFR Direction boxplot in horizontal plane Tropics spring . . . . .	65
7.14	PDF of CFRs' Direction in vertical plane NH mid-latitude spring . . . . .	67
7.15	CFR Direction boxplot in vertical plane NH mid-latitude spring . . . . .	67
7.16	CFR Direction boxplot in vertical plane NH midlatitude winter . . . . .	68

7.17 PDF of CFRs' Direction in vertical plane Tropics spring . . . . .	68
7.18 PDF of CFRs' Direction in vertical plane Tropics summer . . . . .	69
7.19 CFR direction boxplot in vertical plane Tropics spring . . . . .	70
7.20 CFR direction boxplot in vertical plane Tropics summer . . . . .	70
8.1 Meridional Mean of CFRs Coverage Difference in NH midlatitude Spring . . . . .	72
8.2 Meridional Mean of CFRs Coverage Difference in NH midlatitude Summer . . . . .	73
8.3 Meridional Mean of CFRs Coverage Difference in NH midlatitude Autumn . . . . .	73
8.4 Meridional Mean of CFRs Coverage Difference in NH midlatitude Winter . . . . .	74
8.5 Meridional mean CFRs coverage difference in tropics spring . . . . .	75
8.6 Zonal mean CFRs coverage length difference spring . . . . .	76
8.7 Zonal mean CFRs coverage length difference summer . . . . .	76
8.8 Zonal mean CFRs coverage length difference autumn . . . . .	77
8.9 Zonal mean CFRs coverage length difference winter . . . . .	77
8.10 Annual mean surface air temperature averaged over the remaining land regions (Figure obtained from Stefan Brönnimann (2009)) . . . . .	79
8.11 Trend of CFRs' global ocean and land temperature anomalies (figure obtained from NOAA National Centers for Environmental information, Climate at a Glance: Global Time Series, <a href="https://www.ncdc.noaa.gov/cag/">https://www.ncdc.noaa.gov/cag/</a> , published July 2018, retrieved on August 4, 2018) . . . . .	79
8.12 Trend of CFRs' global vertical extension 1983-2018 . . . . .	80
8.13 Trend of CFRs' global vertical extension . . . . .	80
8.14 Trend of CFRs' meridional mean coverage length at 127hPa in the NH mid-latitude re- gions . . . . .	81
8.15 Trend of CFRs' Meridional Mean Coverage Length at 127hPa in the Tropics . . . . .	81
8.16 Trend of CFRs' Meridional Mean Coverage Length at 75hPa in the Tropics . . . . .	82
8.17 Trend of CFRs' meridional mean coverage length at 250hPa in the mid-latitude . . . . .	82
8.18 Trend of CFRs' meridional mean coverage length at 250hPa in the tropics . . . . .	83
A.1 CFR Frequency 200hPa RC2 . . . . .	89
A.2 RC2 PT10 and PT90 comparison of two different months in 1996 . . . . .	90
A.3 Effective Meridional coverage length in Summer . . . . .	90
A.4 Effective Meridional coverage length in Autumn . . . . .	91
A.5 Effective Meridional coverage length in Winter . . . . .	91
B.1 PDF of CFRs' Stretch factor in horizontal plane NH mid-latitude summer . . . . .	93
B.2 PDF of CFRs' Stretch factor in horizontal plane NH mid-latitude autumn . . . . .	94
B.3 PDF of CFRs' Stretch factor in horizontal plane NH mid-latitude winter . . . . .	94

B.4	PDF of CFRs' Stretch factor in horizontal plane Tropics summer . . . . .	95
B.5	PDF of CFRs' Stretch factor in horizontal plane Tropics autumn . . . . .	95
B.6	PDF of CFRs' Stretch factor in horizontal plane Tropics winter . . . . .	96
B.7	PDF of CFRs' Stretch factor in vertical plane NH mid-latitude summer . . . . .	99
B.8	PDF of CFRs' Stretch factor in vertical plane NH mid-latitude autumn . . . . .	99
B.9	PDF of CFRs' Stretch factor in vertical plane NH mid-latitude winter . . . . .	100
B.10	PDF of CFRs' Stretch factor in vertical plane Tropics summer . . . . .	100
B.11	PDF of CFRs' Stretch factor in vertical plane Tropics autumn . . . . .	101
B.12	PDF of CFRs' Stretch factor in vertical plane Tropics winter . . . . .	101
B.13	Direction in horizontal plane NH midlatitude autumn . . . . .	102
B.14	Direction in horizontal plane NH midlatitude winter . . . . .	102
B.15	CFR Direction boxplot in horizontal plane NH mid-latitude spring . . . . .	103
B.16	CFR Direction boxplot in horizontal plane NH midlatitude summer . . . . .	103
B.17	CFR Direction boxplot in horizontal plane NH midlatitude autumn . . . . .	104
B.18	CFR Direction boxplot in horizontal plane NH midlatitude winter . . . . .	104
B.19	PDF of CFRs' Direction in horizontal plane Tropics summer . . . . .	105
B.20	PDF of CFRs' Direction in horizontal plane Tropics autumn . . . . .	105
B.21	PDF of CFRs' Direction in horizontal plane Tropics winter . . . . .	106
B.22	CFR Direction boxplot in horizontal plane Tropics summer . . . . .	106
B.23	CFR Direction boxplot in horizontal plane Tropics autumn . . . . .	107
B.24	CFR Direction boxplot in horizontal plane Tropics winter . . . . .	107
B.25	CFR Direction boxplot in horizontal plane Tropics summer . . . . .	108
B.26	CFR Direction boxplot in horizontal plane Tropics autumn . . . . .	108
B.27	CFR Direction boxplot in horizontal plane Tropics winter . . . . .	109
B.28	PDF of CFRs' Direction in vertical plane NH mid-latitude summer . . . . .	109
B.29	PDF of CFRs' Direction in vertical plane NH mid-latitude autumn . . . . .	110
B.30	PDF of CFRs' Direction in vertical plane NH mid-latitude winter . . . . .	110
B.31	CFR Direction boxplot in vertical plane NH midlatitude summer . . . . .	111
B.32	CFR Direction boxplot in vertical plane NH midlatitude autumn . . . . .	111
B.33	PDF of CFRs' Direction in vertical plane Tropics autumn . . . . .	112
B.34	PDF of CFRs' Direction in vertical plane Tropics winter . . . . .	112
B.35	CFR direction boxplot in vertical plane Tropics autumn . . . . .	113
B.36	CFR direction boxplot in vertical plane Tropics winter . . . . .	113
C.1	Meridional mean CFRs coverage length difference in tropics summer . . . . .	115
C.2	Meridional mean CFRs coverage length difference in tropics autumn . . . . .	116

C.3 Meridional mean CFRs coverage length difference in tropics winter . . . . . 116



# List of Tables

4.1	Examples of CFRs stretch factors . . . . .	20
5.1	Comparison of MOZAIC and EMAC at 200hPa . . . . .	34
5.2	Comparison of MOZAIC and EMAC at 250hPa . . . . .	36
7.1	Stretch factor range of grids combination at different altitude . . . . .	58
B.1	Grid Stretch factor in the vertical plane . . . . .	97
B.1	Grid Stretch factor in the vertical plane . . . . .	98



# Introduction

## 1.1. Thesis Background

"In recent decades, changes in climate have caused impacts on natural and human systems on all continents and across the oceans. Impacts are due to observed climate changes" (Stocker 2014). Radiative forcing (RF) is considered as "an index of the importance of the factor as a potential climate change mechanism" (Solomon 2007). In 2005, aviation emission contributes about 5% to the anthropogenic RF and about 30% of the aviation induced RF are related to contrail (Lee, Fahey, et al. 2009). The number keeps growing due to the long lasting effect of  $CO_2$  and the increasing number of flights every year. According to Airbus, air traffic is growing at an average annual rate of 4% to 5% (Forecast 2015). Therefore, it is very crucial to mitigate the aviation induced climate changes. Since contrails contribute greatly to the aviation induced climate changes, it is necessary to find more methods to reduce the amount of contrails produced everyday by aviation to slow down the global warming situation.

Currently, the options to mitigate the formation of contrails can be classified into three categories. The first one is the technical mitigation option. for example, to alter the engine in such a way that its overall propulsion efficiency temporarily decreases when flying through the Contrail Formation Regions (CFRs) (Haglind 2008). But this may also exacerbate the climate problem of other greenhouse gas like  $CO_2$  as well as an increase of the fuel consumption, both of which are not desirable. Furthermore, to alter an engine also requires a lot of money and time invested on the benchmarking, concept designing, making prototype and full scale testing. The second option is to change the contrail properties, to alter the optical properties of the contrails as the contrail induced RF depends largely on the size and shape of the ice particle (Lee, Pitari, et al. 2010; Meerkötter et al. 1999). This option can be achieved by altering the properties of the exhaust aerosol (Klaus Gierens, Lim, and Eleftheratos 2008), therefore, an alternative fuel is required (Klaus Gierens 2007). The last category is the operational mitigation option, one of the methods is to avoid the aircraft flying through the CFRs, this can be fulfilled by changing the flight altitudes or flight routes. As CFRs are rather thin, a change of one flight level would be sufficient to avoid the formation of contrails (Ulrich Schumann 2012). Another method is to change the flight time, about 25% of the total flights are night flights, however they contributes to about 60% to 80% of the net RF (Stuber et al. 2006). Therefore, schedule more flights in day time instead of night time can also help reducing the global warming impact caused by contrails.

When planning the flight route, knowing the distribution of the CFRs beforehand can help planning the flight route in a way to avoid flying through the CFRs and to mitigate the contrails formed.

However, it is rather unrealistic to predict the exact distribution of CFRs beforehand as the climate system is complex itself. Therefore, it is more feasible for an aircraft to shift the flight route a bit when its surrounding atmosphere is detected to be CFRs. Then the question become: towards which direction is it more recommended to shift the flight route in order to mitigate the contrails formed. This requires a better understanding of the distribution of CFRs and their trends. Thus, the main research questions are: what are the characterizations and seasonal variations of CFRs and their future trends. Therefore, the main objectives of this project is to analyze the CFRs' characterizations and their seasonality as well as their future trends and identifying changes due to the climate impacts in order to have a better prediction of the CFRs distribution base on the weather pattern and climate change.

Currently, there are several different ways to obtain the distribution of the CFRs, they can be classified into two categories. The first one is the real time measurement campaign including far distance detected by satellite sensor, for example, MLS and in-situ measurement by commercial aircraft like MOZAIC. Normally, these methods tend to have some limitations due to the methods those data are measured. For example, the MOZAIC does not have a global coverage and the MLS results have a very low vertical resolution. The second category includes different types of simulation models, for instance, EMAC, EC-EARTH, MIROC5, etc. Those models are available to provide simulation of the global climate for both past and future, therefore, they can be useful when predicting the future climate. As the climate system is very complex, for different simulation models, the accuracy level can vary a lot, depending on the assumptions made when running the simulation.

The ECHAM/MESSy Atmospheric Chemistry (EMAC) is "a modular global climate and chemistry simulation system"<sup>1</sup> with several sets of different simulation that focus on different aspects of the climate. With the help of this simulation model it makes it easier to study the development of climate with a global coverage. Here, in this thesis project, data simulated by two different EMAC simulations are used for analyzing both the contrail distribution and characterisation from the past and future.

## 1.2. Research Objective

The main research objective of this thesis is *to study the characterisations, seasonal variations and future trends of CFRs as well as the impact of the climate changes*. The CFRs analyzed in this thesis have very similar coverage to the Ice Super Saturated Regions (ISSRs), a detailed explanation of the differences between the CFRs and ISSRs are give in Section 2.4. Generally, CFRs are the regions that allow contrails to form and persist when aircraft fly through them. In this research, several characterisations as well as their seasonal variations of the CFRs are analyzed. Chapter 6 presents the analysis of the meridional and zonal mean coverage length of CFRs to help study where are the CFRs mostly distributed. The stretch factor and direction of CFRs in both horizontal and vertical plane are also analyzed in Chapter 7 to have a better understanding of the typical shape and direction of CFRs within different regions. Furthermore, the trend of the characterisations of CFRs are assessed as well as the climate impact on these trends in Chapter 8.

## 1.3. Thesis Structure

The thesis is structured as followed, in Chapter 2 presents an introduction of the CFRs including an introduction of the contrails and the formation of contrails as well as the differences between the CFRs and ISSRs. In Chapter 3, presents an introduction and comparison of the two different

---

<sup>1</sup>[https://www.dlr.de/pa/en/desktopdefault.aspx/tabid-8859/15306\\_read-37415/15306](https://www.dlr.de/pa/en/desktopdefault.aspx/tabid-8859/15306_read-37415/15306) (accessed September 8, 2017)

EMAC simulations used in this thesis project. The methodology of this thesis project is presented in Chapter 4. The validation of both of the EMAC simulations: RC1SD-base-10 and RC2-base-04 is provided in Chapter 5 where the EMAC simulated data are compared with the observed results from both Measurements of Ozone by Airbus in -service aircraft (MOZAIC) and Microwave Limb Sounder (MLS). After the validation process of the two EMAC simulations, the analysis of the CFRs' characterisation and seasonality including the coverage lengths, stretch factors and directions are presented in Chapter 6 and Chapter 7. The future trend of CFRs' distribution are presented in Chapter 8. Finally, the conclusions and recommendations of this thesis project are given in Chapter 9.



# 2

## Contrail Formation Region

In this chapter, presents an introduction of the contrails and the formation of the contrails as well as the differences between the Contrail Formation Regions (CFRs) and Ice SuperSaturated Regions (ISSRs).

### 2.1. Contrail

Contrails or condensation trails are formed by the hot and humid exhaust from aircraft engines mixing with the cold and dry ambient air. Whether a contrail can be formed or not depends on the relative humidity and temperature of the ambient atmosphere as well as the fuel and aircraft specific variables (Burkhardt et al. 2008). Once a contrail is formed, it can expand into contrail cirrus. Whether a region is suitable for a contrail cirrus to persist or not depends on its physical condition and these regions are also known as the ISSRs and will be introduced later. The lifetime of a contrail cirrus can vary from minutes to hours and this is also impacted by the ambient atmosphere condition.



Figure 2.1: Contrails

In Figure 2.1 several contrails can be seen and some have already developed into contrail cirrus. The contrails that persist for more than several seconds are considered persistent contrails and they are the main sources of the contrail induced RF. Generally, the lifetime of a contrail varies from minutes to hours, over 80% of persistent contrails have a lifetime up to 5 hours and only about 5% of the persistent contrails have a lifetime longer than 10 hours (Klaus Gierens and Vázquez-Navarro 2017). Depending on the thickness of the contrails, they can reduce the incoming shortwave radiation as well as the outgoing longwave radiation so that the net RF is slightly positive (Mannstein, Spichtinger, and Klaus Gierens 2005). A more detailed demonstration of the contrails induced RF based on the time of a day is presented in Figure 2.2 as well as a general overview of the contrail coverage throughout the day. Generally, the contrail coverage is higher during the day due to the higher aircraft density during the day, correspondingly, both the contrail induced longwave RF and shortwave RF have higher magnitudes during the day. In the daytime, contrails are both acting like a sun shield blocking the incoming shortwave radiation and a blanket preventing the longwave radiation leaving the Earth surface. Overall, both effects are counteracting with each other leading the net RF during the day very close to 0. However, during night, due to the absence of the shortwave incoming radiation, the contrails are only acting as a blanket, keeping the earth surface warm. Therefore, during night, the net RF induced by contrails is positive which leads to an overall positive net RF for both day and night (Ulrich Schumann and Heymsfield 2017; Haywood et al. 2009). Furthermore, when the contrails are very thin, they allow most of the shortwave radiation along with the incoming energy to reach the Earth surface. However, they are still able to block the outgoing longwave radiation (Avila and Sherry 2016), in this case, the net RF will be higher than the previous case.

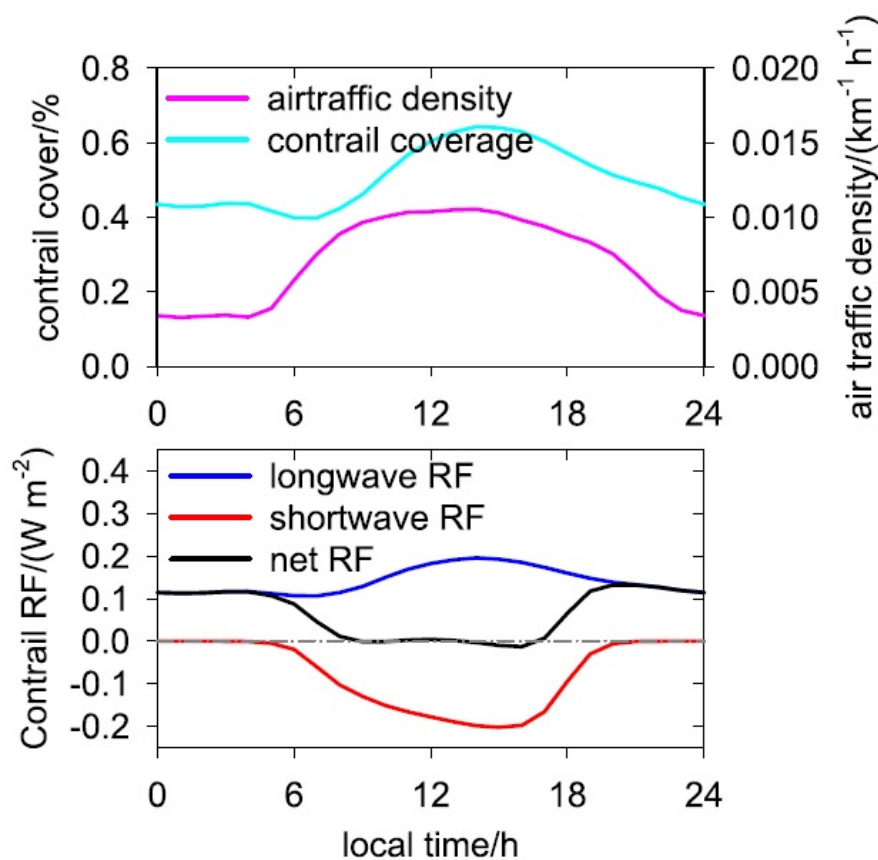


Figure 2.2: Global mean diurnal cycle of (top) air traffic density, contrail cirrus coverage, and (bottom) long wave, short wave, and net RF vs local time (Figure obtained from Schumann et al. (2017))

Figure 2.3 presents the estimation of different components of the aviation induced RF from Lee et al. (2009). From the figure, it can be seen that, the linear contrails formed after aircraft contribute about 21% to the total aviation induced RF. Other than that, the aviation induced cirrus cloudiness contribute even more to the aviation induced RF. Two type of aviation induced cirrus are considered here, the first one is the cirrus developed from contrails and the second type have a different mechanism, they are formed in the atmosphere due to the particles being emitted by the aircraft. If both contrails and induced cirrus cloudiness are taken into account, together they contribute to over 50% of the total aviation induced RF. However, due to the limited study of the aircraft induced cirrus, the level of science understanding is very low and there is a very large uncertainty in the estimated RF amount. And for this project only the contrails and their formation regions are studied.

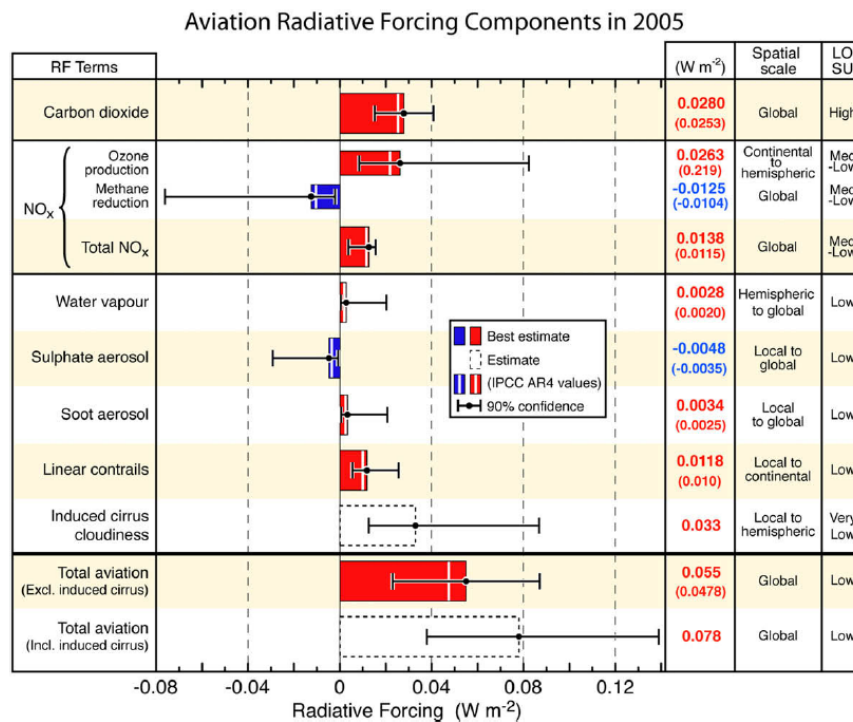


Figure 2.3: Radiative forcing (RF) components from global aviation as evaluated from preindustrial times until 2005. With the total aviation induced RF including and excluding induced cirrus (Figure obtained from Lee et al. (2009))

The formation of a contrail and whether it will be persistent or not depends on two different factors including the conditions of the ambient atmosphere and the physical conditions of the aircraft exhaust and will be introduced in detail next.

## 2.2. Ice Supersaturated Regions (ISSRs)

Naturally, when the exhaust air of an engine is hot and humid, after mixing with the dryer and cooler surrounding air, a contrail will form. And whether the contrail will persist or not depends on the ambient atmospheric condition. The regions that allow the formed contrails to persist for hours are considered the Ice SuperSaturation regions (ISSRs) and will be introduced next. Whether a region is ISSR or not is determined by the Relative Humidity with respect to Ice (RH<sub>i</sub>) as well as the temperature, when the RH<sub>i</sub> is higher than 100% and the temperature is lower than  $-40^{\circ}\text{C}$ , the region is suitable for formed contrails to persist.

Figure 2.4 plots the regions that fulfill the requirements of ISSRs. The green curve represents the saturation line with respect to ice which means that the relative humidity is 100% with respect

to ice. And the red curve is the saturation line with respect to water so the relative humidity is 100% with respect to water. The two colored curves separated the whole atmosphere conditions into three parts.

The first part is when the physical condition of the ambient atmosphere lies in the region above the red curve. In this case, as it indicates the relative humidity is more than 100% saturated with respect to water, then chances are natural cirrus has already formed there.

The second part is when the physical condition of the ambient atmosphere lies in the region in between both curves. Based on the physical conditions of this region, it is also called Ice Super Saturated Region (ISSR). This region is considered sufficient for contrails to persist when the temperature is also lower than  $-40^\circ$ .

The third part is when the relative humidity is lower than 100% with respect to ice which is also the region underneath the green curve. In this case, this regions is considered too dry for contrails to persist. Therefore, a formed contrail will dissolve.

Other than the conditions of the ambient atmosphere, in order to know whether a contrail will form or not in the first place, another criterion also needs to be taken into consideration and is presented next.

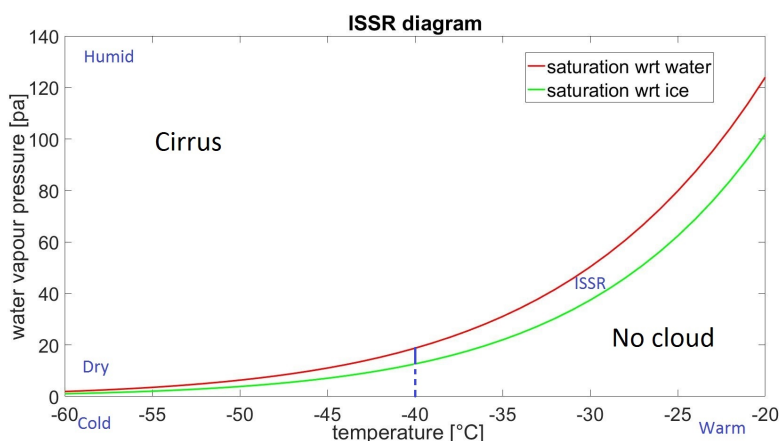


Figure 2.4: Relative Humidity and Temperature of ISSRs

### 2.3. Schmidt-Appleman criterion (SAC)

Whether a contrail will form or not in the first place also depends on the physical conditions of the aircraft exhaust air including temperature and humidity. The mixing process of the contrail formation is described by the Schmidt-Appleman Criterion (SAC). It was first developed by Schmidt and Appleman (Schmidt 1941; Appleman 1953) and later in 1996 it was re-examined by Schumann (Ulrich Schumann 1996). It shows that the process of contrail formation is a thermodynamic problem. The SAC can be used to determine if a contrail will form or not and is expressed as followed (Ulrich Schumann 1996),

$$G = pa * C_p * \frac{M(air)}{M(H_2O)} \frac{EI(H_2O)}{(1 - \eta)Q} \quad (2.1)$$

where,  $G$  is the slope of mixing line,  $pa$  is the atmospheric pressure,  $C_p$  is the specific heat capacity of air,  $M(air)$  and  $M(H_2O)$  are the molar masses of air and water and they are all constant,  $\eta$  is the overall propulsion efficiency and is aircraft dependent,  $EI(H_2O)$  is the water vapour emission index and  $Q$  is the specific heat content and are fuel dependent. Basically, a larger  $G$  indicates a steeper

slope of the mixing line. The diagrams of ISSR and SAC will be combined next, to study together how they determine whether a contrail can form and persist or not.

## 2.4. Contrail Formation Regions (CFR)

By combining the ISSR and SAC, a plot can be made as shown in Figure 2.5, where the two curves represent the saturation with respect to water and ice, the three straight lines describe three different mixing processes with the same slope. The mixing process of the aircraft exhaust air and the ambient air can be described as followed with the purple line in Figure 2.5. The condition of the aircraft exhaust air is represented by the endpoint A of the purple line, and the atmosphere condition is represented by the other endpoint C. As the aircraft exhaust air mixing with the ambient air, it starts to cool down following the mixing line. At the intercept of the purple line with the red curve, its relative humidity is saturated with respect to water, therefore, water droplets start to form. After that, with the temperature keep decreasing, the water droplets turn into ice particles when the temperature is lower than  $-40^{\circ}$ . If the physical condition of the ambient air lies in the ISSRs, then the contrail is persistent. The blue line in Figure 2.5 indicates the threshold condition for a contrail to form. In this case, the mixing line is tangent to the saturation curve with respect to water, and the point of tangency is the condition where contrail starts to form and becomes visible. And for this case, since the physical conditions of the ambient air are not ISSRs, then formed contrail will dissolve. If the mixing line doesn't intercept with the saturation curve with respect to water, then the relative humidity is not large enough for water droplets to form, hence, no contrail will form as indicated by the yellow line in Figure 2.5.

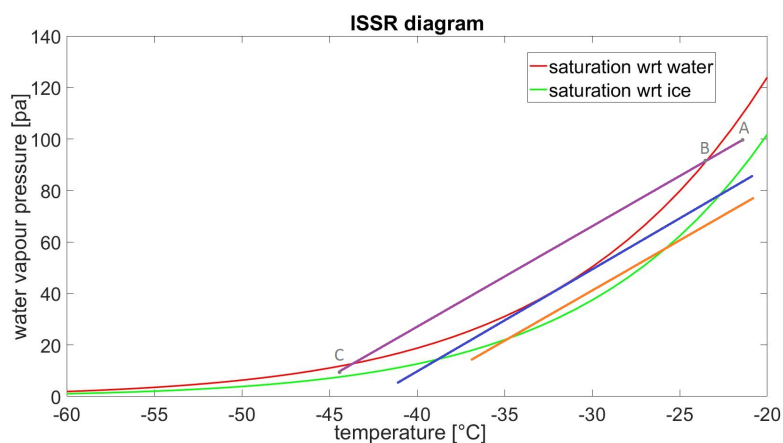


Figure 2.5: ISSR and mixing lines with same slope

In Figure 2.6 shows the effect of the physical conditions of the aircraft exhaust air on the formation of contrails. In Figure 2.6, three different situations are presented with the ambient atmosphere conditions remain ice supersaturated. The threshold condition is depicted by the blue mixing line, where it is tangent to the saturation curve with respect to water. If the slope of the mixing line is steeper as depicted by the purple line in Figure 2.6, means the exhaust air is colder or more humid, then a contrail will form. On the other hand, if the exhaust air is warmer or drier as depicted by the grey line in Figure 2.6, then contrail will not form. The temperature of the aircraft exhaust air depends mostly on the engine efficiency and the humidity of the aircraft exhaust air depends on the fuel type. When the the engine is more efficient, the exhaust air of the engine is colder as more energy are used for propulsion. However, this also lead to a steeper slope of the mixing line, therefore the mixing line slope is inversely proportional to the efficiency of the engine. In conclusion, an aircraft with a more efficient engine have a higher chance of forming contrails when flying through ISSRs.

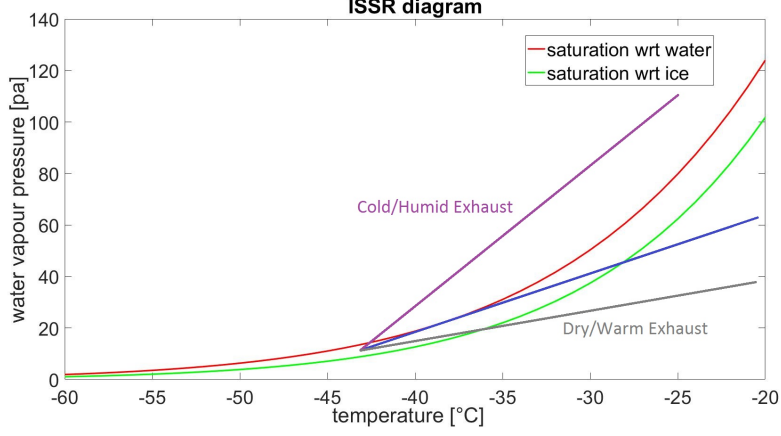


Figure 2.6: ISSR and Mixing Lines with Different Physical Conditions of Aircraft Exhaust Air

Generally speaking, ISSRs are those regions that allow a formed contrail to persist, whether a contrail can form or not in the first place also depends on the physical conditions of the aircraft exhaust air. Burkhardt et al. (2008) performed a study on the "Contrail cirrus supporting areas in model and observations" where they studied the differences between potential contrail coverage and potential contrail cirrus coverage, quantify the influence of the temperature and humidity of the aircraft exhaust air. In this paper, the potential contrail cirrus coverage is defined as ISSRs while the potential contrail coverage is defined as the Contrail Formation Regions (CFRs) in this thesis. In Equation 2.2, they calculate the "grid mean critical relative humidity for supersaturation,  $r_{CC}$ ", where they defined the relative humidity of saturation  $r_{sat}$  as 1.

Different from ISSRs, CFRs also take the physical conditions of the aircraft exhaust air into account. In order to quantify the influence of the temperature and humidity of the aircraft exhaust air, in their paper, instead of  $r_{sat}$ , one "relative humidity over ice at which contrail form during the mixing process between the aircraft jet engine exhaust and the surrounding air"  $r_{SAC}$  is defined as 1.1 in Equation 2.3 while calculating the "critical relative humidity for contrail formation  $r_{CO}$ ". For both equations, the "critical relative humidity for natural cloud formation,  $r_{ci}$ " is set to 0.6.

$$\frac{r_{CC}}{r_{ci}} = \frac{r_{sat}}{a \cdot r_{nuc}} = \frac{1}{a \cdot r_{nuc}} \quad (2.2)$$

$$\frac{r_{CO}}{r_{ci}} = \frac{r_{SAC}}{a \cdot r_{nuc}} = \frac{1.1}{a \cdot r_{nuc}} \quad (2.3)$$

A comparison of the fractional coverage of contrail and contrail cirrus based on the grid mean relative humidity is plotted in Figure 2.7. The black curve represents the natural cloud coverage  $b_{ci}$  and each of the dashed curve represents the sum of  $b_{ci}$  and the respective potential coverage of the corresponding color solid curves. For the potential contrail cirrus coverage, all the regions where formed contrails can persist are included, it only requires the regions to be ice supersaturated and is represented by the red curve from Figure 2.7. The potential contrail coverage includes only the CFRs where contrails can form, therefore, it is defined by both the ISSRs and SAC and is indicated by the green curve from Figure 2.7. A set of more detailed plots of the annual mean percentage of the potential contrail and contrail cirrus coverage simulated by ECHAM4 can be found in Figure 2.8 and Figure 2.9. It can be seen that the potential contrail cirrus coverage has basically a global coverage while the potential contrail coverage covered only the arctic and mid latitude regions at the same pressure level 300hPa.

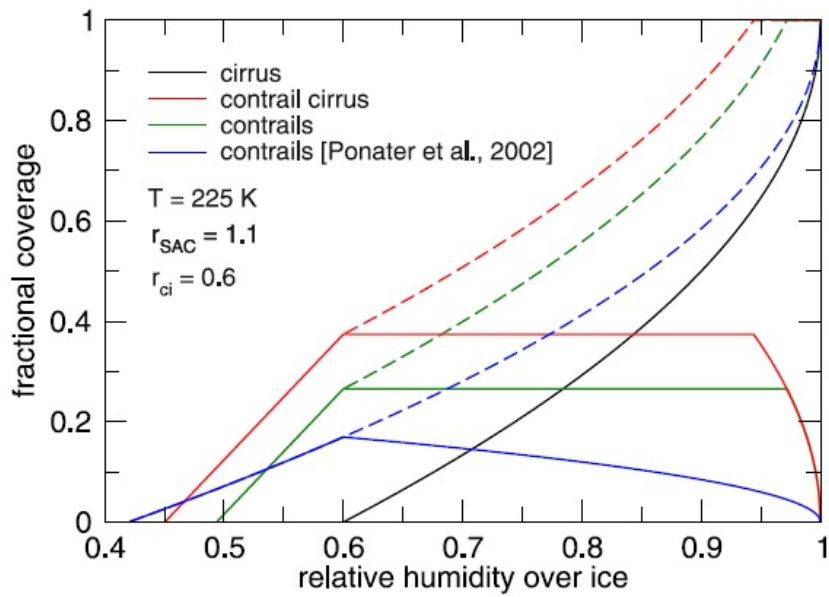


Figure 2.7: Cirrus coverage, potential contrail coverage, potential contrail cirrus coverage and potential contrail coverage according to Ponater et al. (2002)(Figure obtained from Burkhardt et al. (2008))

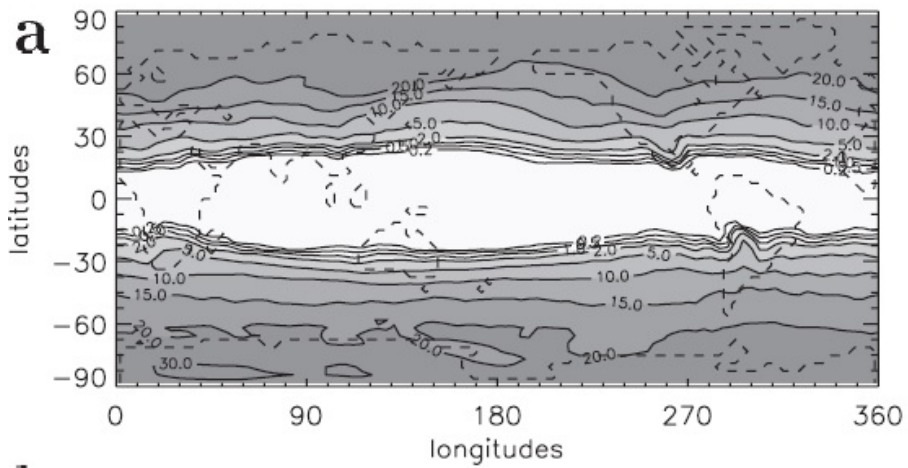


Figure 2.8: Annual Mean Potential Contrail Coverage [%] at 300hPa (Figure obtained from Burkhardt et al. (2008))

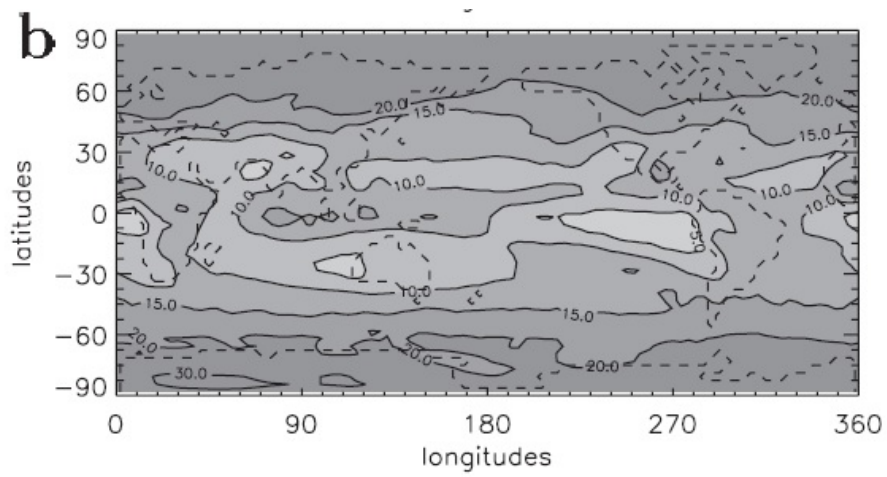


Figure 2.9: Potential Contrail Cirrus Coverage [%] at 300hPa (Figure obtained from Burkhardt et al. (2008))

# 3

## EMAC Model Description

In this thesis, data simulated by EMAC sub-model CONTRAIL were used for analyzing the characterisation and seasonality of the CFRs and their trends. EMAC is the abbreviation of ECHAM/MESSy Atmospheric Chemistry. It is capable of simulating the chemistry-climate interaction over the global scale (Jöckel et al. 2015). The sub-model CONTRAIL consists of several sets of simulations of the potential contrail coverage. Data from two different simulations are used, RC1SD-base-10 and RC2-base-04. The differences between these two simulations and why they are picked are elaborated next.

### **3.1. Hindcast with specified dynamics of the past (RC1SD)**

Reference simulation, REF-C1 with Specific Dynamics (RC1SD) stand for the hindcast simulation with specified dynamics, this simulation is available for the data from 1980 to 2013. For this simulation, the free running data is nudged towards the ERA-Interim reanalysis data (Jöckel et al. 2015). Basically, the nudging process is to insert the observation data from ERA-Interim reanalysis data into the simulation data so that the simulation results are closer to the observation result (Miyakoda, Strickler, and Chludzinski 1978). The resolution of this simulation is T42L90MA, T42 stands for the spectral resolution of a quadratic Gaussian grid of  $2.8^\circ \times 2.8^\circ$  in latitude and longitude, so the size of each grid is around  $300\text{km} \times 300\text{km}$ . L90MA stand for a vertical resolution of 90 model levels from the Earth surface reaching up to 0.01 hPa to the middle atmosphere approximately 80 km high. The 90 model levels are numbered from top to bottom starting from 1 to 90, this is the highest vertical resolution available. In order to describe the complicated chemical reactions in the upper stratosphere, the model level is set denser in the upper level to have a better simulation result.

### **3.2. Free running hindcast and projection simulations of the future (RC2)**

Reference simulation RC2 stand for the free running hindcast and projection simulation, the data simulated cover the year from 1960 to 2100. The data simulated from this simulation is used for analyzing the future trend of CFRs. Same as RC1SD-base-10, RC2-base-04 also has a resolution of T42L90MA, therefore, it is easier and more straightforward to compare the simulation results from these two different simulations.

### 3.3. Temperature and humidity differences between RC1SD and RC2

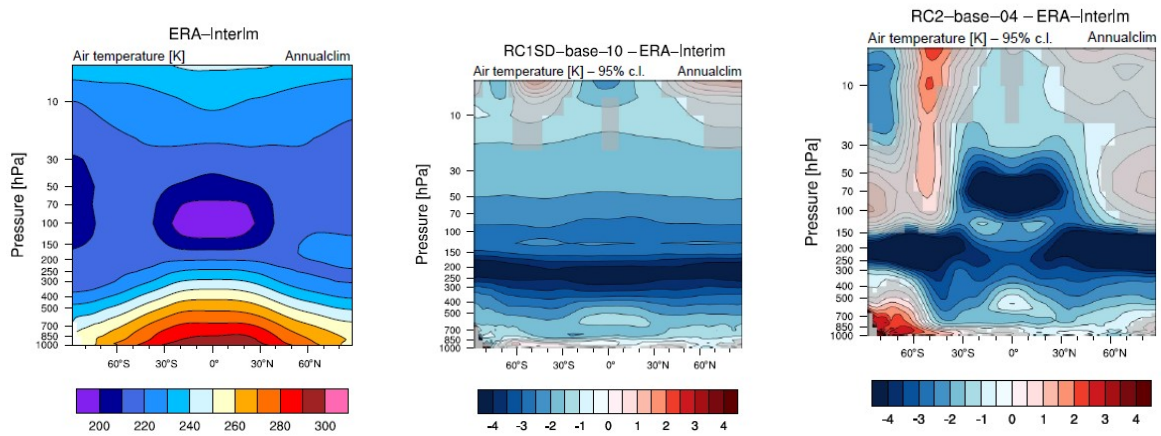
By the name of RC1SD and RC2, one big difference can be noticed, with the SD stand for specified dynamics, it means that RC1SD runs its simulation with specified dynamics. This is done by nudge the free-running hindcast simulation towards ERA-Interim reanalysis data by Newtonian relaxation (Dee et al. 2011). With the nudging process, it actually implies that the Sea Surface Temperatures (SSTs) and Sea Ice Concentrations (SICs) are very close to the ERA-Interim reanalysis data, the global mean data are almost identical with the satellite and in site observations (Jöckel et al. 2015).

For RC2, as this simulation covers the future till year 2100, a different method is used while acquiring the SSTs and SICs, historical data simulated by Hadley Centre Global Environment Model version 2-Earth System Model (HadGEM2-ES) are used for years up to 2005. After that, the Representative Concentration Pathway 6.0 (RCP6.0) simulation are incorporated, initialized with the 2005 year's data. However, the accuracy of the simulation result still needs to be improved, as in some area for the SICs, a deviation of up to 80% are discovered compare to the observed value.

A more detailed differences between the temperatures returned from these different models can be found in Figure 3.1. Figure 3.1a presents the temperature distribution simulated by the ERA-Interim, the simulated distribution of the temperatures are almost identical to the "merged satellite and in situ observations" (Jöckel et al. 2015). Therefore, it is used as a baseline to compare with the distribution of temperatures used in RC1SD-base-10 and RC2-base-04. The comparison results are presented in Figure 3.1b and Figure 3.1c.

From Figure 3.1b, it can be seen that, the simulated temperatures used in RC1SD-base-10 are overall lower than the ERA-Interim simulation results. The highest temperature deviation is around 4 K and locates in the pressure altitude from 150 hPa to 300 hPa. In the mid-latitude regions, This is also where the tropopause located. The simulated temperatures used in RC2-base-04 are presented in Figure 3.1c, the temperature deviation are not very consistent like the RC1SD-base-10 case. In some regions in the southern hemisphere, the simulated temperatures are higher than the base line in the stratosphere and lower troposphere. In most of the region, the simulated temperature used in RC2-base-04 are overall lower than the base line, the largest temperature deviations are located near the tropopause around 150 hPa to 300 hPa within the mid-latitude area in both northern hemisphere and southern hemisphere and around 40 hPa to 100 hPa within the tropics. This might result in the altitude shift of the tropopause as well as an altitude shift of the patterns of CFRs, as "contrail layers are mostly situated around the tropopause (Stuefer and Wendler 2004)".

In Figure 3.2a and Figure 3.2b presents the zonally averaged precipitation in the years 1990 to 2009 from all the sub model that are available from EMAC and their deviation from the GPCP data. The black solid line in both of the figures are plotted by the data from the Global Precipitation Climatology Project (GPCP), this project provide monthly precipitation data by combining both the observation and satellite data, therefore here it is used as the baseline to compare the humidity biases of the data used in other EMAC sub model. "Both simulations overestimate precipitation in the tropics, in the mid latitude regions for both hemispheres RC2-base-04 overestimate the precipitation while RC1SD-base-10 underestimate the precipitation compared to the GPCP simulation, in general, the free running and the nudged simulation show the same large scale deviation pattern from the observations. However they differ in strength and also regional differences can be found" (Jöckel et al. 2015).

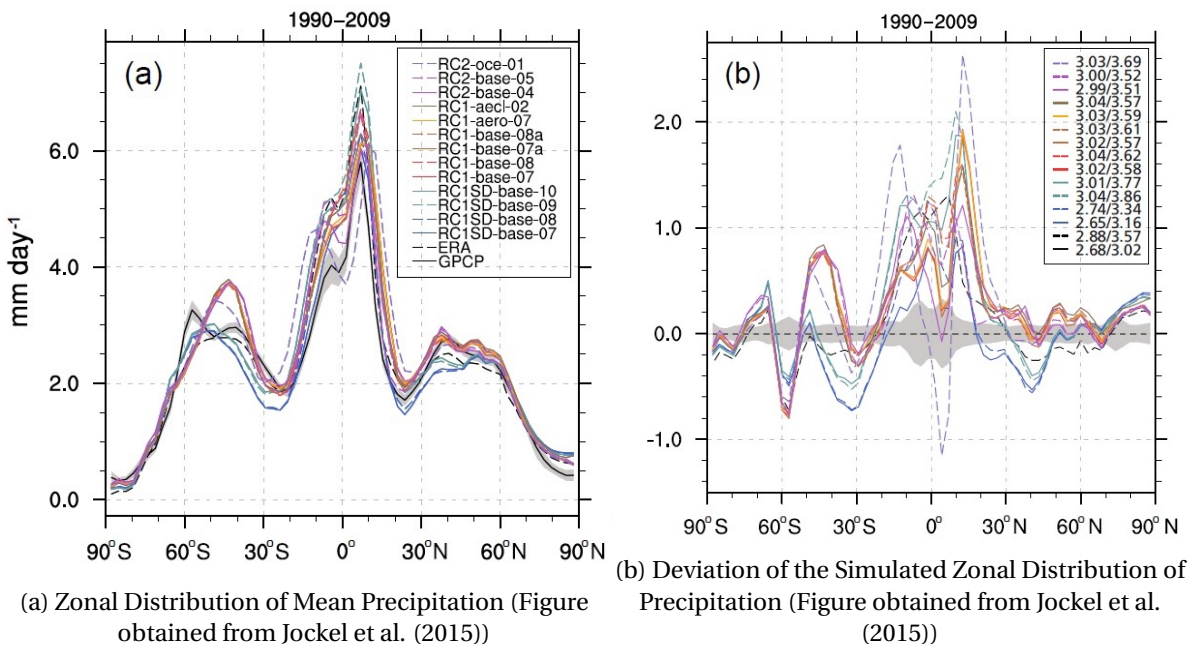


(a) Temperature Simulation Result with ERA-Interim Data (Figure obtained from Jöckel et al. (2015))

(b) Temperature Biases of RC1SD-base-10 (Figure obtained from Jöckel et al. (2015))

(c) Temperature Biases of RC2-base-04 (Figure obtained from Jöckel et al. (2015))

Figure 3.1: Temperature biases



(a) Zonal Distribution of Mean Precipitation (Figure obtained from Jöckel et al. (2015))

(b) Deviation of the Simulated Zonal Distribution of Precipitation (Figure obtained from Jöckel et al. (2015))



# 4

## Methodology

This chapter presents the methodology of this thesis. The general approach of this thesis is given in Section 4.1. Section 4.6 explains in detail how the grids are calculated to be connected and considered as one region for further analysis. Some decision making points including the selection of the time spans, choice of simulations, regions of interest and different potential coverage threshold (PT) selected for different parts of the thesis are explained in this chapter. Lastly, a summarize of the statistical and mathematical methods used to analyze and present the data is introduced in Section 4.8.

### 4.1. General Approach

This section presents the general approach of this thesis and some critical steps are further elaborated in the following sections.

First, a literature review about this thesis was performed and presented in Chapter 2.1 and 3. After that, the EMAC simulations chosen were validated by two different methods that can observe the atmosphere conditions in Chapter 5. Then, the data are prepared for further analysis, the data are simulated by two different EMAC simulations for different purposes. During the data preparation process, several PTs and regions of interests are tested and selected for further analyzing purpose. The CFRs grids that are simulated to be connected are numbered for further analysis. The data are also categorized by regions, seasons, past and future for further analyzing their characterisations, seasonality and trends of the CFRs. After the data are prepared, different statistical and mathematical methods were used to help analyzing and presenting the data.

### 4.2. Selection of time spans

It is commonly agreed that a continuous 30 years of data is minimally required to come up with a standard climate normal as well as to study the trend of climate change (Mason et al. 2015). In this thesis, two 30 years time spans are selected, one representing the current and the other for the future. Based on the availability of the EMAC data, the year 1984 to 2013 are picked for studying the current CFRs characterisation and seasonality, and the year 2700 to 2099 are selected for studying the future trend of CFRs.

Since temperature is one of the determining factors in the persistence of CFRs, a seasonal variation of the CFRs' characterisations is expected due to the different climate conditions in each season. Hence, the CFRs' characterisations are studied separately by each season. The four seasons are de-

fined by the northern hemisphere perspective as followed.

- Spring: March, April, May
- Summer: June, July, August
- Autumn: September, October, November
- Winter: December, January, February

### 4.3. CFR's Characterisation

For each grid from the simulations, the information regarding the fractional coverage of CFRs is available in a 4 dimensions perspective, latitude, longitude, altitude and time step. In order to visualize the data in a 2D plane, the following CFRs' characterisations are adopted.

#### 4.3.1. Zonal mean of CFRs' coverage

Zonal, together with meridional, represent the two directions on the Earth. Zonal is the direction along a latitudinal circle and meridional is the direction along a longitudinal circle. In order to present the regions that CFRs appear the most and have a high coverage in the 2D plane, the data are presented in a latitude-pressure altitude plane. As the Earth is a sphere, the circumference of each latitudinal circle at different latitude is different. Therefore, directly compare the summation of the CFRs along each latitudinal circle is biased. Each of the grid within the plot represents the zonal mean of CFRs' coverage, it is a ratio of length within that latitudinal circle that is covered with CFRs, and is calculated as followed,

$$\overline{Z}_{j,k} = \frac{\sum_{t=1}^{mt} \sum_{i=1}^{128} L_{i,j,k,t}}{mt \cdot C_j} \quad (4.1)$$

$i$  is the longitude,  $j$  is the latitude,  $k$  is the altitude and  $t$  is the time step,  $mt$  is the total number of time steps and 128 is the number of grids along each latitudinal circle.  $L_{i,j,k,mt}$  is the coverage length simulated at each grid for each time step.  $C_j$  is the circumference of the latitudinal circle at latitude  $j$ . The dimensionless quantity  $\overline{Z}_{j,k}$  is the time averaged zonal mean of CFRs' coverage at that latitude and pressure altitude. By dividing the summation of the coverage length along latitude  $j$  for all the time steps with the total number of time steps  $mt$  and the circumference of the latitudinal circle  $C_j$ , the ratio of the CFRs coverage length per unit length averaged by time at certain latitude  $j$  and pressure altitude  $k$  can be obtained.

#### 4.3.2. Meridional mean of CFRs' coverage

Same as the zonal mean of CFRs' coverage, the meridional mean of CFRs' coverage is presented in the longitude-pressure altitude plane. When analyzing the meridional mean of CFRs coverage, two regions are selected: Northern Hemisphere (NH) mid-latitude regions and tropics, the CFRs in these two regions are analyzed separately. The time averaged meridional mean of CFRs coverage is calculated as followed,

$$\overline{M}_{i,k} = \frac{\sum_{t=1}^{mt} \sum_{j=j_n}^{j_s} L_{i,j,k,t}}{mt \cdot C_i} \quad (4.2)$$

where  $C_i$  is the partial circumference of each longitudinal circle within the regions interested (NH mid-latitude regions or tropics).  $j_n$  and  $j_s$  are the latitudes of the northern and southern boundaries

of the regions interested. The dimensionless quantity  $\overline{M_{i,k}}$  is the ratio of the CFRs coverage length per unit length averaged by time within the regions interested at certain longitude  $i$  and pressure altitude  $k$ .

#### 4.3.3. Conditional mean of meridional CFRs' coverage length

Additional to the meridional mean of CFRs' coverage mentioned above, a conditional mean of meridional CFRs' coverage length is also calculated and presented in the longitude-pressure altitude plane. The conditional mean of meridional CFRs' coverage length for each grid in the 2D plane is calculated as followed,

$$\overline{N_{i,k}} = \frac{\sum_{t=1}^{mt} \sum_{j=j_n}^{j_s} L_{i,j,k,t}}{nt} \quad (4.3)$$

where  $\overline{N_{i,k}}$  is the conditional mean of meridional CFRs coverage length within the regions interested (NH mid-latitude regions or tropics). Instead of dividing the summation by the total number of time step  $mt$ ,  $nt$  is the number of time steps that CFRs are discovered within the regions interested at that longitude  $i$  and pressure altitude  $k$ . For example, the simulation have 500 time steps, and within the regions interested at longitude  $i$  and pressure altitude  $k$ , CFRs are discovered 200 times, then  $\overline{N_{i,k}}$  is calculated by dividing the summation with 200. The  $\overline{N_{i,k}}$  has a unit of km for each grid, to have a more straightforward idea of how much regions are covered by CFRs on average.

#### 4.3.4. Vertical Extension of CFRs

The vertical extension of CFRs are calculated to study the trend of the CFRs' distribution in Section 8.2.1. For each year, one summation of all the CFRs' vertical extension simulated globally at all latitude, longitude and altitude is calculated as the total vertical extension for that year.

#### 4.3.5. Stretch factor of CFRs

The stretch factor of CFRs are analyzed to have an overview of the shape of CFRs. For each numbered CFRs (the process of the numbering of CFR is introduced in Section 4.6), it is calculated as followed,

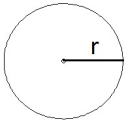
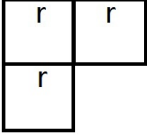
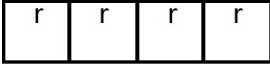
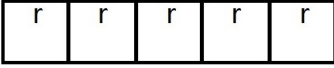
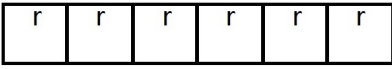
$$\text{Stre\_fac} = \frac{P/4}{\sqrt{S}} \quad (4.4)$$

where  $P$  is the perimeter of the CFR and  $S$  is the surface of the CFR. The stretch factor ( $\text{Stre\_fac}$ ) is a dimensionless quantity that can describe how stretched a shape is. Table 4.1 presents some examples of the stretch factors of some basic geometric shapes and some geometric shapes consist of different amount of grids. According to the definition, the stretch factor of a circle is equal to 0.89 and the stretch factor of a square is equal to 1 and these shapes are considered as not stretched. For a rectangle as shown in Table 4.1, the stretch factor is always larger than 1, when the shape is more elongated, then the stretch factor also increase. Basically, when the stretch factor of a geometric shape is smaller than 1, then that shape is considered as not stretched. When the stretch factor is bigger than 1, the geometric shape is considered as stretched, and when the shape is more stretched, the stretch factor is bigger.

#### 4.3.6. Direction of CFRs

Furthermore, when the stretch factor of a CFR is calculated to be larger than 1.1, then that CFR is considered to be stretched and its direction is then calculated. The detailed definitions of the CFRs' di-

Table 4.1: Examples of CFRs stretch factors

Shape	Illustration	P	S	Stre_fac
Circle		$2\pi r$	$\pi r^2$	0.89
Square		$4r$	$r^2$	1
Equilateral Triangle		$3r$	$\frac{\sqrt{3}}{4}r^2$	1.14
Rectangle with 2 grids		$6r$	$2r^2$	1.06
Random shape of three grids		$8r$	$3r^2$	1.15
Rectangle with 4 grids		$10r$	$4r^2$	1.25
Rectangle with 5 grids		$12r$	$5r^2$	1.34
Rectangle with 6 grids		$14r$	$6r^2$	1.43

rection within the horizontal plane (latitude-longitude plane) and vertical plane (Longitude-altitude plane) are given in Section 7.2.

#### **4.4. Regions of Interest**

In this research, different regions of interest are selected when analyzing different CFRs' characterisations. For the zonal mean of CFRs' coverage length, the whole Earth is covered. For the CFRs' coverage length in the meridional direction, two different regions are analyzed separately, the NH mid-latitude regions and tropics. Same for the CFRs' stretch factor and direction, the CFRs located in the NH mid-latitude regions and tropics are analyzed separately. The detailed selection of each region analyzed and the reasons are explained next.

First of all, in order to have an overview of the CFRs' distribution globally, two parts of the study were conducted on a global scale which are the zonal mean of CFRs coverage length and the Vertical extension of CFRs.

Next, according to the common flight routes and different typical atmosphere conditions, the NH mid-latitude regions  $23^{\circ}\text{N}$  to  $66^{\circ}\text{N}$  and tropics  $23^{\circ}\text{S}$  to  $23^{\circ}\text{N}$  are selected. As most of the commercial flight routes take place in the NH mid-latitude and Tropics, its worthy of a thorough study of these regions about their CFRs' characterisations and trend. And due to the different typical atmospheric conditions of these two region, hot and humid over the year for Tropics and for NH mid-latitude there is a clear distinction between the four seasons, more seasonality of the distribution of CFRs are expected in the NH mid-latitude regions. Therefore, when studying the Meridional mean of CFRs coverage length, these two regions where studied separately.

For studying the stretch factor and direction of the CFRs, as the purpose of this part of research is to study the pattern of the distribution of the CFRs so that it can help the airline to plan their routes or to alter their routes to avoid the formation of contrails. Therefore, for this part, the regions of interest are also selected to be the air traffic busy regions, NH mid-latitude and tropics.

#### **4.5. RC1SD and RC2**

Due to the different temperature and humidity configuration used in RC1SD-base-10 and RC2-base-04 as mentioned in Section 3.3, a temperature bias is discovered in both of the simulations. However, for RC2-base-04, more regional temperature deviations are discovered. Therefore, for the first part of the study, only the results simulated by the RC1SD-base-10 are studied, mainly to figure out the current characterisations and seasonal variations of the CFRs including the zonal and meridional mean of CFRs' coverage length, direction and stretch factor of the CFRs in both horizontal and vertical plane. For the second part of this master thesis, in order to study the future trends of the CFRs, the simulation results from RC2-base-04 are used, as this simulation is available till year 2100.

#### **4.6. Definition of connected region**

In this research, when one grid and its adjacent grids are simulated to be CFRs, then all the connected grids are considered as one region. A detailed demonstration is given in Figure 4.1.

Figure 4.1 presents a 5 by 7 grids map, each of the grids are numbered by its row and column number. The grey coloured grids are the grids that are simulated to be CFRs. This process is done by scanning through the grids in each 2D plane, eg. horizontal plane (longitude-latitude plane). When a CFR grid is scanned, for example G22, then it is numbered as region number 1, next the eight grids adjacent to it, in this example, they are G11, G12, G13, G23, G33, G32, G31 and G21 are scanned next,

and G23 as a CFR grid is also numbered as region 1. Then, the 8 grids adjacent to G23 are scanned next and any grid that has already been number before will not be processed again. In this case, G34 will be numbered as region 1 as well as G43. After that, when scanning the 8 grids adjacent to G43, no more grid is discovered to be CFR, then the program will move on to the next CFR grid it discovered. In this example, it is G26 and this grid is then numbered as region number 2, and by scanning through the 8 grid adjacent to G26, G36 will also be numbered as region 2. Same process is applied to the whole 2D plane in order to find and numbered all the grids connected in that 2D plane.

The stretch factor and direction of the covered regions of each numbered CFR are further calculated. This algorithm is also applied to the vertical plane (longitude-altitude plane) in order to analyze the CFRs stretch factor and direction in the vertical plane. It is worth mentioning that a similar algorithm is also applied to the 3D space covering the whole atmosphere. Basically, it is scanning through all the grids available from the ground to the top and numbered the grids that are connected. However, due to the complex nature of CFRs, for many time step, only one region is returned. It means that all the CFR grids turned out to be connected somehow, therefore, it is pointless to further study the CFRs stretch factor and direction in the 3D space.

G11	G12	G13	G14	G15	G16	G17
G21	G22 1	G23 1	G24	G25	G26 2	G27
G31	G32	G33	G34 1	G35	G36 2	G37
G41	G42	G43 1	G44	G45	G46	G47
G51	G52	G53	G54	G55	G56	G57

Figure 4.1: Demonstration of how the CFR grids are numbered

The chance for a grid simulated to CFRs largely depends on the PT selected, and it will be explained in the next section.

#### 4.7. Potential Coverage Threshold (PT)

POTential contrail COVERAGE is represented by POTCOV in EMAC and is calculated according to the paper by Burkhardt et al. (2008) as mentioned in Section 2.4. Both the theories of ISSR and SAC are taken into consideration while calculating it. A Potential coverage Threshold (PT) is used in this thesis as a boundary for considering a grid as a CFR or not. When the POTCOV of a grid is larger than the set PT, then that grid is considered as a CFR and will be taken into account for further analysis of their characterisations and trends. For each grid of  $2.8^\circ \times 2.8^\circ$ , the amount of the POTCOV indicates the percentage of the total grid area that are covered with CFRs. Overall, a higher PT adopted indicates

a lower chance for each grid to be considered as CFR, therefore, the chance for CFR grids discovered to be connected are lower.

In this section, the sensitivity of the PT are tested for both of the simulations, RC1SD-base-10 and RC2-base-04. The sensitivity and selection process of PT in this research are explained next.

#### 4.7.1. Sensitivity of PT

A set of 4 PTs range from 10 to 90 are tested for each simulation. For RC1SD-base-10, to analyze the sensitivity of PT, the CFRs' frequency for different PTs are compared to see the sensitivity of the PT. The definition of the frequency of CFRs is given in detail in Section 5.3. Furthermore, to compare the detailed differences caused by the different PT selected, the distribution of the CFRs within the same altitude level are studied when two different PTs are applied.

First, Figure 4.2 shows the CFRs' frequency at 200 hPa pressure altitude for the year 1995 to 1997. The parameter used in this part of the simulation is the same as the validation of EMAC by MOZAIC that will be discussed in Chapter 5 later. Therefore, the color scale used here are the same as the one used in 'Measurement of ozone and water vapor by Airbus in-service aircraft: The MOZAIC airborne program, An overview' (Marenco et al. 1998). It can be seen that with the increase of the PT, overall, the frequency of CFRs is decreasing globally. The frequency pattern seems quite different as the color for different plot are quite different, especially when compare the two plots with PT=10 and PT=90. However, the pattern are similar for the four plots with different PTs. They all have high values above the tropics and comparatively higher frequency in the American-Europe-Asia flight corridor and some part of the South Pacific and South America as well as the Intertropical Convergence Zone (ITCZ).

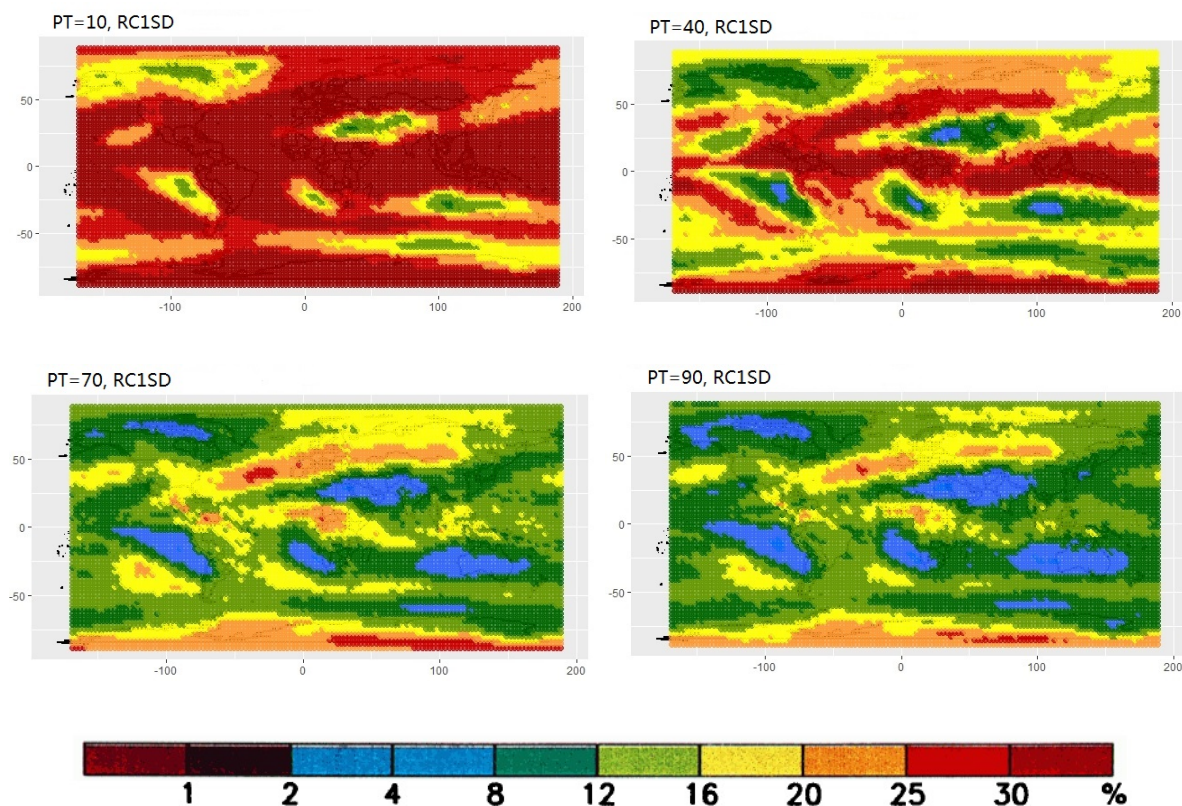


Figure 4.2: CFR Frequency 200hPa RC1SD

Same pattern is also noticed for the simulated results from RC2-base-04, and the CFRs' frequency at 200 hPa with four different PTs simulated by RC2-base-04 can be found in Appendix A.1.

Figure A.2 presents a comparison between a set of two different PTs, PT=10 and PT=90. The results are plotted by RC1SD-base-10, the fractional coverage of CFR at each grid is simulated according to paper by Burkhardt et al. (2008). Two different time steps from 1996 are selected here, one in June representing the contrail pattern in summer, the other one is from December representing the situation in winter. Both of the CFRs plotted are at the pressure altitude around 200 hPa. Figure 4.3a and Figure 4.3b show the differences between the two PTs selected. Figure 4.3a presents the plot for summer with a PT=10, a high coverage of contrail presents in the Antarctica as well as some scattered region in the tropics and mid-latitude regions. Most of the grids simulated to be CFRs are connected, this is due to the PT selected is quite low. For PT=10, when more than 10% of the grid is calculated to be CFR, then the whole grid is considered to be a CFR. This way more grids are simulated to be CFRs, therefore, there is a higher chance for the CFR grids to be connected and considered as one region.

Figure 4.3b is the plot at the same time step as Figure 4.3a but with a PT=90. In this case, the grids calculated to be CFRs are only those with CFR coverage of more than 90% of the whole grid area. Therefore, compared to the case with PT=10, less grids are simulated to be CFRs. Furthermore, if several grids are calculated to be connected and are considered as one region, there is a higher chance for real life contrails formed there to be connected at these regions. By comparing Figure 4.3c and Figure 4.3d, the differences between the two PTs selected for a winter climate can also be noticed. In winter, at 200 hPa pressure altitude, there are less contrail coverage in the Antarctica, the CFRs in the tropics and mid-latitude regions are more concentrated compared to the summer climate. Same as the summer case, when PT=10, more grids are considered to be CFRs, therefore, higher chance for CFRs grids simulated to be connected as one region.

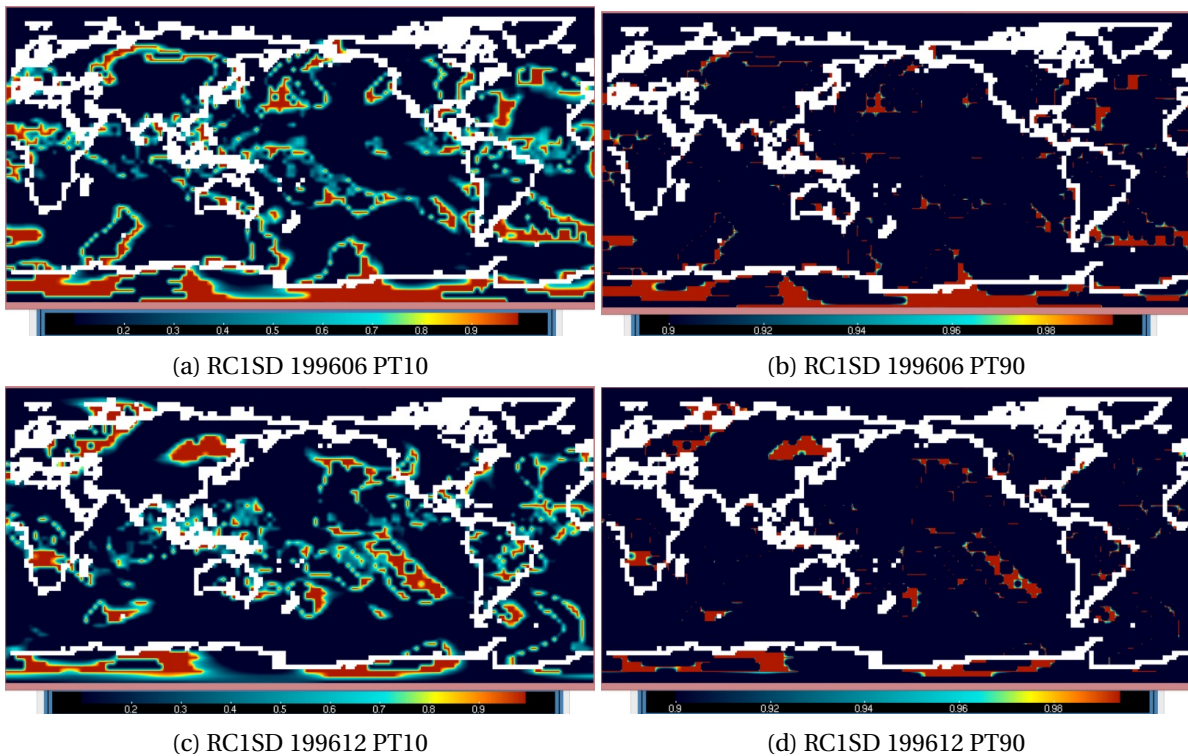


Figure 4.3: RC1SD PT10 and PT90 Comparison of Two Different Months in 1996

Same pattern is also noticed for the simulated results from RC2-base-04, and the CFRs' fre-

quency at 200 hPa with four different PTs as well as the CFRs' distribution with PT=10 and 90 simulated by RC2-base-04 can be found in Appendix A, Figure A.1 and A.2.

#### **4.7.2. Selection of PT**

For the first part of this project, the CFRs characterisations are studied with the simulated result from RC1SD-base-10 only. The CFRs characterisations analyzed are separated into two groups. The first group includes the zonal and meridional mean coverage length of CFRs, a PT=10 is applied to make sure all the sufficient regions are covered. As the purpose of this part of study is to calculate the overall coverage length of CFRs, therefore, every bits count. The second group includes the stretch factor and direction of CFRs, when analyzing the typical stretch factor and direction pattern of the CFR for different latitude and longitude, PT is set to 90%. It means that only when more than 90% of a grid area is simulated to be CFR, then this whole grid is considered as a CFR. By setting the PT to 90%, it means that in real life when an aircraft fly through a grid that is simulated to be CFR, there is a higher chance that contrail will form. Furthermore, if two connected grids are both simulated to be CFRs, there is a higher chance for these CFRs to be really connected in really life situations and more contrails will be formed if the aircraft does not change its route accordingly. Furthermore, with a PT=90, the over estimation of the connectivity of the CFR grids are avoided, the stretch factor and direction of CFRs calculated are closer to the real life situation.

For the second part of the research where the simulation results from RC2-base-04 is analyzed. The zonal and meridional mean CFRs' coverage length of 30 years from the past and 30 years from the future are compared to study the CFRs' trend as well as the vertical extension of CFRs, PT=10 is selected for the reasons mentioned above.

### **4.8. Data Analyzing and Presenting Methods**

This section introduces the statistical methods used for analyzing and presenting the data.

#### **4.8.1. Boxplot**

For depicting the distribution of the CFRs' direction verses the latitude, the boxplot is used. For each group of data, boxplot uses boxes and whiskers to display the distribution of the data by presenting the minimum, first quartile, median, third quartile, maximum as well as the outlier. The boundary of the box is set by the first quartile and third quartile and the range of the box is defined as the likely range of variation (LQR). When a data point is deviate from the boundary of the box more than 3 times of LQR, then these data points are considered to be outliers. And they will be plotted as black solid points in the box plot. The two end of the whisker is set by the maximum and minimum data point except the outliers. With the help of boxplot, it is easier to spot the the most appeared direction of CFRs and their distribution verses the latitude.

#### **4.8.2. Kernel Density Estimation**

Other than the boxplot, the Kernel Density Estimation (KDE) is also used in this thesis when analyzing the CFRs' stretch factors and directions. By selecting the proper bandwidth, the kernel density plot can present a smooth distribution of a large amount of data points. In this thesis, the bandwidth is selected by the unbiased cross validation. The kernel density plot can be used to present the probability of the interested variables, when both the density and area under the curve at one value are high, then the probability of the variable at that value is also high.

### **4.8.3. Welch's Two Sample T-test**

When analyzing the trend of the CFR, the data simulated for 30 years in the past (1984 to 2013) and for 30 years in the future (2070 to 2099) are compared by calculating the differences between their mean values. Therefore the statistical significance is required to determine if the results are statistically significant. The Welch's two sample t-test is used since the variance between the past and future data are varied largely (Welch 1947). A Welch's t-test is performed on each of the two data sets compared. For each Welch's t-test, the null hypothesis is: the difference between mean value of the data obtained for 30 years in the past and future are 0. Therefore, the alternative hypothesis is the mean value of the data for 30 years from the past and future are not the same. In this thesis, the significance level threshold is set to 5%, so when the probability (p-value) calculated is lower than 5%, the null hypothesis is rejected and the difference calculated are considered to be statistically significant with a confidence level of 95%.

# 5

## Model Validation

This chapter presents the validation process of the two simulations from EMAC sub-model CONTRAIL. The data from both of the simulations are compared to the observed ISSRs frequency by two different methods: MOZAIC and MLS, and these two methods are introduced next.

### 5.1. ISSRs Measurement by in Service Aircraft: MOZAIC

MOZAIC is the abbreviation of Measurements of ozone by Airbus in-service aircraft. It is a project that equipped measurement devices on Airbus wide body aircraft that fly daily and internationally to collect real time data such as water vapour data which is used here to calculate if a region is ice supersaturated. The observation results used here are obtained by Gierens et al. (1998) from their paper "Ice-supersaturated regions and subvisible cirrus in the northern mid-latitude upper troposphere". In their paper, the frequency of the ISSRs were calculated for two 50 hPa pressure layers centered at 200 hPa and 250 hPa for a three year period from 1995 to 1997. The probability of Ice Super Saturation (ISS) is used in this paper to show the frequency of ISSRs, it is defined as "the ratio of the number of measurements that indicate ice supersaturation and the total number of measurements in a cell" (Marengo et al. 1998). Only when a flight flies in a certain grid for more than 8 minutes, then that certain measurement was considered as a valid one and was used for further averaging, and only those grids that have more than 30 valid measurements were taken into account (Marengo et al. 1998).

However, for MOZAIC, the areas where measurements are available are limited to the regions where the aircraft has flown through since the data are collected on board of in-service aircraft. These regions are mostly at the common altitude for international flights, and the time slot where data are measured are also limited to the common flight hours for these flight. Therefore, to have a better validation of the EMAC data on a global scale, observation results from MLS are also used and are introduced next.

### 5.2. ISSRs Observation by Satellite: MLS

MLS is the abbreviation of Microwave Limb Sounder, the data are obtained from Upper Atmosphere Research Satellite (UARS). MLS can remotely sense vertical profiles of atmospheric gases, temperature, pressure, and cloud ice.<sup>1</sup> The data used here for validation purpose is obtained from paper

---

<sup>1</sup><https://mls.jpl.nasa.gov> (accessed September 13, 2017)

"The global distribution of ice-supersaturated regions as seen by the Microwave Limb Sounder" by Spichtinger et al. (2003). This paper presents the observation results at two different pressure levels: 147 hPa and 215 hPa from year 1991 to 1997. The frequency of occurrence of ice supersaturation is defined as for each grid "the number of measurements with  $RHi > 100\%$  divided by the total number of measurements at this grid point", and a clearance of cloud is fulfilled by removing the measurement with  $RHi > 230\%$ , and only when there were more than 50 valid measurements then the grid points are taken into final averaging (Spichtinger, Klaus Gierens, and Read 2003).

The detailed comparisons between the simulation results from EMAC and the observation results from MOZAIC and MLS are presented next.

### 5.3. Validation of EMAC

For the EMAC simulation results present in this section, a frequency of CFR for each grid is calculated as followed:

$$\text{Frequency of CFR} = \frac{\text{Number of time steps one grid is simulated to be CFR}}{\text{Total number of time steps}} \times 100\% \quad (5.1)$$

The frequency of CFRs is compared with the frequency of the ISSRs from both "Measurement of ozone and water vapor by Airbus in-service aircraft: The MOZAIC airborne program, An overview" and "The global distribution of ice-supersaturated regions as seen by the Microwave Limb Sounder". The grid resolution in both MOZAIC and MLS are the same as EMAC, so it is easier to have a direct comparison between the EMAC simulation result and the observation result from MOZAIC and MLS.

#### 5.3.1. EMAC and MLS

In this section, a comparison between EMAC and MLS at pressure levels 147 hPa and 215 hPa is presented, the year covered are from 1991 to 1997. As mentioned in Section 4.7.1 that with a different PT selected, the frequency of CFRs basically have a similar pattern, but the magnitude of CFRs' frequency decreases with the increase of the PT selected. First, four different PTs: 10, 40, 70, 90 are set in the simulation to find the PT that provides the CFRs' frequency within the range that is most similar to the Figure 5.2a from MLS. In order to have an easier comparison with the ISSRs' frequency observed by MLS, here we use the same colour scale as the one used in their paper to have a visually more direct comparison. The simulation results by EMAC at the pressure altitude of 147 hPa with the 4 different PTs selected can be found in Figure 5.1. By comparing Figure 5.1 to Figure 5.2a, the EMAC simulation result with a PT of 40% has the CFRs frequency that are closest to the range observed by MLS at this pressure level. They both have a maximum around 40% within most of the tropical regions. Therefore, PT equal to 40% is selected during the validation process of EMAC for a comparably more straightforward comparison.

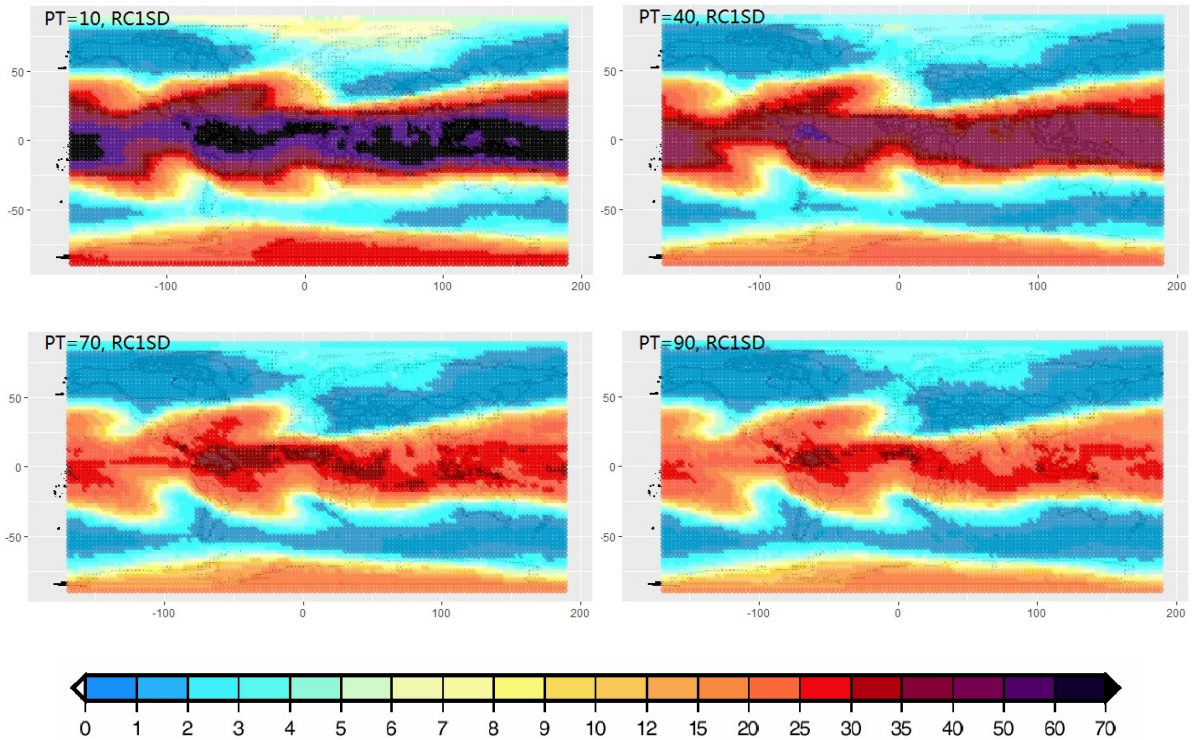
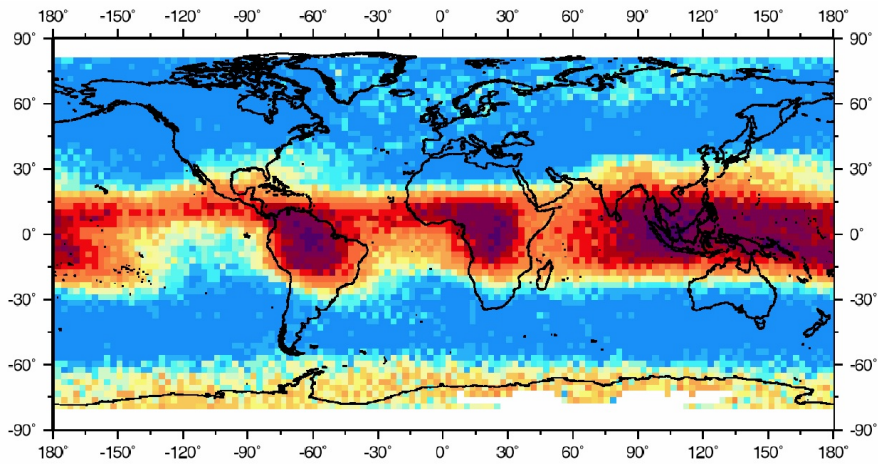


Figure 5.1: CFRs' Frequency at 147 hPa Simulate by RC1SD with Four Different PTs

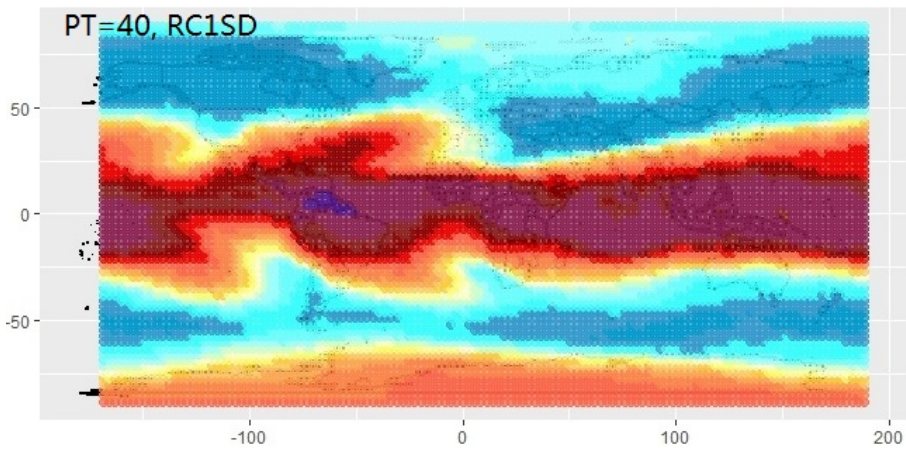
### Pressure Altitude: 147 hPa

By comparing Figure 5.2b, 5.2c to Figure 5.2a, the EMAC simulation results at 147hPa level are compared to the results observed by MLS. According to Figure 5.2a, the frequency of ISSRs reach the maximum in the tropics between 15°S and 15°N. The highest frequency is around 40-50%, and are mostly presented above the continent including the southern America, tropical Africa as well as the Indonesian archipelago, these maxima regions are connected by the InterTropical Convergence Zone (ITCZ) between the equator and 15°N with a ISSRs frequency around 25%. Furthermore, within the tropical regions, low frequency of ISSRs are mostly discovered above the Tropical Eastern Pacific. In the subtropics of both hemisphere (15° – 30°) there is a strong poleward decrease of the ISSRs' frequency. Within the Antarctica, the frequency of ISSRs is around 15%, higher than the mid-latitude regions. In both mid-latitude regions at 147 hPa, ISSRs are rarely discovered with a frequency around 1%, this is due to the dry stratospheric air (Spichtinger, Klaus Gierens, and Read 2003).

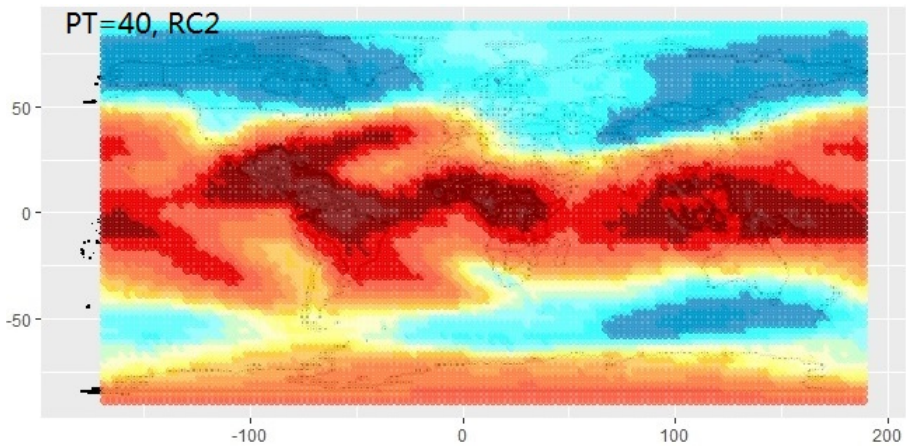
Figure 5.2b and 5.2c present the CFRs frequency at 147hPa level with a PT of 40% for both of the EMAC simulations RC1SD-base-10 and RC2-base-04. Overall, both of the plots are showing a similar pattern to the MLS plot. High CFRs' frequency are discovered within most of the tropics except the Tropical Eastern Pacific. CFRs' frequency are very low within the mid-latitude regions in both hemisphere, and a slightly higher frequency of CFRs is discovered above the Antarctica. Some differences can be noticed that the EMAC plots show a high frequency of CFRs in the North Atlantic and North Pacific till 50°N. For RC2-base-04, the CFRs frequency calculated are a bit lower than the RC1SD-base-10 result and the high frequency regions are a bit dissipated compared to the RC1SD in the south hemisphere mid-latitude regions, but overall both plots are following a similar pattern.



(a) Frequency of Occurrence of ISSRs at 147 hPa by MLS (Spichtinger, Klaus Gierens, and Read 2003)



(b) CFRs' Frequency simulated by RC1SD at 147 hPa



(c) CFRs' Frequency simulated by RC2 at 147 hPa

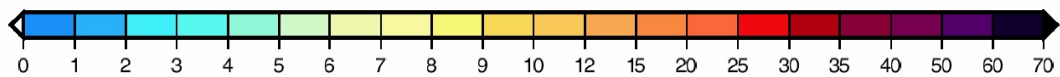


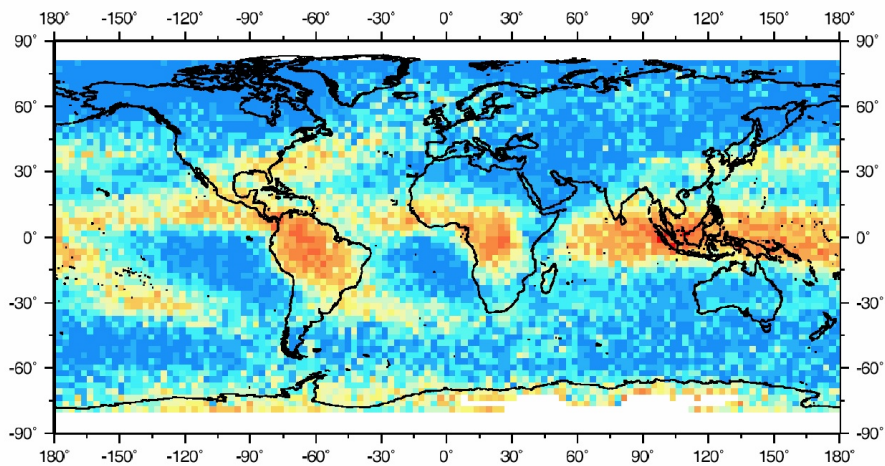
Figure 5.2: CFRs' Frequency by MLS and EMAC Simulations at 147 hPa

## Pressure Altitude: 215 hPa

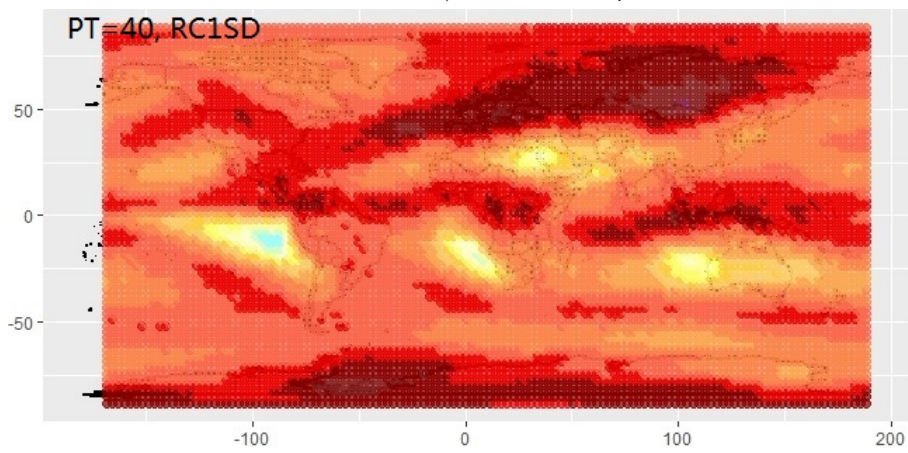
Next, the results from the two EMAC simulations at 215 hPa level as shown in Figure 5.3b and 5.3c are compared to the MLS observation result plotted in Figure 5.3a. Generally, the ISSRs' frequency observed by MLS at 215 hPa have a very similar pattern to the ISSRs' frequency observed at 147 hPa level by MLS, but the maximal frequency value is around 20%, this is way lower than the one observed at 147 hPa level. Unlike the results at 147hPa level, the simulated results from both of the EMAC simulations seem to be drastically different from the MLS plot at first glance. As shown in Figure 5.3b and 5.3c, overall, the CFRs' frequency are higher than 25% globally. For the region in between 30°S and 30°N, it is actually following the same pattern as the MLS result especially for the RC1SD-base-10 results. High frequency fo CFRs are discovered over the continent including the Amazonia, tropical Africa and the Indonesian archipelago. For the region northern to the 30°N and southern to the 30°S, there are rarely ISSR being observed by MLS. Generally, the result from RC2-base-04 have a lower CFRs' frequency within the tropics than the result from RC1SD-base-10. This is probably due to the temperature bias mentioned in Section 3.3. At 215 hPa level in the tropics, the temperature used in RC2-base-4 are higher than that in RC1SD-base-10, hence the CFRs' frequency might be lower in RC2-base-04 for these regions.

Most of the difference are notice as followed, according to RC1SD-base-10, especially over the continent of Eurasia, a very high frequency of CFRs around 30% are discovered. For RC2-base-04, a high frequency of CFRs are discovered covering most of the regions northern to 50°N. The same difference is also discovered by Spichtinger et al. (2003) when they compare their results to the MOZAIC data and in their paper "The global distribution of ice-supersaturated regions as seen by the Microwave Limb Sounder", they presented the reason that might lead to this deviation, which is due to the poor vertical resolution (ca. 3km) of the limb sounder. Since both of the pressure level measured are in its field of view, this might lead to an underestimation of the ISSR frequency at the lower level which is the 215 hPa level over the Eurasia. (Spichtinger, Klaus Gierens, and Read 2003)

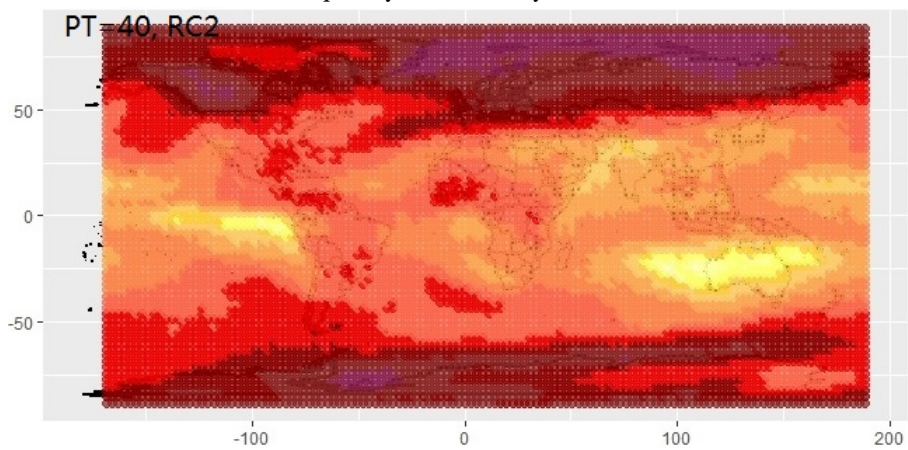
Overall, it's pointless to directly compare the result numerically, as the exact CFRs' frequency returned by EMAC largely depend on the PT chosen. Furthermore, the specific definition of the ISSRs' frequency from both MLS and MOZAIC are still slightly different from the CFRs' frequency calculated by EMAC simulations. Therefore, despite some differences, the results from the EMAC simulations have very similar pattern to MLS observation results.



(a) Frequency of occurrence of ISSRs at 215 hPa by MLS (Spichtinger, Klaus Gierens, and Read 2003)



(b) CFRs' Frequency simulated by RC1SD at 215 hPa



(c) CFRs' Frequency simulated by RC2 at 215 hPa

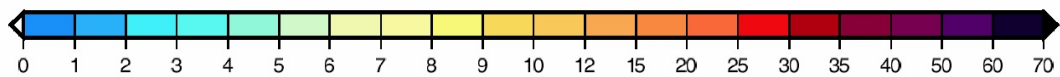


Figure 5.3: CFRs Frequency 215hPa RC1SD and RC2

### 5.3.2. EMAC and MOZAIC

This section presents the simulation results from EMAC and the in-situ observation results from MOZAIC for year 1995 to 1997 at pressure levels 200 hPa and 250 hPa. To make the comparison more straightforward, the color scale used here are the same as the one used in their paper "Measurement of ozone and water vapor by Airbus in-service aircraft: The MOZAIC airborne program, An overview".

As mentioned earlier, simply comparing the exact value of the ISSRs' and CFRs' frequency at each grid are pointless. This is due to the exact CFRs' frequency returned by EMAC largely depend on the PT chosen, and the specific definition of the ISSRs' frequency from MOZAIC are slightly different from the CFRs' frequency calculated by EMAC simulations. Therefore, here mainly the trends of the available regions from MOZAIC are studied and compared with the EMAC simulations' results.

#### Pressure Altitude: 200 hPa

For pressure level 200 hPa, the MOZAIC in-situ measured data are plotted in Figure 5.4 and the EMAC simulation results from both simulations are presented in Figure 5.5. First, the results simulated by the two EMAC simulations are compared. As plotted in Figure 5.5, in most of the regions, the CFRs frequency calculated by both of the EMAC simulations have a similar pattern, most of the discrepancies located in the tropics as well as the regions northern to the 50°N. In the tropics, the results calculated by RC2-base-04 are overall lower than that from RC1SD-base-10, on the other hand, in the regions northern to the 50°N, the RC2-base-04 simulated result are higher than that of the RC1SD-base-10. Same contrast was also discovered in the case at 147hPa level. As mentioned in Section 4.5, despite the temperature bias discovered for both simulations, more regional temperature deviations are discovered from the temperature data used in RC2-base-04. Therefore, compared to RC2-base-04, RC1SD-base-10 have a relatively better and more detailed simulation results, and the following detailed trend comparison between MOZAIC and EMAC, only the comparison between the results from MOZAIC and RC1SD-base-10 is presented.

As shown in Figure 5.4, the MOZAIC results are rather scattered and limited, it is quite difficult to have a direct comparison with the plot of the EMAC results. Therefore, a summary of the trend within the MOZAIC result are presented as well as some crucial grids including the maximum and minimum value points. For 200 hPa level, the maximums located in the equatorial Africa, upper edge at the Amazonia, upper edge of Indochina and at the boarder of Russia and Kazakhstan, all the maximums have a value over 30%. Overall, the data points that are available from MOZAIC can be categorized into 6 routes considering Europe as their starting point. They are named by both of their endpoints, the Europe→North America, Europe→Brazil, Europe→South Africa, Europe→South Asia, Europe→ Eastern China and Europe→Japan.

A comparison of the trend along these routes obtained by both MOZAIC and RC1SD-base-10 is presented in Table 5.1. Generally, the CFRs' frequency simulated by RC1SD-base-10 have a very similar range as the in-situ observed results from MOZAIC, expect for the regions above Europe and North America. One of the deviation that is noticeable from Table 5.1 is the CFRs' frequency over Europe. From MOZAIC, the value obtained are around 8% which is a rather low value. However, from RC1SD-base-10, the CFRs frequency simulated were higher than 30%, this is in the highest range of CFRs' frequency in this plot. Therefore, when considering a trend of these routes simulated by RC1SD-base-10, it always starts with a decreasing trend of CFRs' frequency in the first place, which lead to all the trends returned by MOZAIC quite different from the one simulated by RC1SD-base-10 in the very beginning. One other region that MOZAIC and EMAC results do not quite agree with each other is the region above North America, the RC1SD-base-10 simulated results are much higher than the MOZAIC in site observed results. Other than these two regions, the rest of the regions where MOZAIC

data are available, the trend of these routes are quite identical between MOZAIC and RC1SD-base-10, despite some minor differences between the exact values. Overall the CFRs' frequency simulated by RC1SD-base-10 are higher than the MOZAIC observed data. And according to Figure 5.4, within the Eurasia continent, "the more northern latitudes tend to show low fractional coverage of ice supersaturation (Marenco et al. 1998)", this also fits with the trend plotted by RC1SD-base-10.

Table 5.1: Comparison of MOZAIC and EMAC at 200hPa

Route	MOZAIC	MOZAIC Trend	RC1SD-base-10	RC1SD Trend
EU→North America	8 → 16 → 8	↗↘	30+ → 16 → 25	↘↗
EU→Brazil	8 → 8 → 16	↗	30+ → 20 → 30+	↘↗
EU→South Africa	8 → 1 → 30+ → 8	↘↗↘	30+ → 8 → 30+ → 16	↘↗↘
EU→South Asia	8 → 8 → 12 → 25	↗	30+ → 12 → 16 → 20	↘↗
EU→Eastern China	8 → 30+ → 20 → 12	↗↘	30+ → 30+ → 20 → 12	↘
EU→Japan	8 → 20 → 16 → 12	↗↘	30+ → 20 → 16 → 12	↘

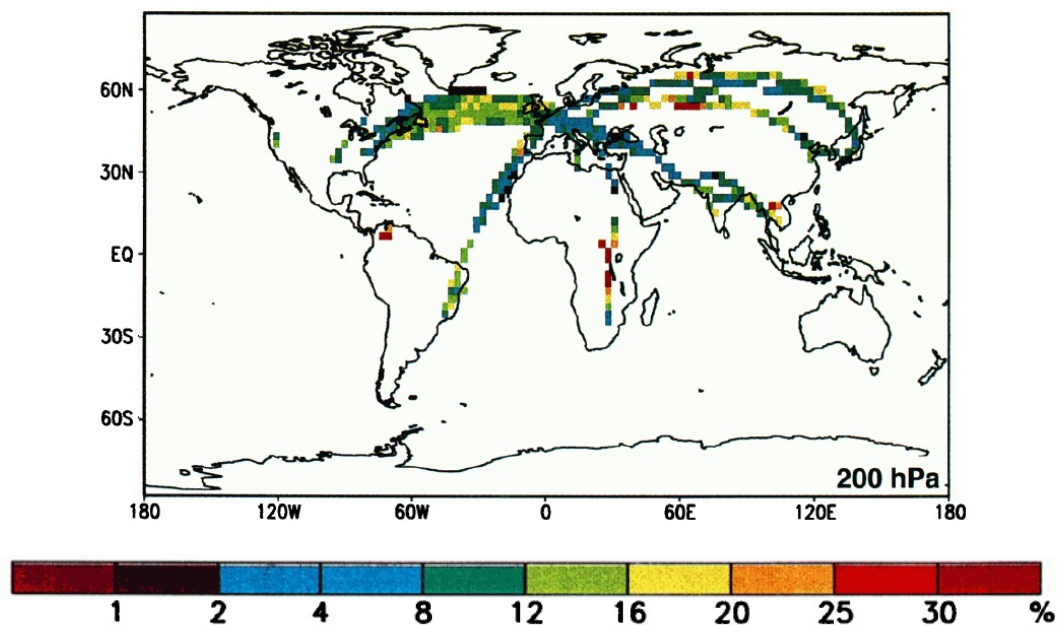
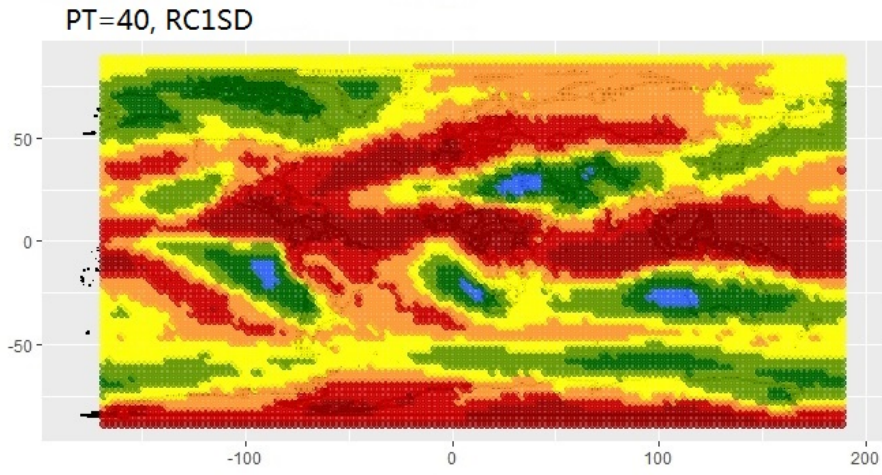


Figure 5.4: Frequency of occurrence of ISSRs at 200 hPa by MOZAIC (Marenco et al. 1998)

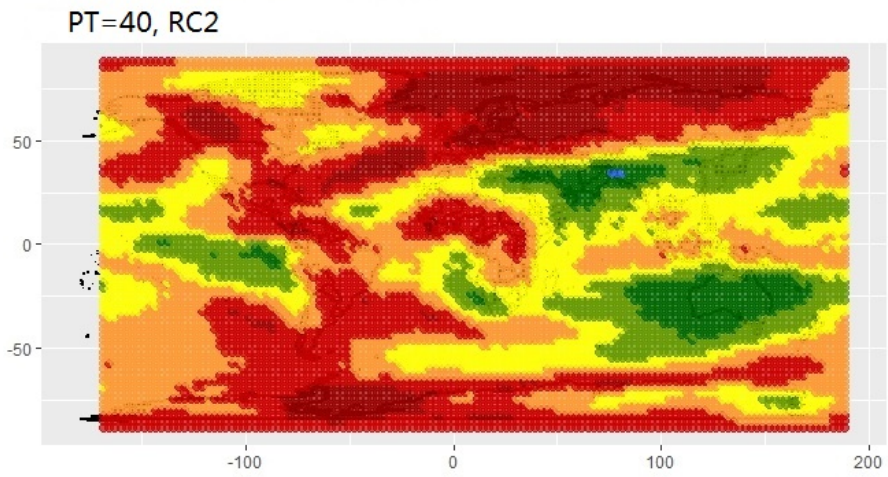
### Pressure Altitude: 250 hPa

Figure 5.7 presents the EMAC simulation results from both of the simulations at 250 hPa and the MOZAIC in situ observed results are presented in Figure 5.6. As observed by MOZAIC, the minimum of ISSRs' frequency over part of Sahara is less than 1%, and the maximum is discovered with a value of 36% at 10° west of Brittany in France (Marenco et al. 1998). And in the Northern latitude, the ISSRs frequency are generally higher than 20%.

The same comparison of the trend for the six specific routes that are available in MOZAIC data are presented in Table 5.2. It can be seen that, at 250 hPa, most of the trend of these six routes are identical between RC1SD-base-10 and MOZAIC, this is partly due to the CFRs' frequency simulated by RC1SD-base-10 over Europe is again greater than 30%, but this time in this region, EMAC also observed quite a high ISSR frequency of 25%. Likely to 200hPa level, the ISSR frequency simulated



(a) CFRs' Frequency simulated by RC1SD at 200 hPa



(b) CFRs' Frequency simulated by RC2 at 200 hPa

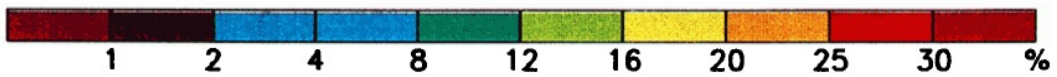


Figure 5.5: ISSR Frequency 200 hPa RC1SD and RC2

by RC1SD-base-10 are higher than the MOZAIC in situ observed data globally. Despite that, as mentioned earlier, due to the definition of the CFRs' frequency from EMAC and ISSRs' frequency from MOZAIC are not exactly the same, it is more important to compare the trend than directly comparing the exact value of the ISSRs and CFRs frequency.

Table 5.2: Comparison of MOZAIC and EMAC at 250hPa

Route	MOZAIC	MOZAIC Trend	RC1SD-base-10	RC1SD Trend
EU→North America	25 → 20 → 12 → 25	↘↗	30+ → 30 → 25 → 30+	↘↗
EU→Brazil	25 → 8 → 16 → 8 → 20	↘↗↘↗	30+ → 30 → 12 → 20 → 16	↘↗↘
EU→South Africa	25 → 1 → 30+ → 8	↘↗↘	30+ → 4 → 30 → 16	↘↗↘
EU→South Asia	25 → 4 → 12	↘↗	30+ → 8 → 16	↘↗
EU→Eastern China	25 → 20 → 12	↘	30+ → 20 → 16	↘
EU→Japan	25 → 12 → 20 → 16	↘↗↘	30+ → 30 → 20 → 16	↘

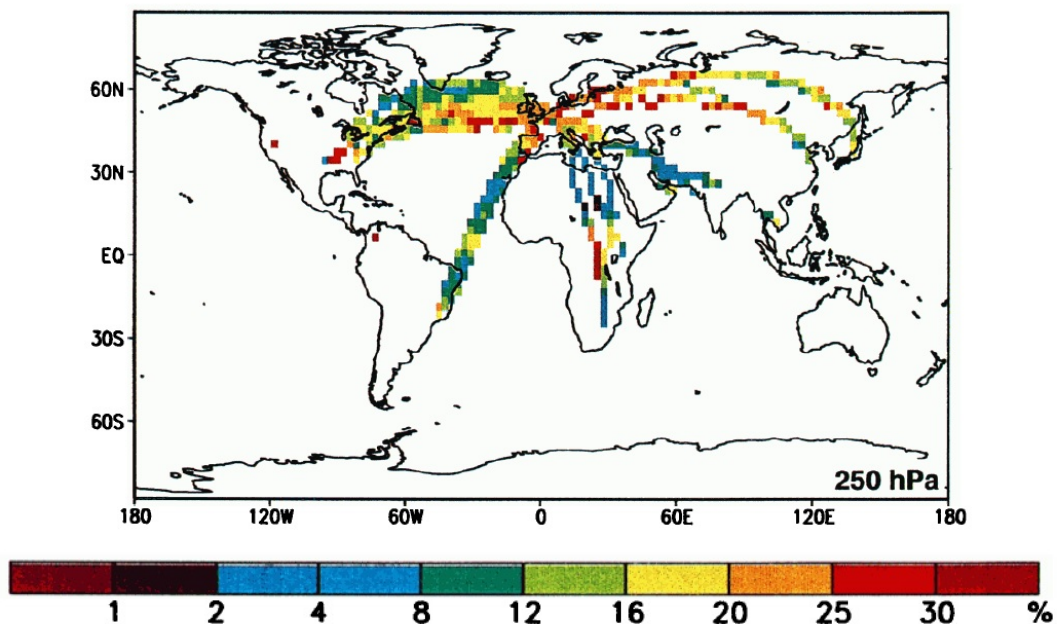
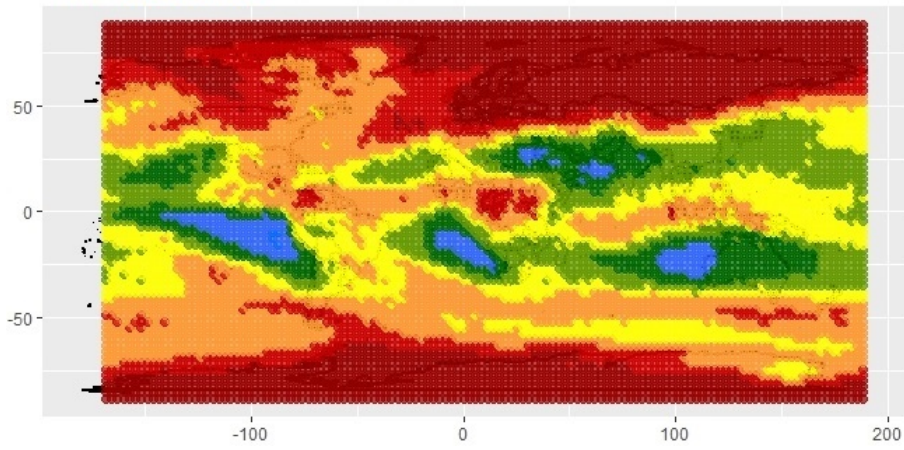


Figure 5.6: Frequency of Occurrence of ISSRs at 250hPa by MOZAIC (Marenco et al. 1998)

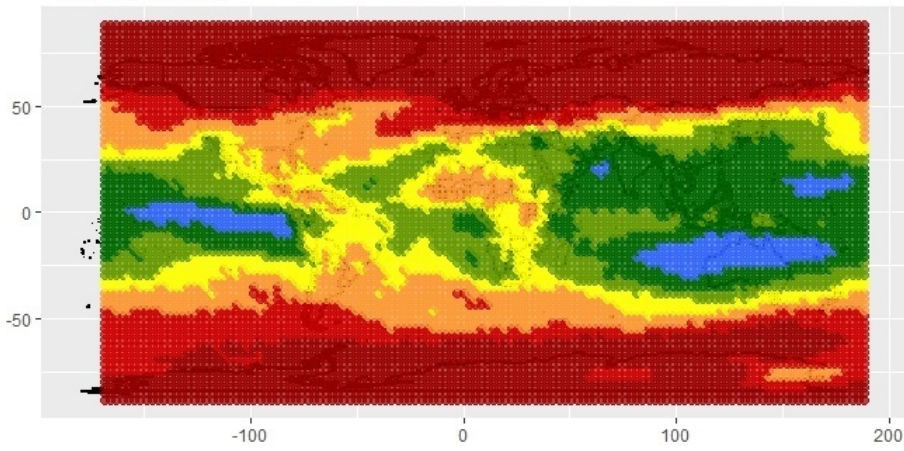
Overall, it can be said that the simulation results from EMAC are validated by MOZAIC and MLS together. Due to the slight difference between the definition of ISSRs and CFRs, simply compare the exact value of the CFRs' frequency simulated by EMAC and the ISSRs' frequency observed by both MOZAIC and MLS is not useful. The validation is done by comparing the significant trends discovered within the results simulated by EMAC and the observed results from both MOZAIC and MLS.

PT=40, RC1SD



(a) CFRs' Frequency simulated by RC1SD at 250 hPa

PT=40, RC2



(b) CFRs' Frequency simulated by RC2 at 250 hPa

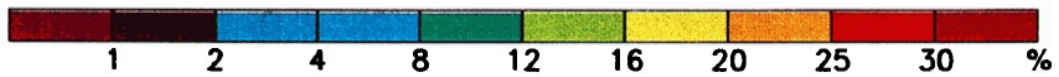


Figure 5.7: ISSR Frequency 250hPa RC1SD and RC2



# 6

## Characterizations and Seasonality of CFRs: Coverage Length

Analyzing the current distribution of CFRs is essential for predicting the future trend of CFRs' distribution. This chapter presents the analysis of the current CFRs' characterizations and their seasonality including the zonal and meridional mean of CFRs' coverage as well as the conditional mean of meridional CFRs' coverage length.

Throughout this part of study, PT is set to 10% as explained in Section 4.7.2. Therefore, when calculating the total coverage length, each grid that have a fractional CFR coverage of more than 10% of its grid length is considered as CFR grid. Those grids are then counted for further calculating the CFRs' coverage length. Furthermore, when calculating the CFRs' coverage length, in order not to overestimate the total coverage length of CFRs, when adding up the coverage length at each grid, only the part of the grid length that are actually simulated to be CFRs are summed up as the total CFRs coverage length.

### 6.1. Meridional mean of CFRs' coverage

Meridional, together with zonal, represent the two directions on the Earth. Meridional is the direction along a longitudinal circle. A more detailed introduction of the meridional mean of CFRs' coverage and how it is calculated are elaborated in Section 4.3.2.

In addition, the meridional mean of CFRs' coverage is studied for NH mid-latitude and Tropics separately for the reasons mentioned earlier in Section 4.4. The simulation results from RC1SD-base-10 is presented in the following sections.

This section presents the simulation results of the meridional mean of CFRs' coverage from the RC1SD-base-10 for the 30 year time spans from the past (1984-2013). A comparison between the simulation results for the four different seasons are presented in order to study the seasonal variations of these characterisations. First, the simulation results of the CFRs appear in the North Hemisphere (NH) mid-latitude regions are presented.

#### 6.1.1. NH Mid-latitude Regions

Figure 6.1, 6.2, 6.3 and 6.4 present the CFRs Meridional mean coverage for the four different seasons in the NH mid-latitude regions. In these figures, the value at each grid represents the dimensionless

quantity: the time averaged CFRs' coverage length per unit length at that altitude and along that longitude circle within the NH mid-latitude regions. The value at each grid is represented by both size and color of the grid. A bigger grid size implying a higher ratio of the interested region are covered with CFRs. The grid with a lower ratio is represented by a series of green colors and the grid with a higher ratio is represented by a series of brownish colors till the highest ratio is indicated as grey color. Hence, the large and grey grids in these figures indicate where are the regions that have a higher coverage of CFRs.

Figure 6.1, 6.2, 6.3 and 6.4 presents the meridional mean of CFRs' coverage in spring, summer, autumn and winter, it can be seen that in the NH mid-latitude regions, CFRs are mostly found distributed along the pressure altitude from 600 hPa to around 100 hPa. The regions with higher coverage of CFRs are located between the layer from 400 hPa to 200 hPa pressure altitude. Overall, spring and autumn are showing very similar pattern of the distribution of the CFRs' coverage due to their similar weather conditions. On the other hand, since there is a temperature threshold for the formation and persistence of CFRs, in summer, these regions are shifted a bit upward to 350 hPa to 150 hPa pressure altitude, this is due to the overall higher temperature in summer causing the temperature in the lower altitude too high for contrails to form and persist. On the contrary, due to the overall lower temperature in winter, these regions are extended to a lower level around 550 hPa pressure altitude especially in the eastern hemisphere. Overall, for summer, autumn and winter, the maximal ratio discovered is higher than 0.1. It means that, for these three seasons, within the NH mid-latitude regions at certain pressure altitude where the maxima are discovered, over 10% of the regions are covered by CFRs on average. The maximal ratio discovered in spring is slight lower than 10%. For spring, autumn and winter, most of the maximal ratios appear over the continent including Asia, Europe and America as well as some part of the Atlantic Ocean. In summer, different from the rest three seasons, the highest ratio is discovered over the western North Pacific Ocean.

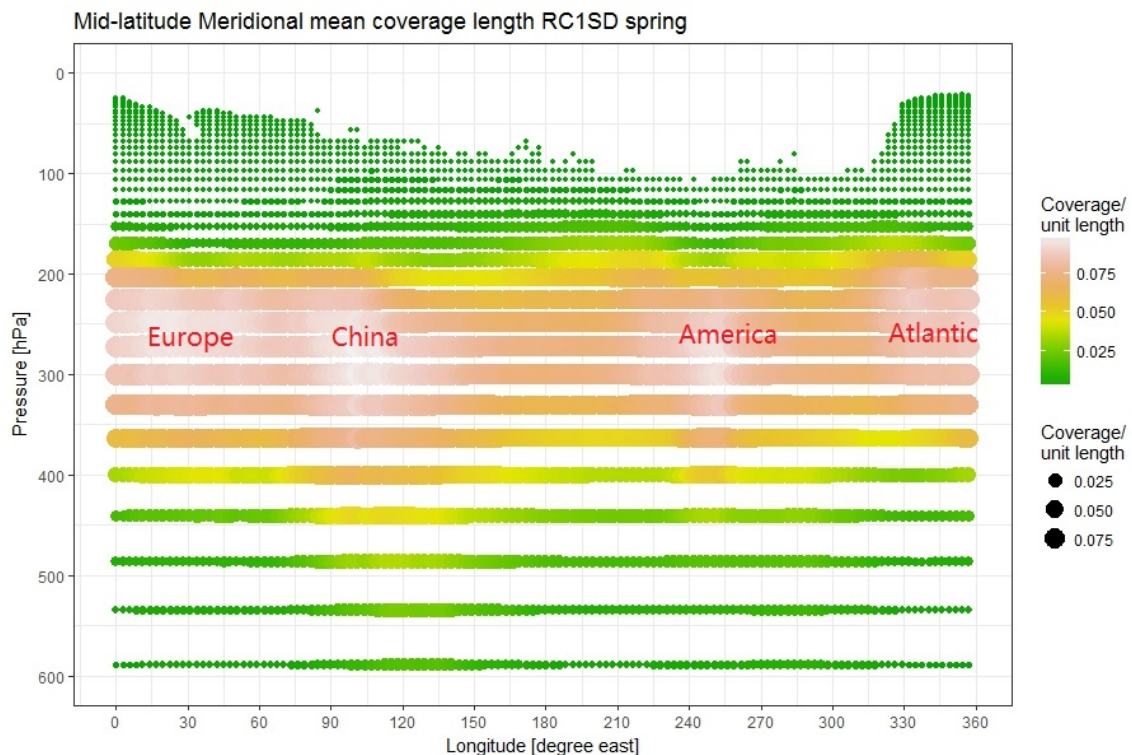


Figure 6.1: Meridional Mean of CFRs' Coverage in Spring NH Mid-latitude

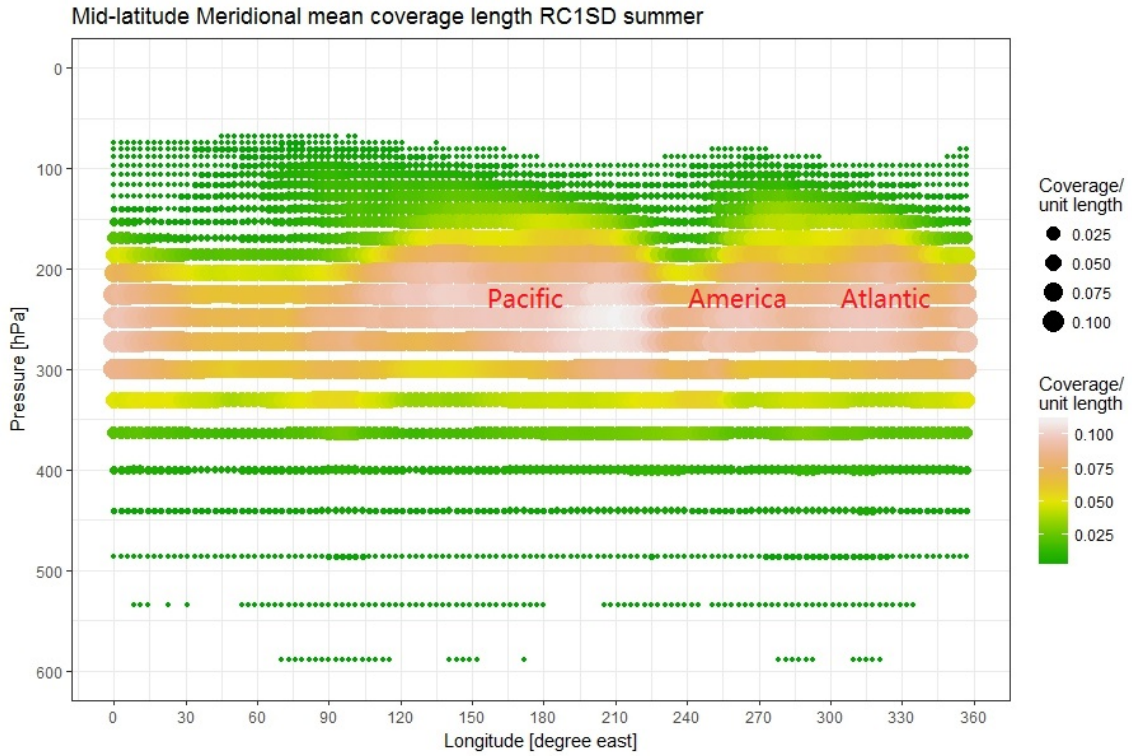


Figure 6.2: Meridional Mean of CFRs' Coverage in Summer NH Mid-latitude

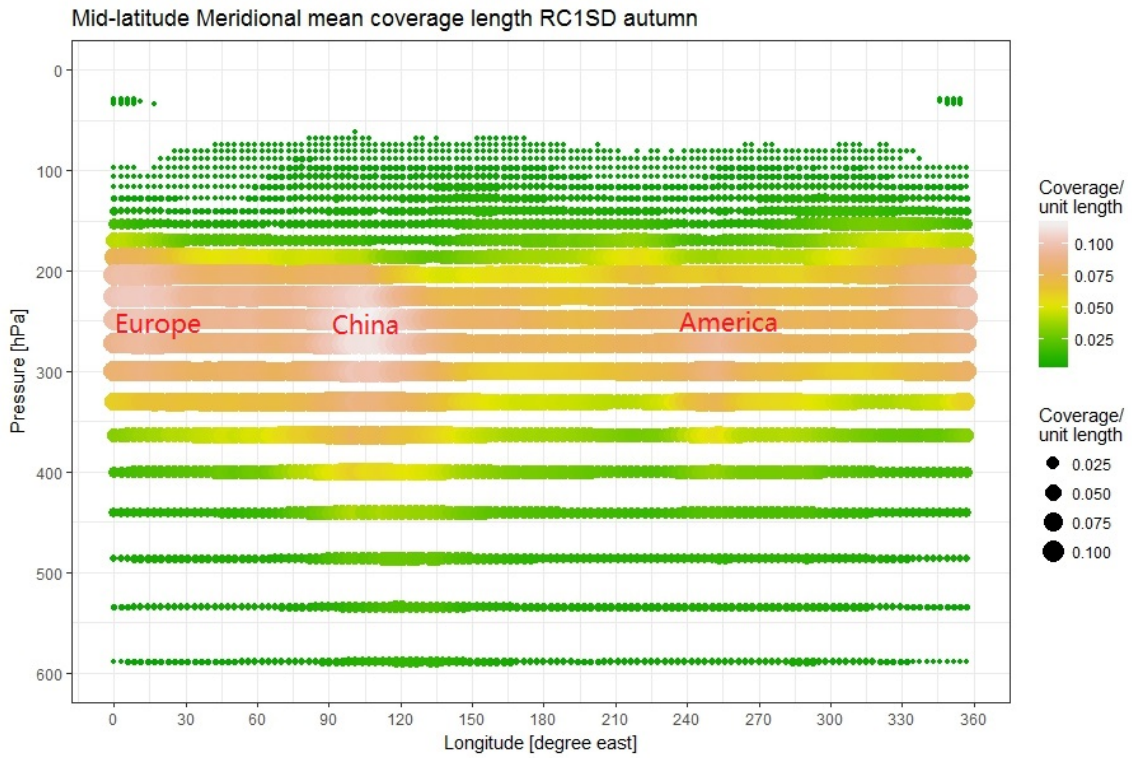


Figure 6.3: Meridional Mean of CFRs' Coverage in Autumn NH Mid-latitude

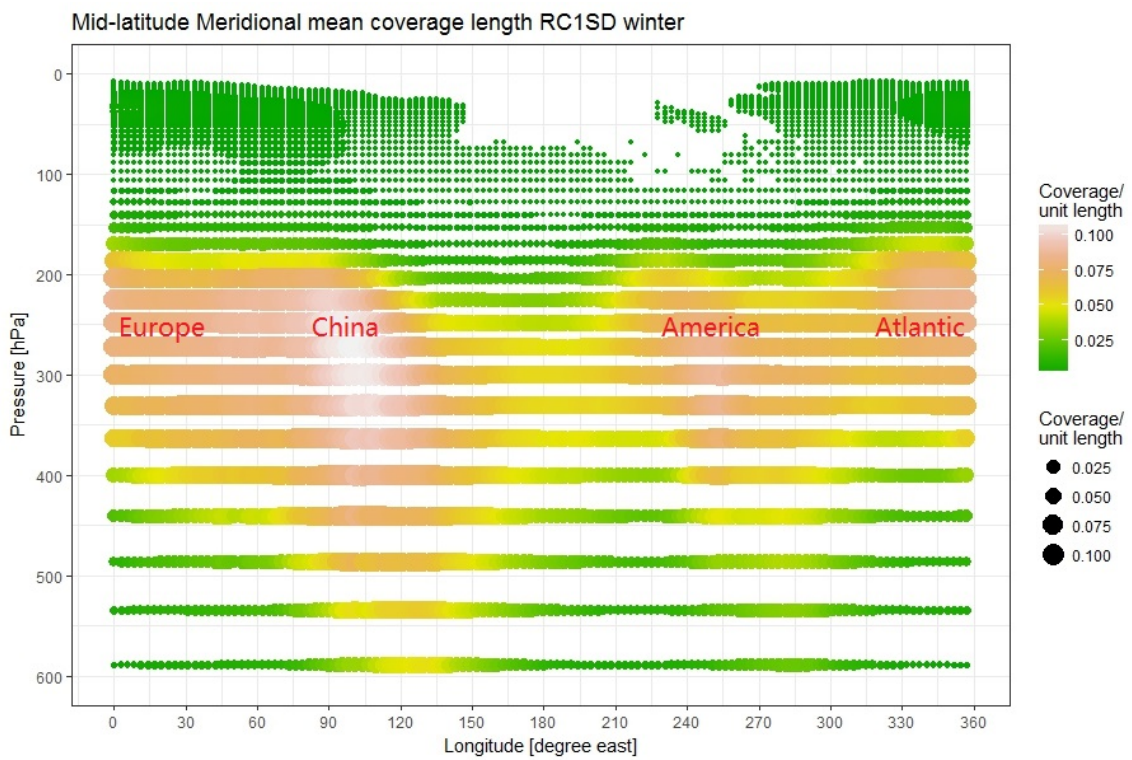


Figure 6.4: Meridional Mean of CFRs' Coverage in Winter NH Mid-latitude

### 6.1.2. Tropics

Figure 6.5, 6.6, 6.7 and 6.8 present the meridional mean of CFRs' coverage for spring, summer, autumn and winter in the tropics. Each of the grid point in these figures represent the dimensionless quantity: the time averaged CFRs' coverage length per unit length at that altitude and along that longitude circle within tropics.

It can be seen that in tropics, most of the CFRs are only discovered between 300 hPa and 50 hPa pressure altitude. The maximal ratios are mostly discovered between 180 hPa and 90 hPa pressure altitude. Compares the CFRs' mostly discovered pressure altitude within the NH mid-latitude regions to that in the tropics, CFRs are located at higher pressure altitudes in tropics. Overall, the layer with a high coverage of CFRs are thinner in tropics, and the ratio of the meridional mean of CFRs' coverage are higher than that of the NH mid-latitude. In tropics, the maximal ratios are found to be higher than 0.2 which means more than 20% of the regions above tropics at the pressure altitude around 100hPa are covered with CFRs and it is more than double of the maximal ratio discovered in the NH mid-latitude.

In tropics, the regions with high CFRs' ratio are very similar for all four seasons due to their similar weather patterns. As in the tropics, instead of four seasons, the weather pattern can be classified into a dry and wet seasons with a general hot weather throughout the year. For all four different seasons, the maximal ratio are mostly appeared in the regions from 75°E to 210°E which is above the tropical eastern Indian Ocean and tropical western Pacific Ocean. The biggest deviation appears in the regions between 210°E and 270°E which is above the Tropical Eastern Pacific Ocean. Above the Tropical Eastern Pacific Ocean, much less CFRs are discovered in spring and winter compares to summer and autumn. Other than that, some seasonal variations can also be spotted in the regions between 0°E to 45°E which is above the Tropical Africa and in the regions within 270°E and 330°E which is above the tropical South America, in both regions, less contrail coverage are detected in summer and winter and more contrail coverage are discovered in spring and autumn.

Since the presence of the CFRs mostly depend on the ambient atmospheric condition, the seasonal variations spotted within tropics can be related to the seasonal variation of the Hadley cell (Dima and Wallace 2003). Furthermore, a study by Peixoto et al. (1996) focused on "the climatology of relative humidity in the atmosphere" where they studied the seasonal variation of the relative humidity over land and ocean separately. At the same latitude, more seasonal variations are discovered over land than over the ocean. Generally, the relative humidity is higher in winter than in summer and the difference is more pronounced above the land. This can be a possible explanation for the less seasonal variation of CFRs' coverage discovered above the ocean and most of the seasonal deviations are discovered above the continent within tropics.

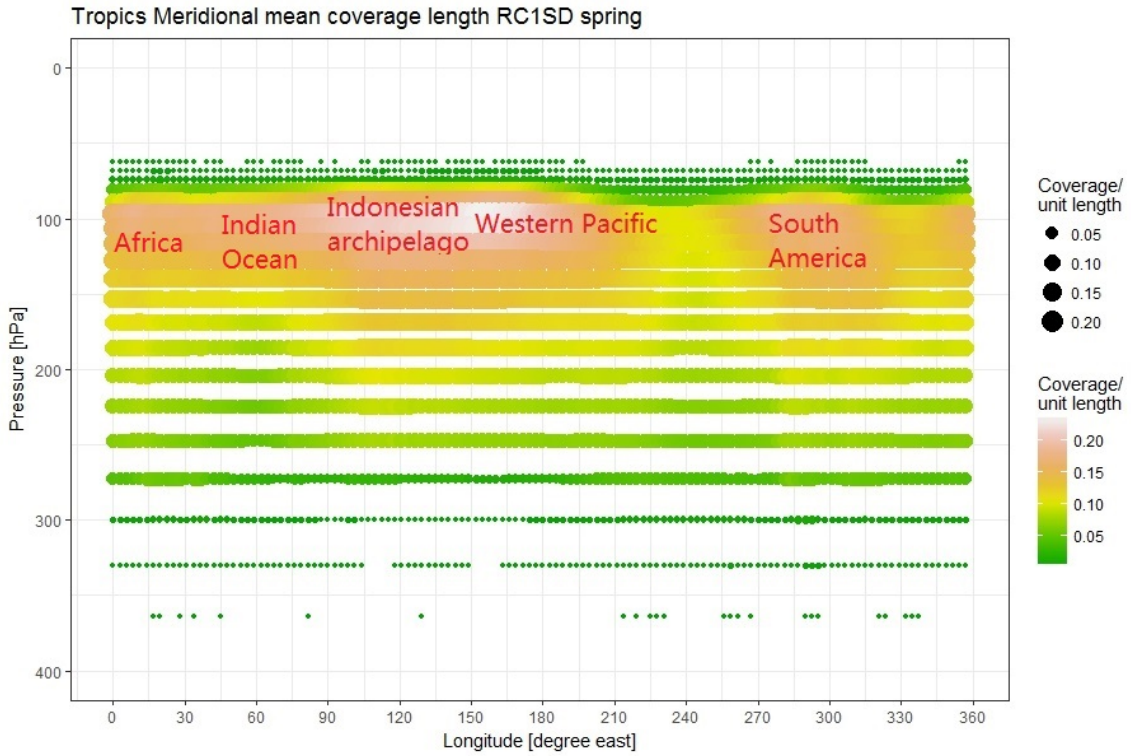


Figure 6.5: Meridional Mean of CFRs' Coverage in Spring Tropics

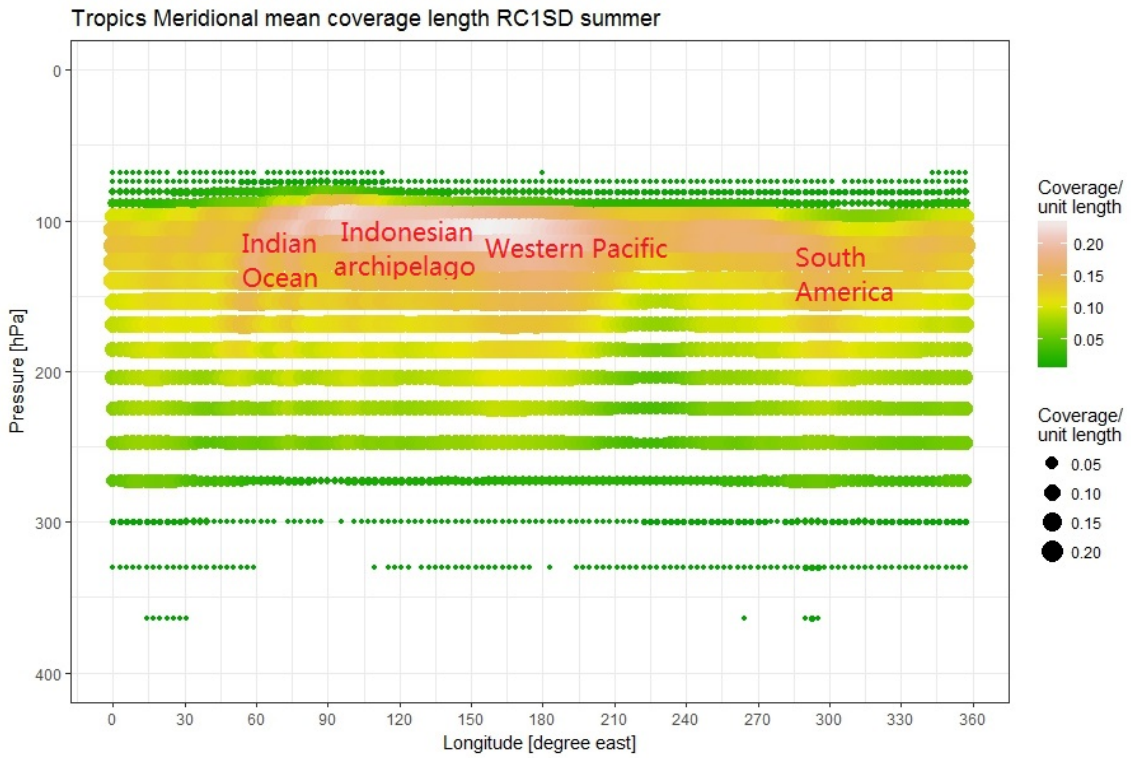


Figure 6.6: Meridional Mean of CFRs' Coverage in Summer Tropics

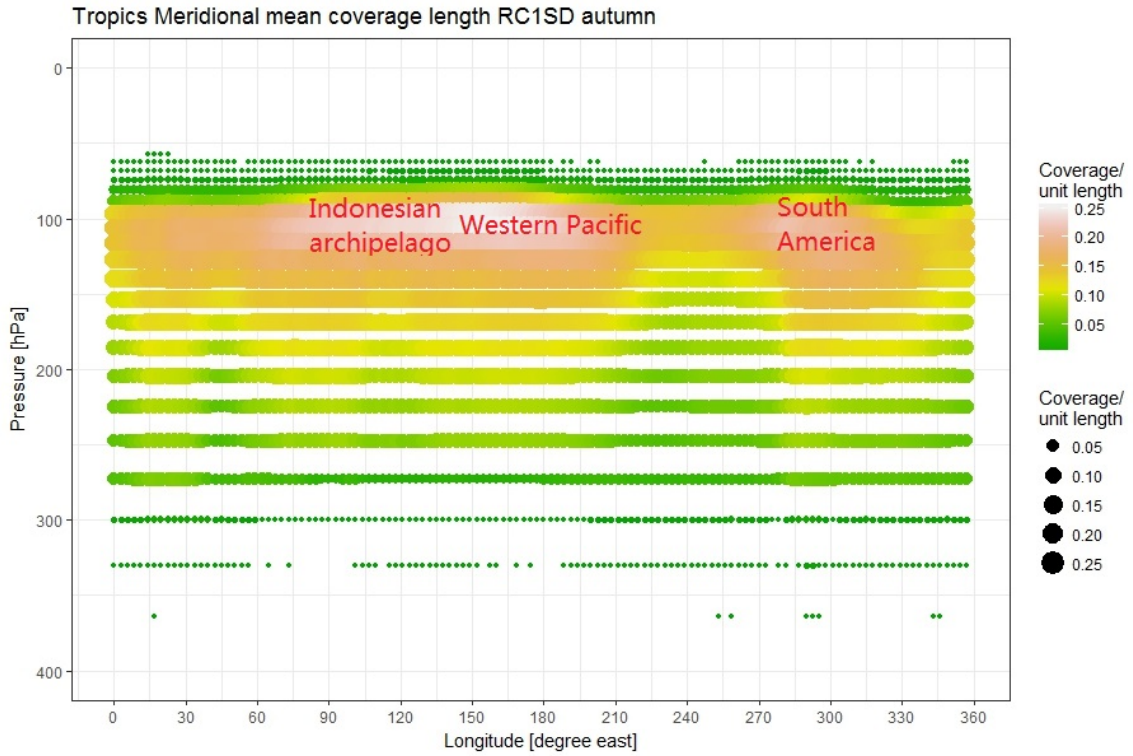


Figure 6.7: Meridional Mean of CFRs' Coverage in Autumn Tropics

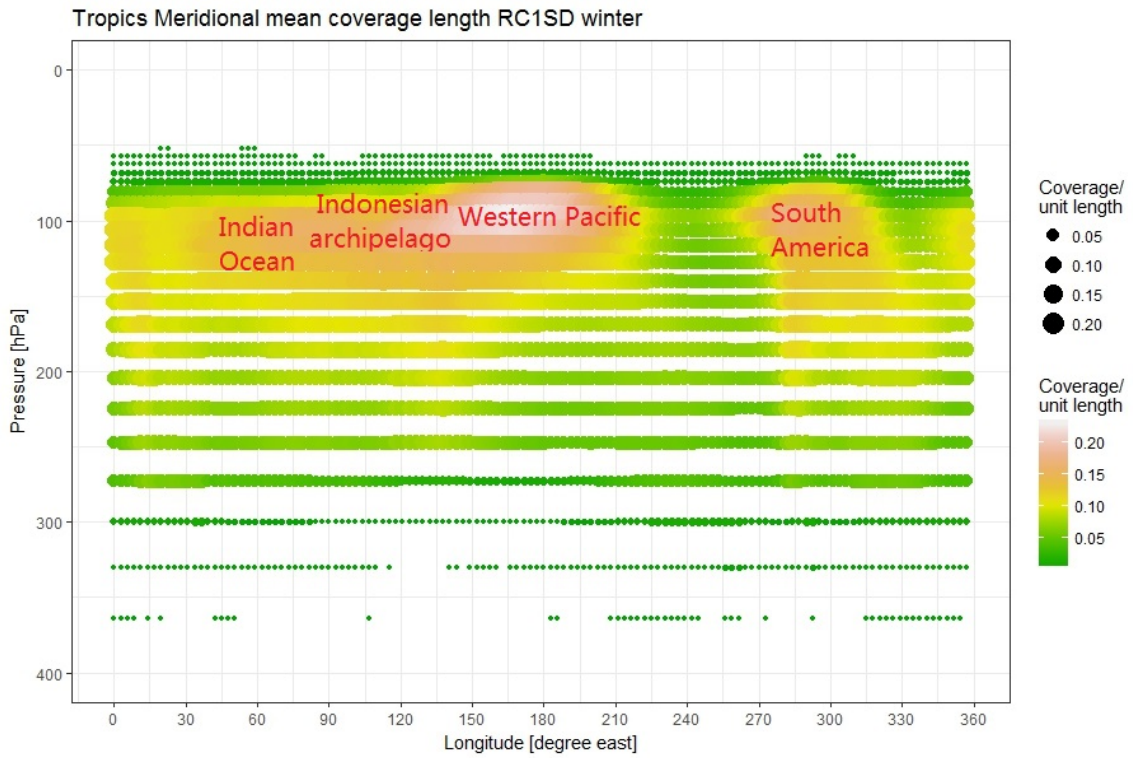


Figure 6.8: Meridional Mean of CFRs' Coverage in Winter Tropics

## 6.2. Conditional Mean of Meridional CFRs' Coverage Length

The RC1SD-base-10 simulation results of the conditional mean of meridional CFRs' coverage length are presented in this section. Unlike the dimensionless quantity: meridional mean of CFRs' coverage, the conditional mean of meridional CFRs has a unit of km. A more detailed definition of the conditional mean of meridional CFRs' coverage length can be found in Section 4.3.3.

The purposes of analyzing both the meridional mean of CFRs' coverage and conditional mean of meridional CFRs' coverage length are that the meridional mean CFRs' coverage represents overall how likely is it for certain longitude to have a certain portion of length covered by CFRs. The conditional mean of meridional CFRs' Coverage Length indicates how big of the regions along that longitude is likely to be covered by CFRs if certain longitude is actually detected to be covered by CFRs. There are three possible cases for the different combination of the two meridional mean values. The first combination is when the two meridional mean values are both high. Together, they indicate a high chance for that longitude to be discovered largely covered with CFRs. The second one is when both of the Meridional mean values are small, then they indicate that there is a small chance for CFRs to be discovered at this longitude and when CFRs are actually discovered, the CFRs' coverage length are small. The last possible case is for a certain longitude, the meridional mean CFRs' coverage is comparably small while the conditional mean of meridional CFRs' coverage length are very high. This case, it means that it is not very likely for CFRs to be discovered at this longitude, however, if CFRs are actually detected then there is a big chance that the CFRs' coverage length are large.

### 6.2.1. NH Mid-latitude Regions

First, the simulation results for the NH mid-latitude regions in spring, summer, autumn and winter are presented in Figure 6.9, 6.10, 6.11 and 6.12. Overall, the conditional mean of meridional CFRs' coverage length of the four seasons follow similar trends as the meridional mean of CFRs' coverage presented in Figure 6.1, 6.2, 6.3 and 6.4. Furthermore, the maximal conditional mean of Meridional CFRs coverage length discovered are above 700km for spring and winter, and the maximum discovered in summer and autumn are slightly shorter than that in spring and winter. In spring, summer and autumn, the conditional mean of meridional CFRs' coverage length are generally large covering Europe, China, Eastern Pacific Ocean, America and Atlantic Ocean. For winter, less regions are simulated to have a large conditional mean of meridional CFRs' coverage length. Most of the deviations discovered are located in the pressure altitude between 200 hPa and 100 hPa where at these regions, the meridional mean of CFRs' coverage are simulated to be very low but the conditional mean of meridional CFRs' coverage length are quite large. This means in these region, it is not very often for CFRs to be discovered but if CFRs are actually discovered, they tend to cover a very large area. Therefore, it is still necessary to detect the CFRs at that altitude over the NH mid-latitude, and if CFRs are discovered, it is recommended to change the flight route in a way to avoid the further formation of contrails.

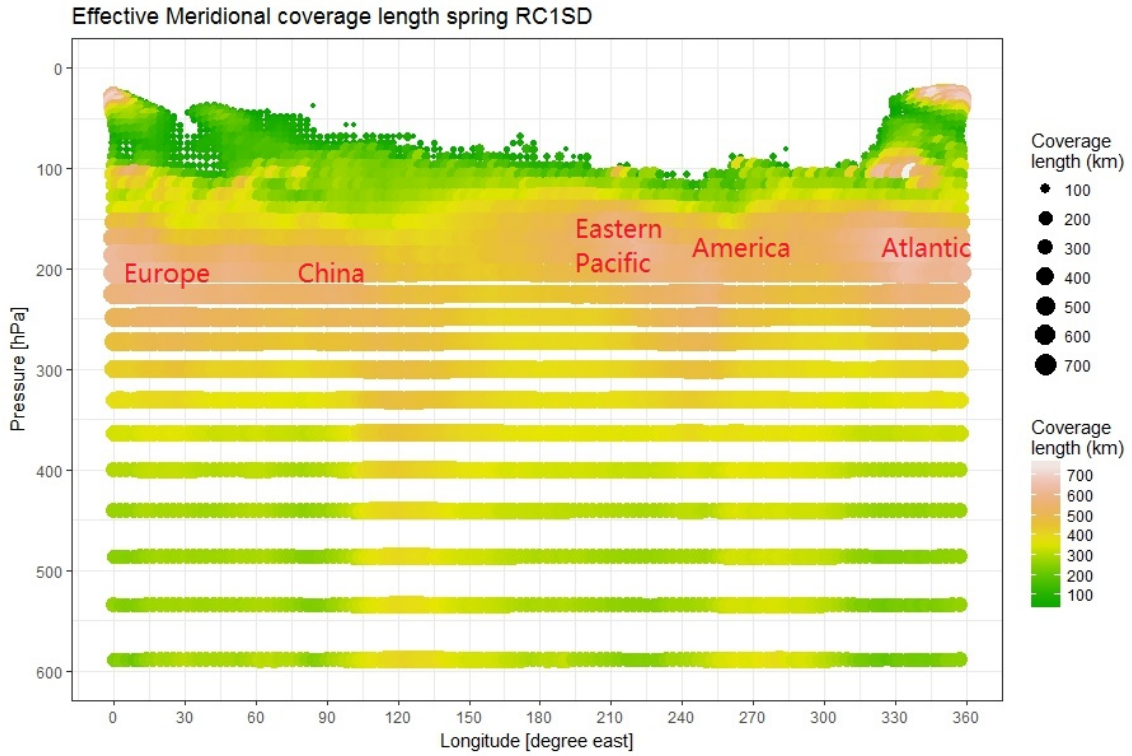


Figure 6.9: Conditional Mean of Meridional CFRs' Coverage Length in Spring

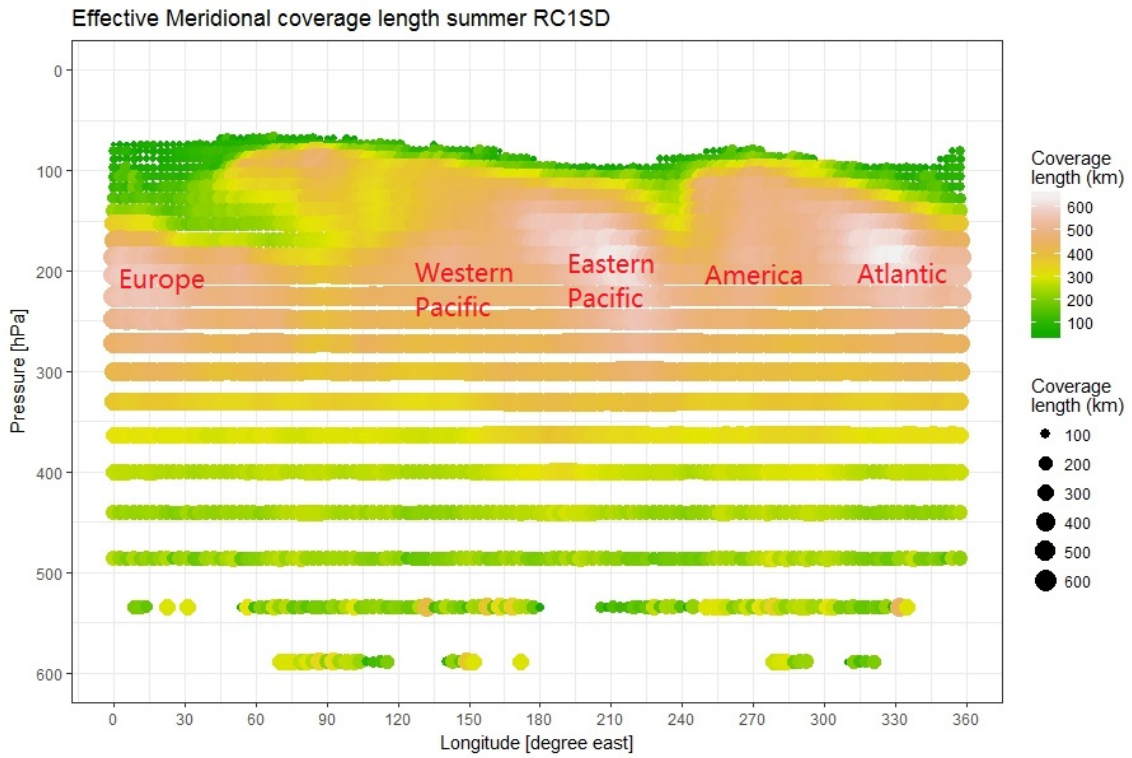


Figure 6.10: Conditional Mean of Meridional CFRs' Coverage Length in Summer

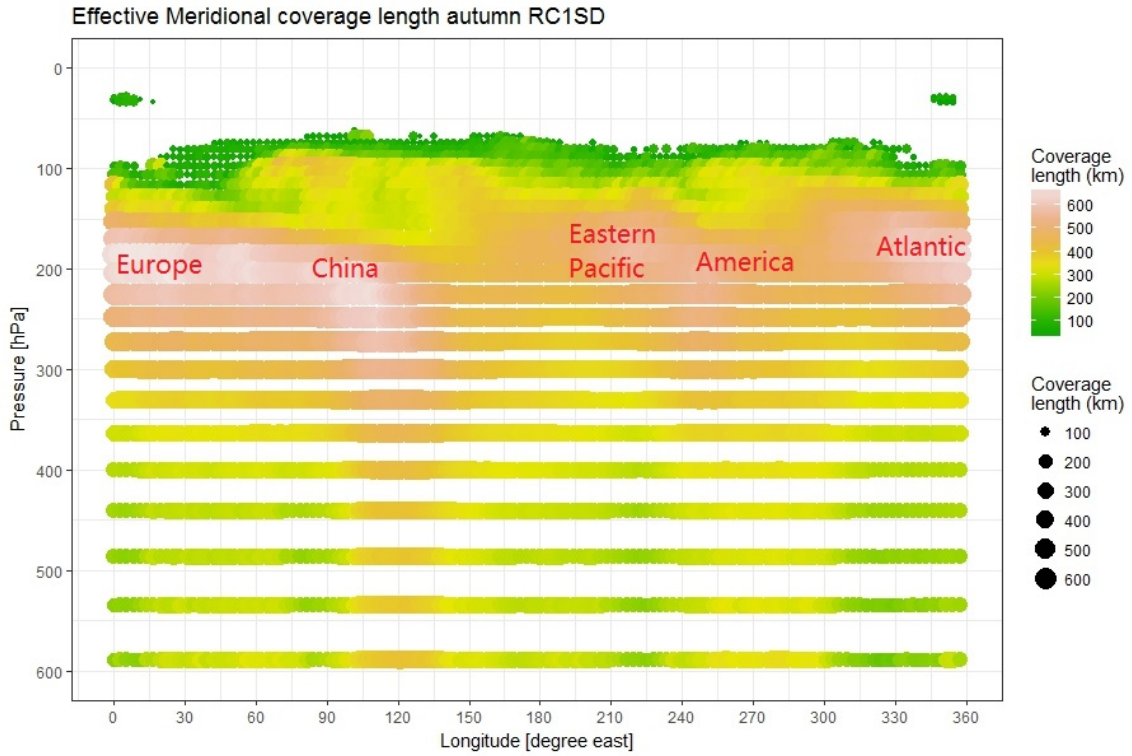


Figure 6.11: Conditional Mean of Meridional CFRs' Coverage Length in Autumn

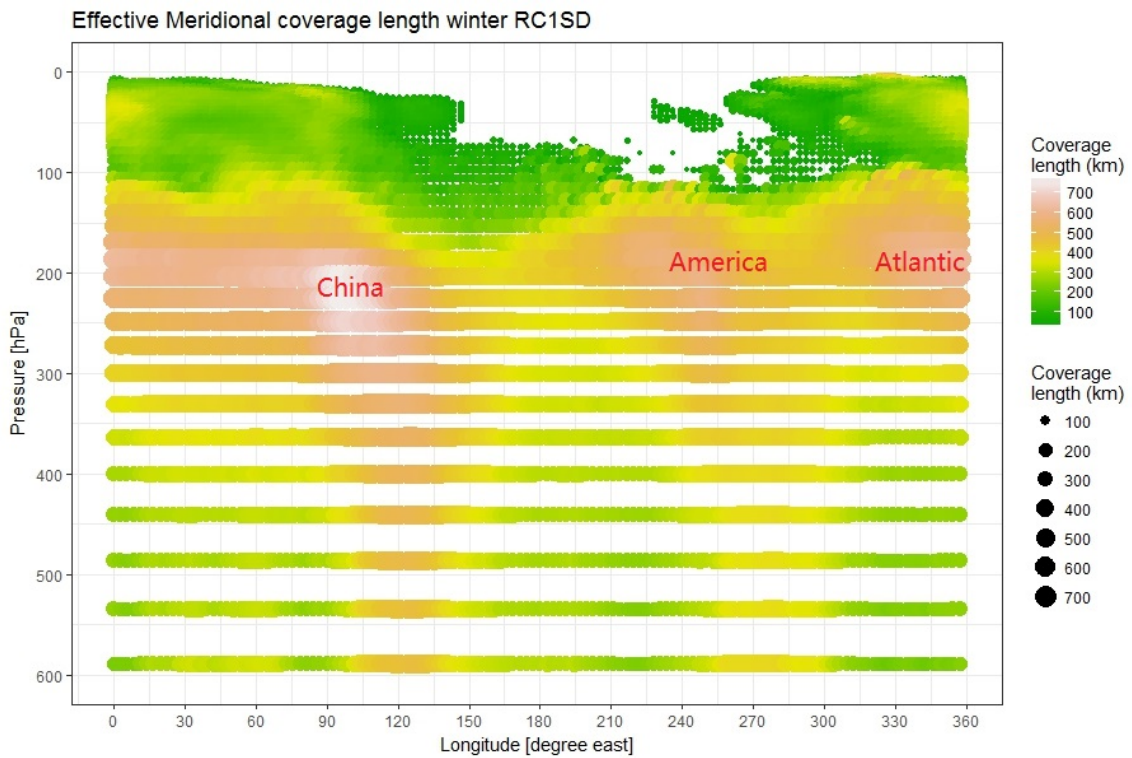


Figure 6.12: Conditional Mean of Meridional CFRs' Coverage Length in Winter

## 6.2.2. Tropics

Figure 6.13 presents the conditional mean of meridional CFRs' coverage length in spring in tropics. The maximal coverage length within tropics is around 2400km and is discovered above the Western Pacific Ocean. Same as the meridional mean of CFRs' coverage, CFRs are mostly discovered between the pressure altitude 300 hPa and 50 hPa, but regions with a maximal coverage of CFRs are limited at a rather thin layer around the 100 hPa pressure altitude. With the increase of pressure altitude, it is closer to the earth surface and the conditional mean of meridional CFRs' coverage length also decrease. A combination of both high meridional mean of CFRs' coverage and high conditional mean of meridional CFRs' coverage length indicates a higher chance for large CFRs to appear very frequently at the thin layer around 100 hPa. And at the layer between 200 hPa to 140 hPa where the meridional mean CFRs coverage length is large while the effective meridional coverage length is relatively small indicates in these regions, CFRs appears very frequent there but their average size are comparably small than those appear at a higher pressure altitude. For commercial airline, the cruising altitude are mostly between FL340 and FL420 which correspond to pressure altitude is around 250 hPa and 165 hPa. Thus, in the tropics, it is less likely for flight to fly through the CFRs within 250 hPa (FL340) to 200 hPa (FL380) pressure altitude compares to the pressure altitude between 200 hPa (FL380) and 165 hPa (FL420).

Very similar pattern of the conditional mean of meridional CFRs' coverage length is also obtained for the other three seasons and the figure for summer, autumn and winter can be found in Appendix, Figure A.3, A.4 and A.5.

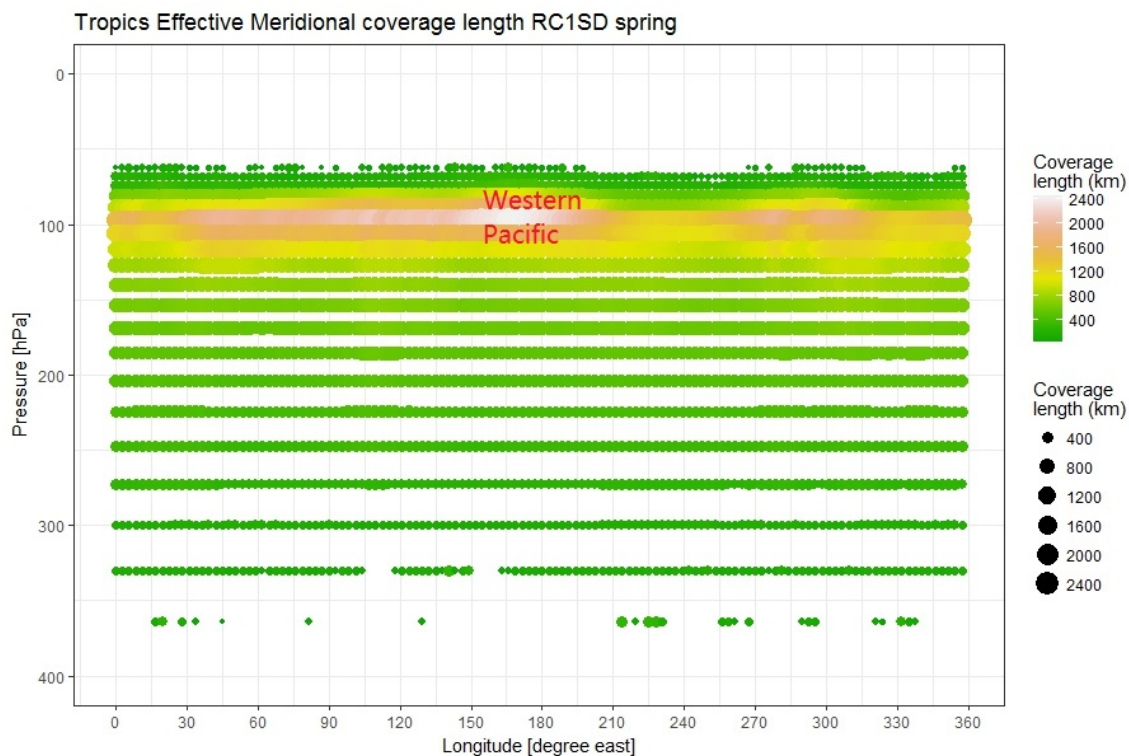


Figure 6.13: Effective Meridional Coverage Length in Spring

## 6.3. Zonal Mean of CFRs' Coverage

This section presents the analysis of the zonal mean of CFRs' coverage. The zonal mean of CFRs' coverage is a dimensionless quantity, it represents the ratio of the latitudinal circle that are covered

by CFRs at that latitude and pressure altitude. As the Earth is a sphere, the circumference of each latitudinal circle is different depends on its geographical location. Therefore, by comparing the ratio of the latitudinal circle that are covered by CFRs, it is more straightforward to see which regions are covered with more CFRs. A more detailed definition is given in Section 4.3.1.

As mentioned by Spichtinger et al. (2004) that the ice-supersaturation layers "appear mostly in a broad region below the tropopause, sometimes their tops reach into the stratosphere", therefore, an overview of the tropopause pressure altitude is presented first to help better understanding the distribution of the CFRs and their seasonal variations. Figure 6.14 presents the zonally averaged pressure altitude of the tropopause and its seasonal variation. Generally, the location of the tropopause can be separated into two regions. In the tropics, tropopause mainly are at pressure altitude around 130 hPa, and in the mid-latitude regions and in the polar regions, mainly the tropopause is at the pressure around 290 hPa. Overall, for different seasons, the location of the tropopause are following very similar pattern with slight seasonal variations within different regions. In summer, the tropopause above the NH mid-latitude regions are higher than the tropopause in winter. In tropics, the tropopause is slightly higher in winter compared to summer (Hoinka 1998).

The simulation results from RC1SD-base-10 are presented in Figure 6.15, 6.16, 6.17 and 6.18. Overall, the zonal mean coverage length for spring, autumn and winter have very similar pattern, with a high coverage of CFRs in the tropical regions at the pressure altitude between 200hPa and 100hPa. Within mid-latitude regions, the zonal mean of CFRs' coverage is high at the pressure altitude between 400 hPa and 200 hPa. Generally, the maximum of the zonal mean of CFRs' coverage appears around the location of the tropopause which also fits the theory mentioned earlier that CFRs appear the most around the tropopause. In summer, the regions with large contrail coverage are overall at a higher pressure altitude compare to the rest three seasons. This is mainly due to the higher temperature in summer. Therefore, in order to allow contrail persist, the pressure altitude need to be higher to meet the temperature threshold. At the southern hemisphere within the antarctic circle, the zonal mean of CFRs' coverage are high above this region even in the very top of the atmosphere, this is mainly due to the temperature and humidity in the polar regions increase in summer,<sup>1</sup> As the seasonal variation of the temperature in the antarctic circle appears the most in the Stratosphere than that in the troposphere (Wexler 1959)

### 6.3.1. Discussions

Overall, the regions that have a larger density of CFRs are located around and underneath the tropopause, where in the topics, they are mostly at a higher pressure altitude at around 100 hPa. In the mid-latitude regions, CFRs appears at a wider layer from around 400 hPa to 200 hPa. The CFRs in the tropics are more concentrated and have a higher CFRs coverage per unit length compared to that in the mid-latitude regions. The maximum ratio of the CFRs' coverage is discovered in the tropics region with more than 40% of the regions are calculated to be covered with CFRs.

Generally, for the four different seasons, the CFRs distribution are mostly located within similar regions. In the NH mid-latitude regions, most of the deviations can be found between summer and winter due to their largely different temperature. In the tropics, CFRs are more concentrated within the layer from 180hPa to 90hPa, and seasonal variation of the tropical CFRs' distribution are not very pronounced except for the regions above the tropical east pacific ocean and the continents.

According to the analysis of both meridional mean of CFRs' coverage and the conditional mean of meridional CFRs' coverage length, it can be tell that in the tropics, the regions where large CFRs appears a lot are mostly at a comparably thin layer between 110 hPa and 90 hPa which is not within

<sup>1</sup>[https://nsidc.org/cryosphere/arctic-meteorology/factors\\_affecting\\_climate\\_weather.html](https://nsidc.org/cryosphere/arctic-meteorology/factors_affecting_climate_weather.html) (accessed on June 15, 2017)

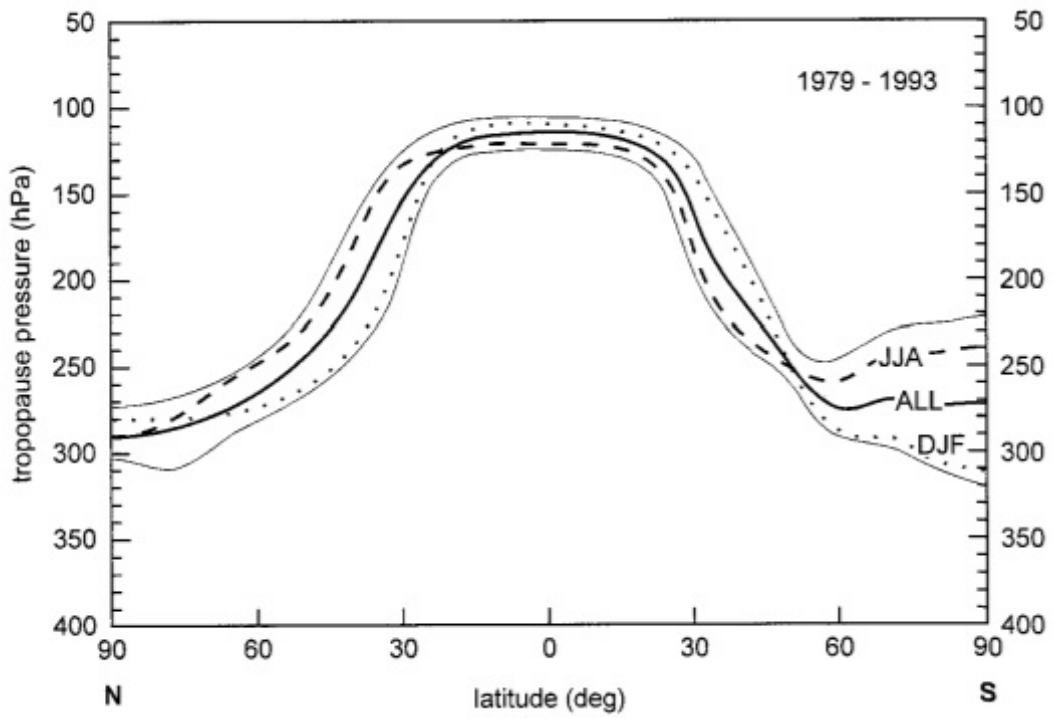


Figure 6.14: Seasonal variation of the meridional profile of the zonally averaged TRG tropopause (1979-93; 1200 UTC): annual mean (full line), DJF (dotted), and JJA (broken). The outermost lines represent the envelope lines for all monthly mean values (Figure obtained from (Hoinka 1998))

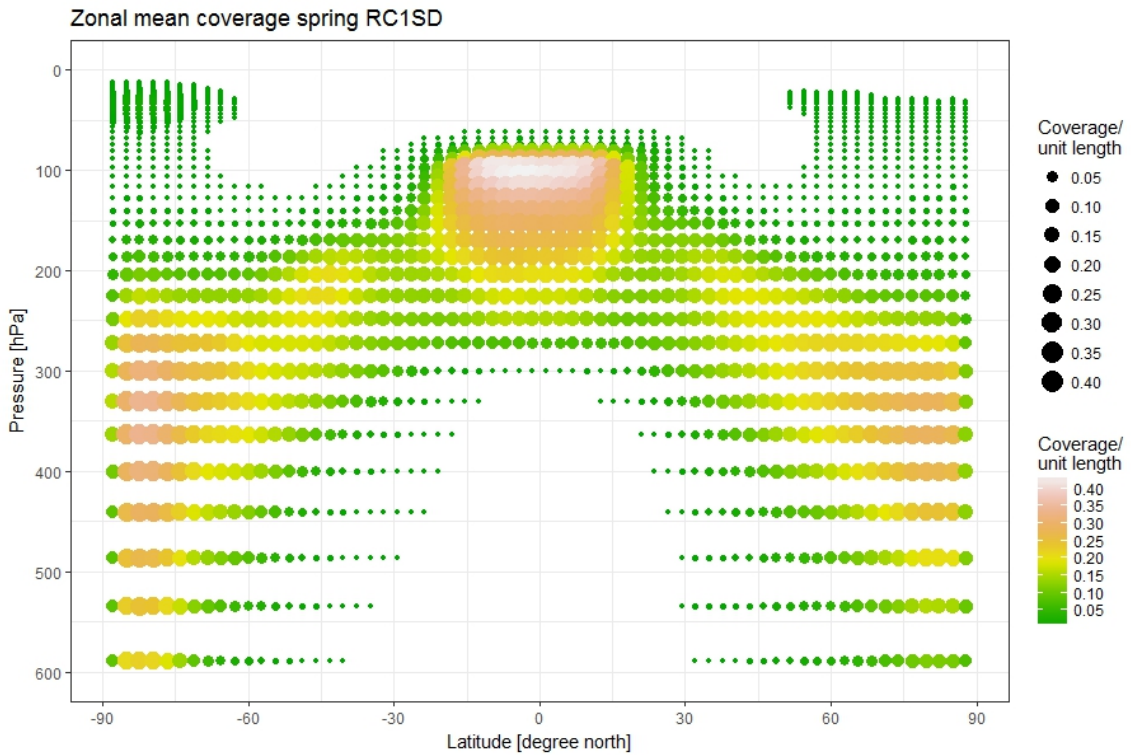


Figure 6.15: Zonal Mean Coverage Length in Spring

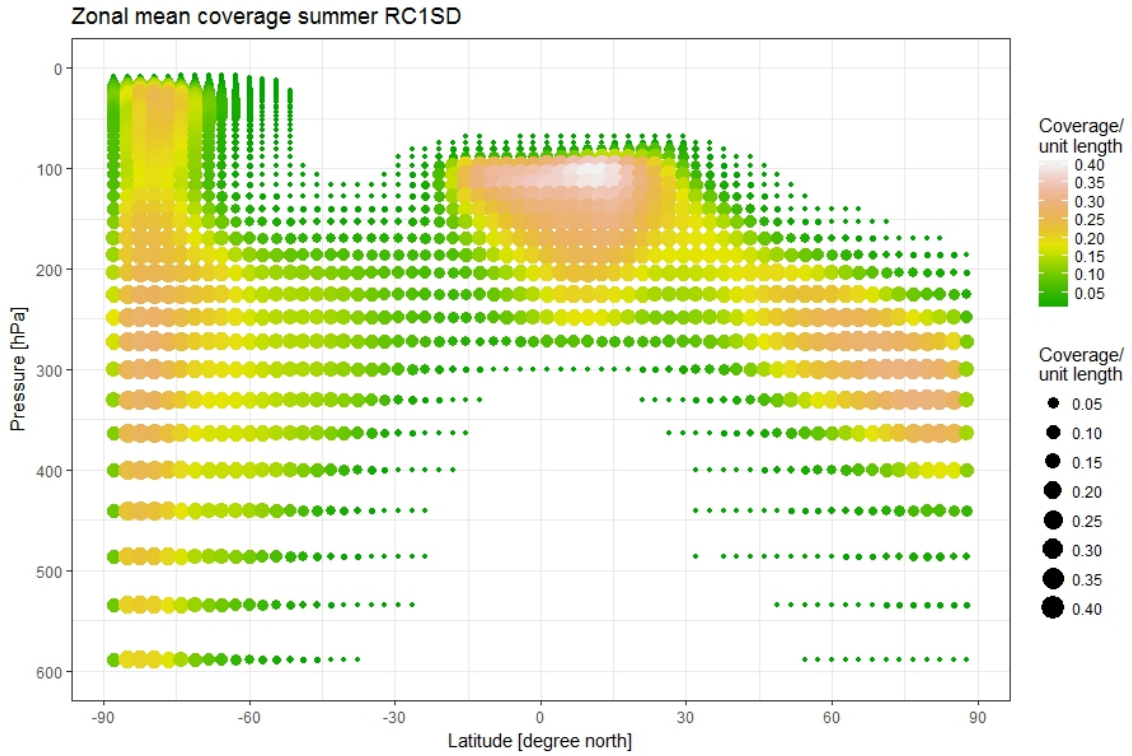


Figure 6.16: Zonal Mean Coverage Length in Summer

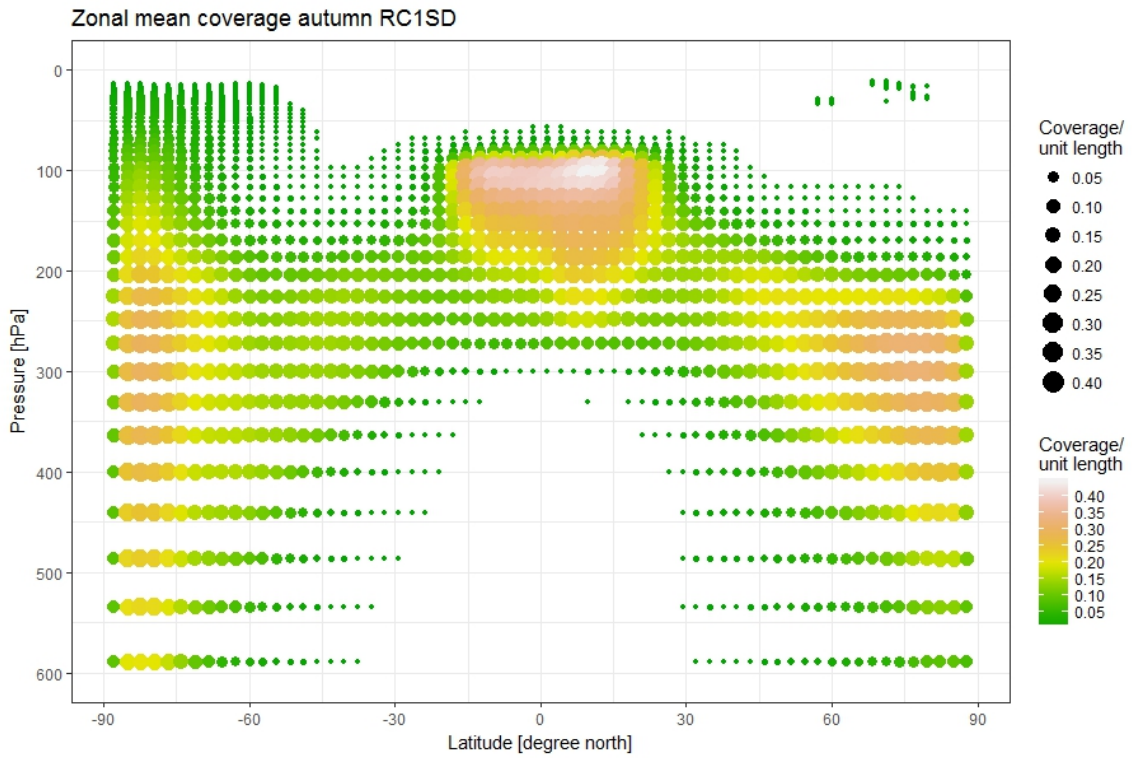


Figure 6.17: Zonal mean coverage length in autumn

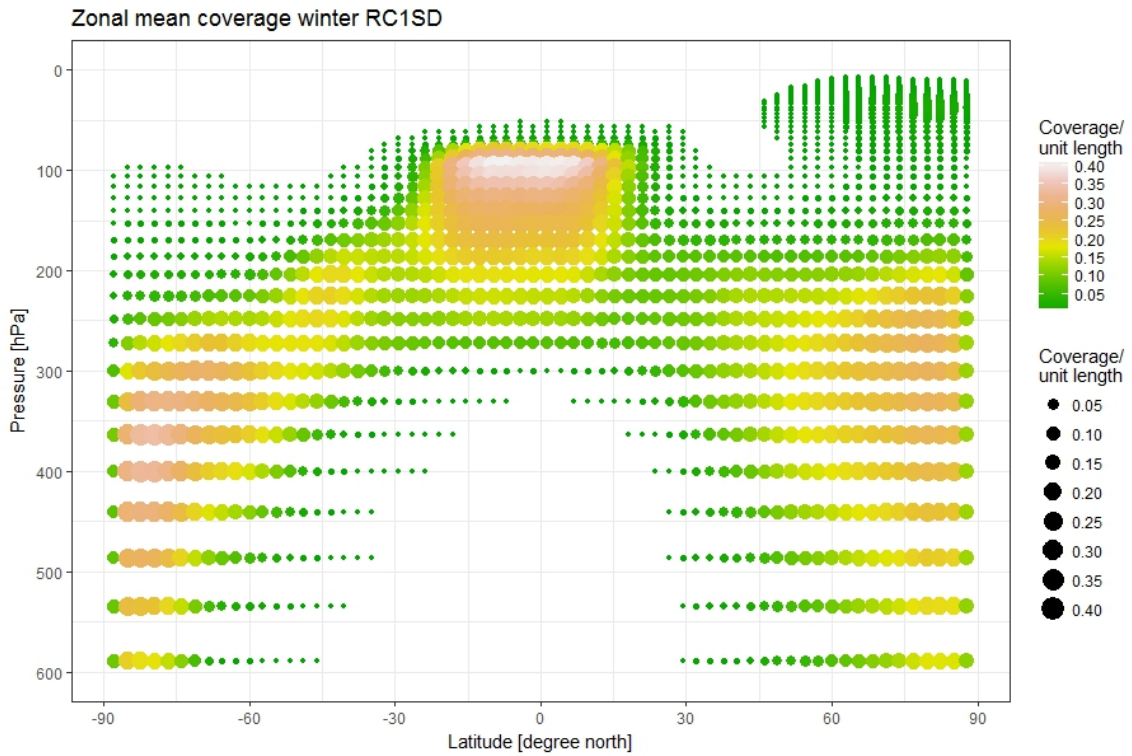


Figure 6.18: Zonal Mean Coverage Length in Winter

the range of the common Flight Level (FL). At the common cruising altitude, less CFRs are discovered within the range from 250 hPa (FL340) to 200 hPa (FL380) compare to a higher level. Overall, both the meridional mean of CFRs' coverage and the conditional mean of meridional CFRs' coverage length in the NH mid-latitude regions are smaller than half of those in the tropics regions, but with a more dispersed distribution between 400 hPa and 100 hPa. Therefore, it is unrealistic to fully planned the flight route totally avoid this rather thick layer, so a further analysis of the CFRs direction is required to help better understanding the CFRs' characterizations.



# 7

## Characterisation of CFR: Stretch Factor and Direction

As contrails contribute about 30% to the aviation induced RE, it is crucial to avoid aircraft from flying through the CFRs. The distribution of CFRs largely depends on the local atmospheric conditions and weather conditions. Other than roughly predict the distribution of the CFRs beforehand, it is also helpful to analyze the typical direction of CFRs within different regions. When an aircraft detected itself is flying through a CFR, it can slightly shift its flight route correspondingly to avoid further flying in that CFR, hence fewer contrails are formed. In this Chapter, presents an analysis of the typical stretch factor and direction of CFRs in different regions within both horizontal and vertical planes.

For this part of study, when simulating the CFRs to analyze both their stretch factors and directions, the PT is set to 90% for the reasons mentioned in Section 4.7.2. The PT is set to a rather high value so that only when more than 90% of the grids area are simulated to be CFRs then the whole grid is considered as a CFR grid. Therefore, if several connect grids are simulated to be connected, then the CFRs at these regions are probably also connected in real life. Hence, the stretch factors and directions calculated for the CFRs are closer to the reality.

### 7.1. Stretch factor of CFRs

First, the stretch factor for each of the numbered CFR is calculated. Basically, when the shape of a CFR is more stretched, then the stretch factor is larger. The detailed definition of stretch factor of CFRs is presented in Section 4.3.5. After that, the calculated stretch factors of CFRs are statistically analyzed by kernel density estimation in both the horizontal plane and vertical plane.

#### 7.1.1. Stretch Factor of CFRs in Horizontal Plane

The CFRs are simulated in both horizontal plane and vertical plane. First, the analysis of the CFRs in the horizontal plane is presented in this section. The horizontal plane is defined as the planes that are parallel to the Earth surface and each horizontal plane is represented by its geographic position, its pressure altitude. Furthermore, the grids that simulated to be CFRs are only considered to be connected as one region if these grids are within the same horizontal plane. In the horizontal plane, each grid in EMAC is a square with a dimension of  $300\text{km} \times 300\text{km}$ , therefore, the stretch factor of each grid is 1. In the following sections, CFRs located in the NH mid-latitude regions and tropical regions are analyzed separately.

## NH Mid-latitude Regions

In Figure 7.1 presents the Probability Density Function (PDF) of the CFRs' stretch factor in spring within NH mid-latitude regions. The first peak is at stretch factor between 1 and 1.1 and the second peak is at stretch factor around 1.4. Compared these stretch factors with the one presented in Table 4.1, the CFRs with stretch factor within 1.1 are in the shape of a rectangle with the length about twice its width and the CFRs with stretch factors around 1.4 are having a similar stretch factor as the rectangle with the length six times its width. In general, in the horizontal plane in the NH mid-latitude regions, the majority of the CFRs are not very stretched, and most of the stretched CFRs have a length around six times its width.

Similar PDF of the stretch factor of CFRs in the horizontal plane in NH mid-latitude regions can also be found in the three other seasons, summer autumn and winter, and their plot can be found in Appendix, Figure B.1, B.2 and B.3.

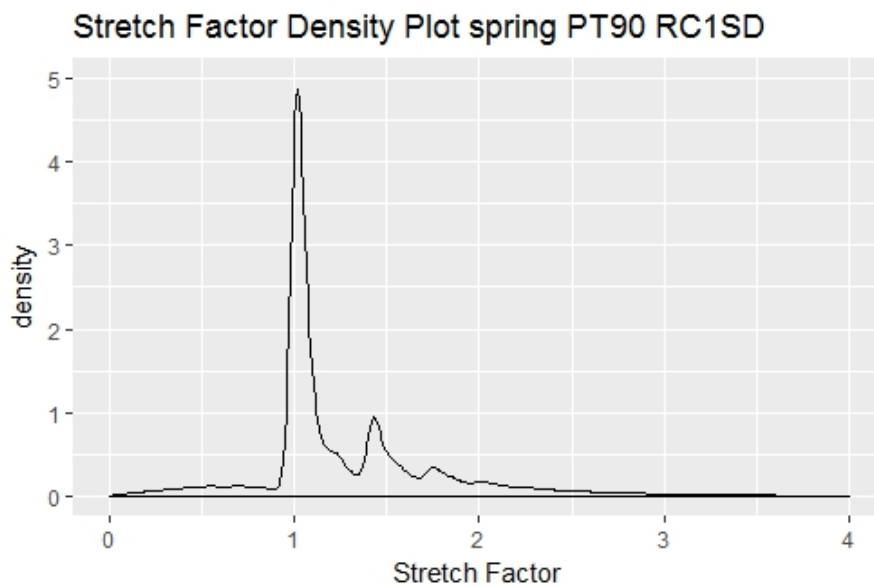


Figure 7.1: PDF of CFRs' Stretch factor in horizontal plane NH mid-latitude spring

## Tropics

In Figure 7.2 presents the PDF of the stretch factor of CFRs in spring within tropics. The stretch factors for both of the peaks are a little bit smaller than those discovered in the NH mid-latitude regions, for tropical CFRs, the first peak appeared at the stretch factor very close to 1 and the second peak is at around 1.4, furthermore, in the Kernel Density Estimation (KDE), both the density and the covered area are larger than that in the case for NH mid-latitude. So, compared to the CFRs in the NH mid-latitude regions, in the tropics, more CFRs are less stretched or even not stretched at all and for the CFRs that are stretched, their lengths are six times of their widths.

Similar PDF of the stretch factor of CFRs in the horizontal plane in Tropics can also be found in the other three seasons, summer autumn and winter, and their plot can be found in Appendix, B.4, B.5 and B.6.

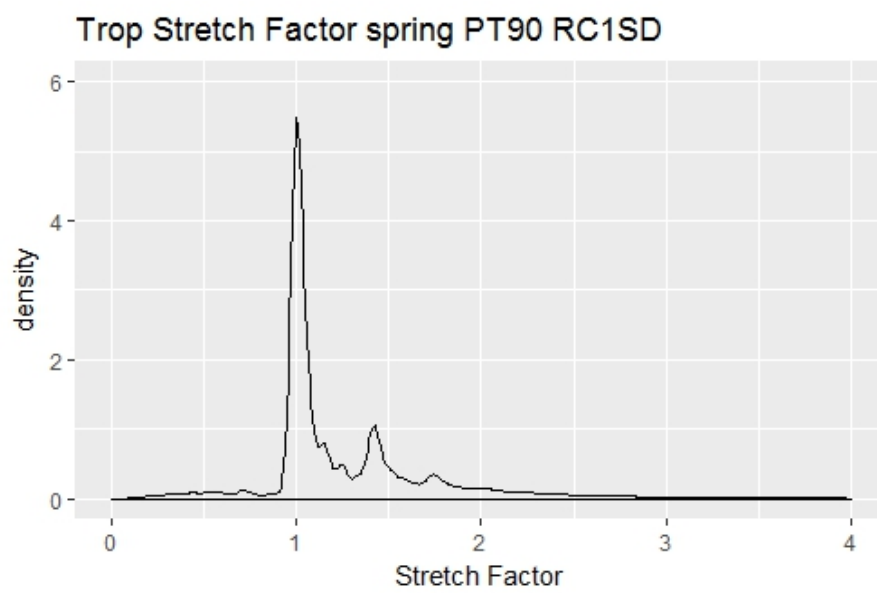


Figure 7.2: PDF of CFRs' Stretch factor in horizontal plane Tropics spring

### 7.1.2. Stretch Factor of CFRs in Vertical Plane

The vertical plane is defined as the plane that is perpendicular to the Earth surface, and each vertical plane is represented by its latitude. Different from the grid within the horizontal plane, in the vertical plane, the shape of each grid differed by its geometric position. The stretch factor of each grid actually depend on their altitude. The length of each grid is 300km, this is same for every grid, however the width of each grid varied a lot, due to the height of each vertical layer in the EMAC model are defined differently. Depends on the pressure altitude of the grid, its width can vary from 0.11km to 1.22km and compare to its 300km length, all these grids in the vertical plane are already very stretched. Their original grid stretch factor varied from 7.86 to 25.6 as shown in Figure 7.3. A detailed table of the grid stretch factor related to different pressure altitude at each model level can be found in Table B.1.

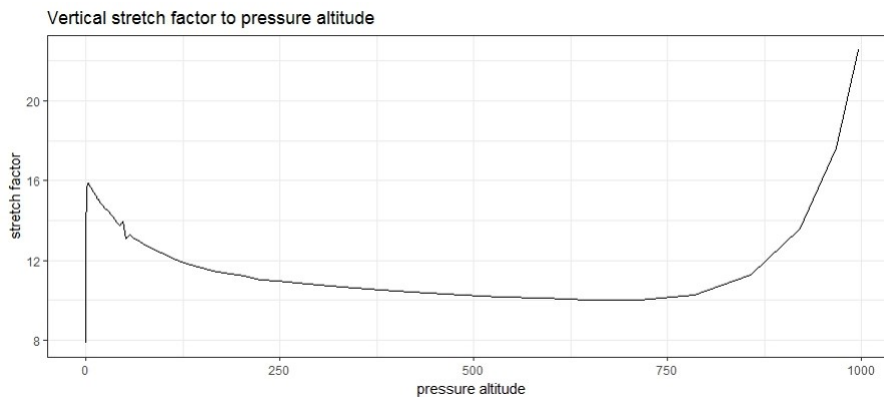


Figure 7.3: Vertical Stretch factor at Different Pressure altitude

Table 7.1 presents the stretch factor range of several sets of different combination of two, three and four grids that are connected vertically at different levels. Generally, more grids connected vertically will have a smaller stretch factor compared to the stretch factor of a very slender single grid at that level. Typically, due to the set up of the vertical level, the stretch factor of a single grid at pressure altitude above 16hPa are larger than 15 , and below pressure altitude 250hPa, the stretch factor are around 10. For the shape that have two grids stacked vertically, the stretch factor are between 7.2 and 11.2, and for three grids stacked vertically, the stretch factor are between 5.8 and 9.2, and for four grids stacked vertically, the stretch factor are between 5.3 and 7.9. Furthermore, for two grids that are connected within the same level, their stretch factor are between 14.4 and 22.4 which is about 1.4 times the stretch factor of a single grid at that level.

Table 7.1: Stretch factor range of grids combination at different altitude

Pressure altitude (hpa)	1 grid	2 grids horizontal	2 grids vertical	3 grids vertical	4 grids vertical
1~16	15~16	21~22.5	10.5~11	8.6~9.2	7.5~8
16~40	14~15	20~21	10~10.5	8~8.6	7~7.5
40~116	12~14	17~20	8.5~10	6.9~8	6~7
116~225	11~12	15.6~17	7.8~8.5	6.3~6.9	5.5~6
225~785	10~11	14~15.6	7.2~7.8	5.8~6.3	5~5.5

### NH Mid-latitude Regions

As the basic stretch factor of each grid in the vertical level is way larger than the basic stretch factor of all the grids in the horizontal plane. The peak of the CFRs' stretch factor in spring, appears at

around 10.6 as shown in Figure 7.4. Overall, most of the stretch factor of CFRs within the vertical plane in the NH mid-latitude regions range from 5 to 20. The largest peak is around 10, this stretch factor mostly are from the one grid CFRs located at pressure level around 440hPa to 300hPa. This stretch factor around 10 also fits with the stretch factor of two grids stacked vertically within 40 hPa to 16 hPa, however, this pressure altitude is already too high to be largely covered by CFRs according to the previous finding in Section 6.3. Other than that, there is a second peak around 7.5, this is possible for vertically stacked 2 grids CFR at pressure altitude below 225hPa or CFR consist of more grids connected vertically at a higher pressure altitude above 116hPa.

Similar PDF of the stretch factor of CFRs in the vertical plane in NH mid-latitude regions can also be found in the three other seasons, summer autumn and winter, and their plot can be found in Appendix, Figure B.7, B.8 and B.9.

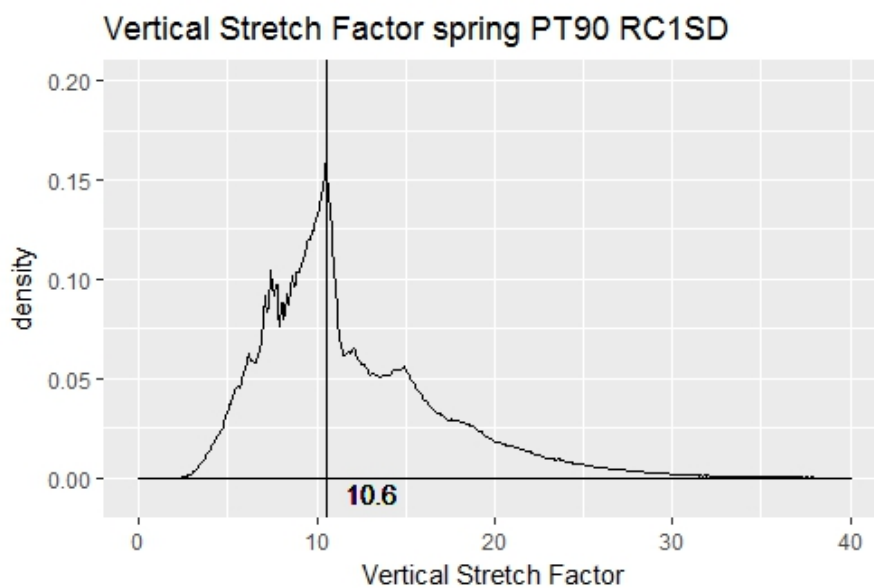


Figure 7.4: PDF of CFRs' Stretch factor in vertical plane NH mid-latitude spring

## Tropics

The PDF of the stretch factor of CFRs in the vertical plane in spring within tropics is presented in Figure 7.2. Same as the NH mid-latitude regions, the CFRs' stretch factor mostly range from 5 and 20. However, the statistical distribution has a distinct pattern. The two peaks are very significant at around 7.5 and 11, both of the peak values are slightly higher than that in the NH mid-latitude regions. The stretch factor around 11 mostly applies to the one grid CFRs at the pressure altitude around 250hPa to 125hPa. And the stretch factor around 7.5 are mostly likely related to the 2 grids stacked vertically CFRs within the same pressure altitude range. This also correspond with the previous discovered CFR distribution pattern presented in Section 6.3, that the pressure altitude of the CFRs located in the tropics are higher than CFRs located in the NH mid-latitude regions.

Similar PDF of the stretch factor of CFRs in the vertical plane in tropical regions can also be found in the three other seasons, summer autumn and winter, and their plot can be found in Appendix, Figure B.4, B.5 and B.6.

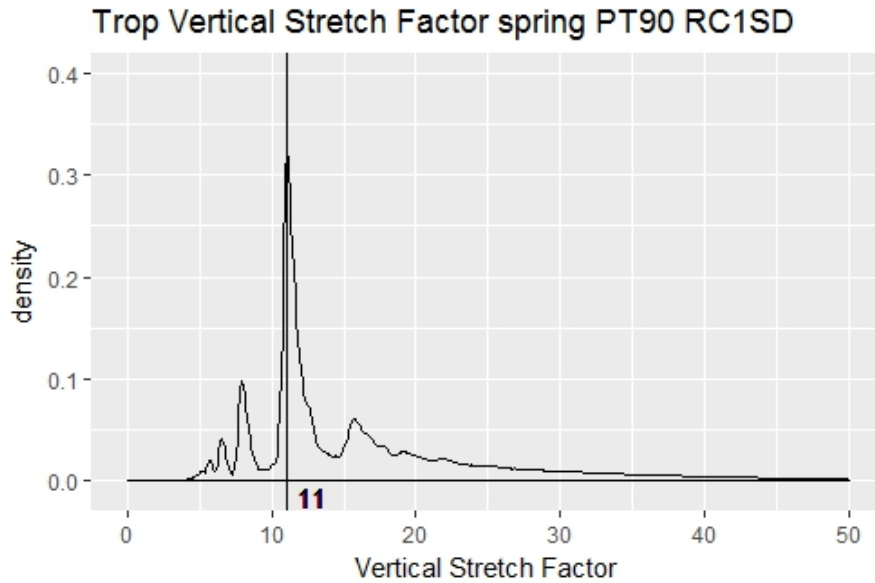


Figure 7.5: PDF of CFRs' Stretch factor in vertical plane Tropics spring

## 7.2. Direction of CFRs

Based on the previous calculated stretch factor of CFRs, the direction of each of these CFRs are also computed and investigated statistically in this section. Only CFRs with stretch factor larger than 1.1 are included in further calculating the direction of these CFRs, so the single grid CFRs in the horizontal plane are excluded. Due to the varied shapes of different CFRs, each CFR is simplified as a vector point from its most right grid to the most left grid of that CFR, and some examples of the CFRs' direction is given in Figure 7.6 including  $45^\circ$ ,  $63.5^\circ$ ,  $71.6^\circ$  and  $135^\circ$ . Furthermore, the specific CFR's direction is defined by the angle between the vector of the CFR and a reference vector, in the horizontal plane the direction of the reference vector was set to north and in the vertical plane, the reference vector was set to point directly upward.

In Figure 7.7 and 7.8 demonstrate the direction of the CFRs representing by the angles calculated in both horizontal plane and vertical plane. Basically in the horizontal plane, when the CFR's angle is calculated to be  $0^\circ$  and  $180^\circ$ , then the CFR is in the north-east direction align with the longitude. When the CFR's angle is  $90^\circ$ , then the CFR is in the east-west direction align with latitude. When the angle calculated is in between  $0^\circ$  to  $90^\circ$ , then the CFR direction is within the northwest sector, when the angle calculated is in between  $90^\circ$  to  $180^\circ$ , then the CFR direction is within the northeast sector. And in the vertical plane, the direction of the reference vector is pointing directly up. Therefore, when the angle calculated is either  $0^\circ$  or  $180^\circ$ , then the CFR is considered as a vertical CFR, if the angle calculated is  $90^\circ$ , then the CFR is considered as a horizontal CFR, other than these three angle, when the angle of CFR is calculated to be within  $0^\circ$  to  $90^\circ$  and  $90^\circ$  and  $180^\circ$ , than the CFR is considered to be a tilted one.

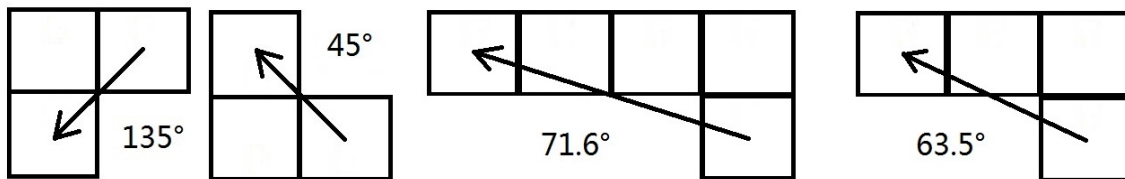


Figure 7.6: Example of the CFR direction definition

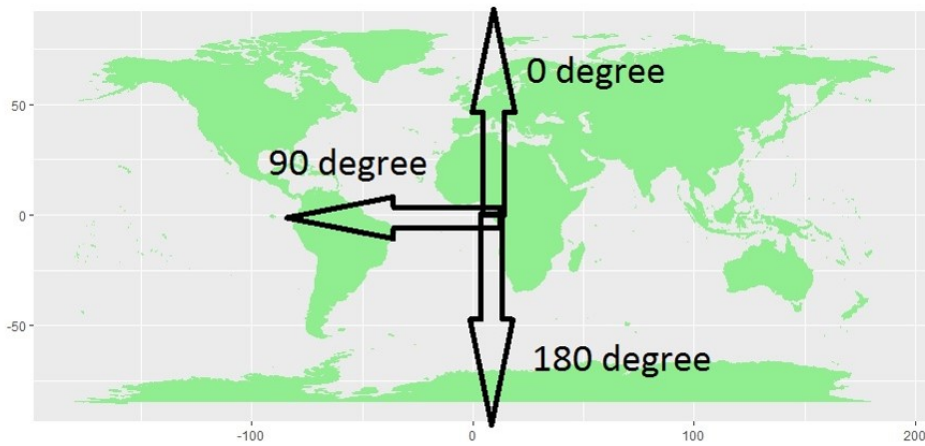


Figure 7.7: CFR direction in horizontal plane

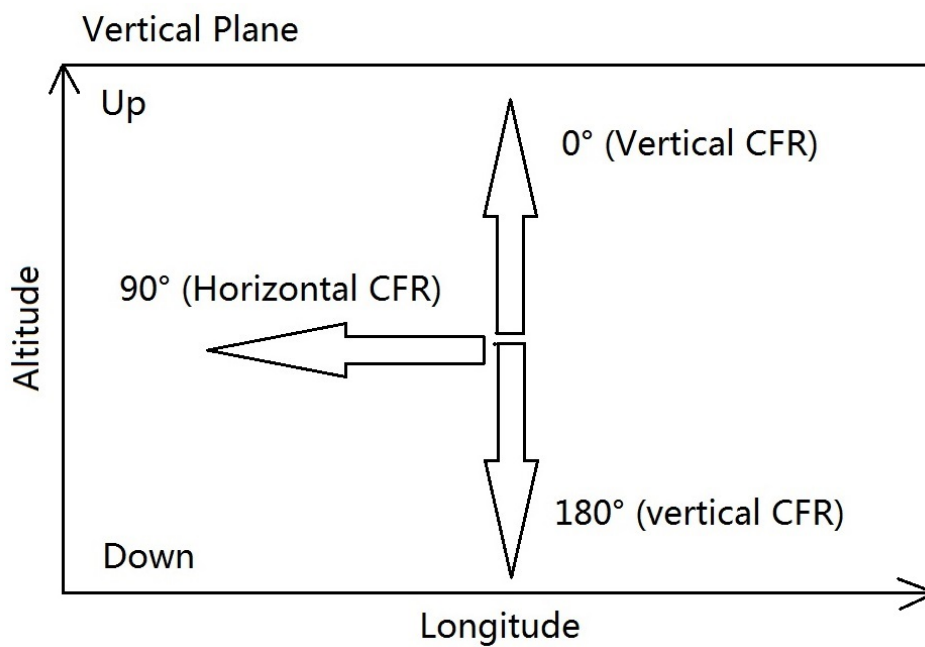


Figure 7.8: CFR direction in vertical plane

### 7.2.1. Direction of CFRs in the Horizontal Plane

In this section presents an overview of the statistical distribution of the CFRs' direction within the horizontal plane in both NH mid-latitude regions and tropics. Both boxplot and Kernel Density Estimation (KDE) are applied to analyze the pattern of CFRs' direction.

In order to have a better comprehension of the simulated CFRs' direction, the atmospheric circulation pattern is demonstrated first. As shown in Figure 7.9, within each hemisphere, there are three global scale atmospheric circulations, Hadley cell located in tropics, mid-latitude cell (Ferrel cell) in mid-latitude regions and polar cell within the polar regions. These atmospheric circulations dominate the general direction of the wind pattern within each of its covered regions. Since in this part of study, only the CFRs appear in the NH mid-latitude and tropics are analyzed, hence, mainly the patterns of the Hadley cell and NH mid-latitude cell are introduced. Within NH tropics, the atmospheric circulation are in a general northeast-southwest direction. In SH tropics the atmospheric circulation are in a general northwest-southeast direction. Generally, in tropics the air are moving poleward at high altitude dominated by the Hadley cell, in the NH mid-latitude, the atmospheric circulation are also in a general northeast-southwest direction, with the air moving equatorward at high altitude (Pauluis, Czaja, and Korty 2008).

To correspond the atmospheric circulation pattern with the definition of the CFRs' direction introduced in the previous section, in the NH tropics as well as the NH mid-latitude, the air are generally moving in a direction of  $135^\circ$ . In the SH tropics, the air are generally moving in a direction of  $45^\circ$ .

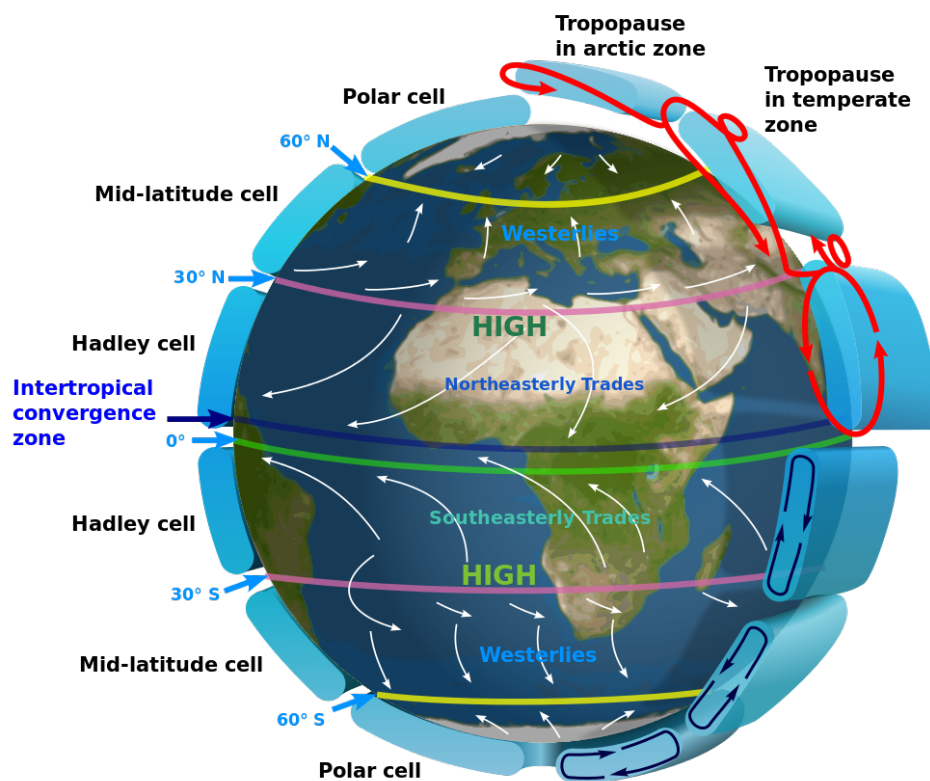


Figure 7.9: Atmospheric Circulation Pattern (Figure obtained on July 16, 2018 from: <https://commons.wikimedia.org/wiki/User:Kaidor>)

## NH Mid-latitude Regions

The kernel density plot of CFRs' direction within the horizontal plane in the NH mid-latitude regions for the spring and summer are presented in Figure 7.10, 7.11. For both seasons, despite the density are different for each peak for different seasons, the angle corresponding with each peak are basically the same. There are in total five significant peaks in each plot, the largest peak is at an angle equals to  $90^\circ$ , and the rest four are mirroring round the  $90^\circ$  peak, which are at  $45^\circ$ ,  $63.5^\circ$ ,  $116.5^\circ$  and  $135^\circ$ . Overall, more than 20% of the CFRs have an angle of  $90^\circ$  and are in the west-east direction, this is probably caused by the general movement of the air is in the west-east direction due to the Earth's rotation.<sup>1</sup> In general, more CFRs tend to be tilted, and the reason why tilted CFRs tend to have a direction of  $45^\circ$ ,  $63.5^\circ$ ,  $116.5^\circ$  and  $135^\circ$  is partly due to the definition of the CFR's direction, where these angles are easy to achieve for the basic grids combination of a line shaped CFRs.

In spring, the largest peak have a density slightly above 0.2 and the second large peak at  $45^\circ$  and  $135^\circ$  have a density around 0.15. The density of  $135^\circ$  is also slightly higher than the density of  $45^\circ$ , this is probably due to atmospheric circulation pattern as shown in Figure 7.9, in the NH mid-latitude regions, due to the westerlies, it is more likely for contrails to have a angle of  $135^\circ$ . Other than that, for summer, compared to the rest three seasons, less CFRs are tilted, this can be caused by weaker westerlies in summer.

The statistical distribution of CFR's direction in autumn and winter are very similar to that in spring and the Figure for autumn and winter can be found in Appendix, Figure B.13 and B.14. Figures B.15, B.16, B.17 and B.18 present the boxplot of the distribution of the CFRs' direction related to the latitude showing similar results.

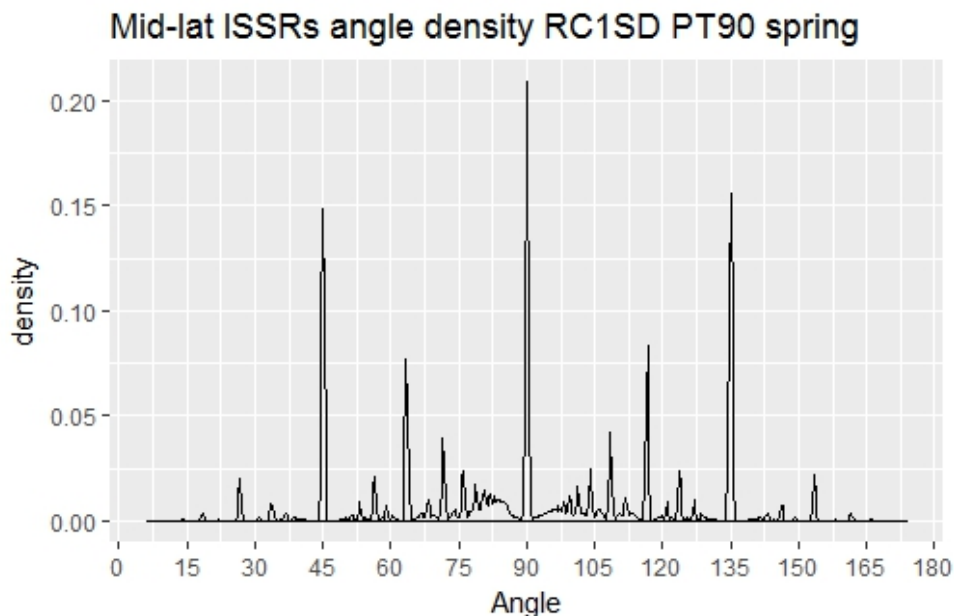


Figure 7.10: PDF of CFRs' Direction in horizontal plane NH mid-latitude spring

## Tropics

Figure 7.12 presents the kernel density plot of the CFRs' direction in the Tropics for the four different seasons. Similar to the CFRs in the NH mid-latitude regions, there are five directions that appeared

<sup>1</sup>[https://www.eoas.ubc.ca/courses/atsc113/sailing/met\\_concepts/09-met-winds/9a-global-wind-circulations/](https://www.eoas.ubc.ca/courses/atsc113/sailing/met_concepts/09-met-winds/9a-global-wind-circulations/) (accessed on July 17, 2018)

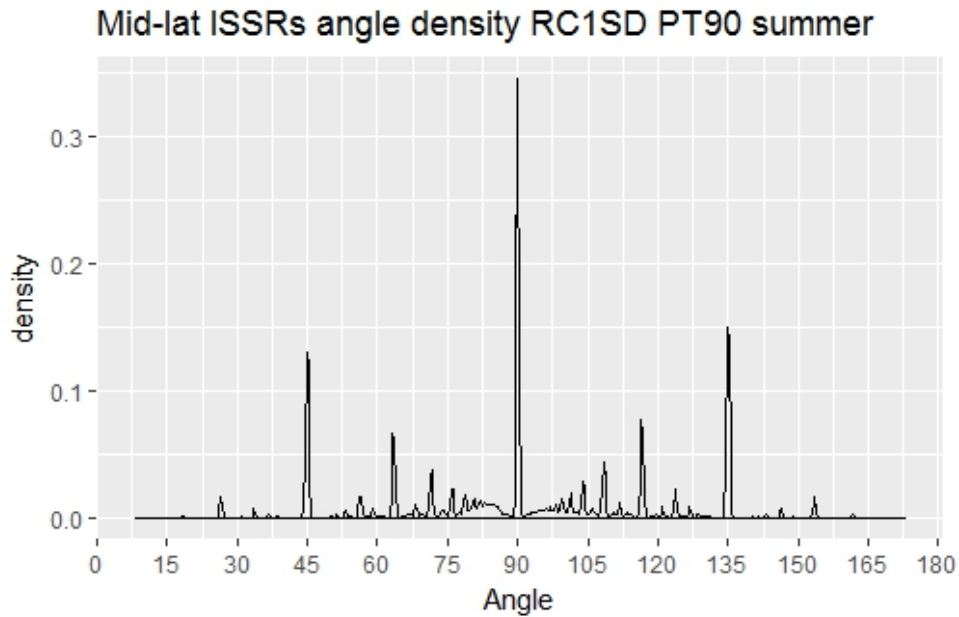


Figure 7.11: PDF of CFRs' Direction in horizontal plane NH mid-latitude summer

most frequently which are again  $45^\circ$ ,  $63.5^\circ$ ,  $90^\circ$ ,  $116.5^\circ$  and  $135^\circ$ . In the tropics, as shown in Figure 7.9, is dominated by the Hadley cell. In the NH, the air generally flow in the direction of  $135^\circ$  and in the Southern Hemisphere(SH), the air generally flow in the direction of  $45^\circ$ . In tropics, more than 40% have a direction of  $90^\circ$  which is in the north-east direction. Compared to the CFRs in the NH mid-latitude, the CFRs are less likely to be tilted in tropics. Therefore, when a aircraft fly within tropics, if encountered a CFR, shifting the flight route poleward is more likely to avoid the aircraft keep flying within that CFR. Same results are also discovered as the boxplots shown in Figure 7.13, B.25, B.26 and B.27.

The statistical distribution of CFR's direction in summer, autumn and winter are very similar to that in spring and the Figure for the three other seasons can be found in Appendix, Figure B.19, B.20 and B.21.

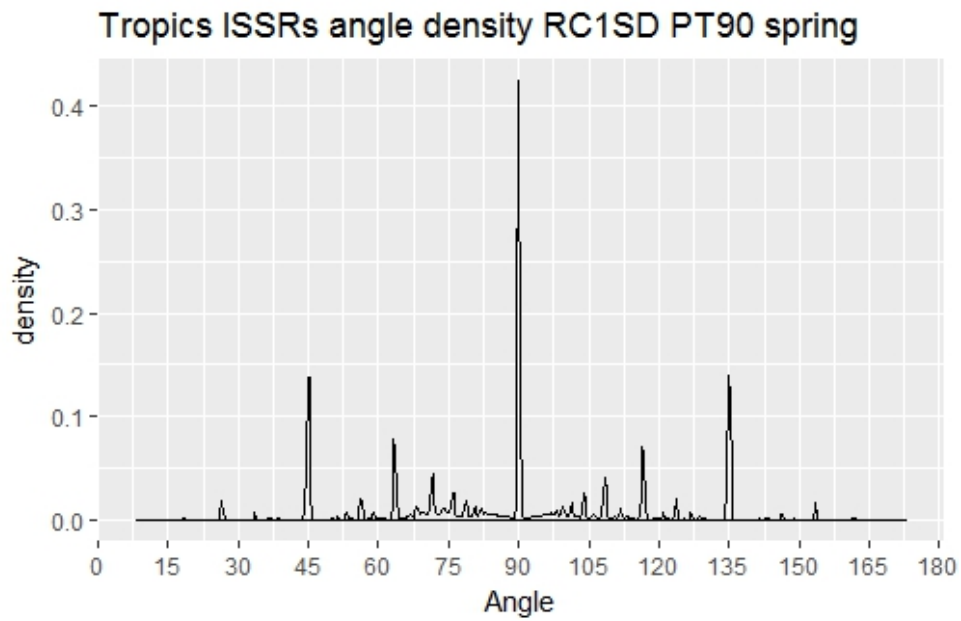


Figure 7.12: PDF of CFRs' Direction in horizontal plane Tropics spring

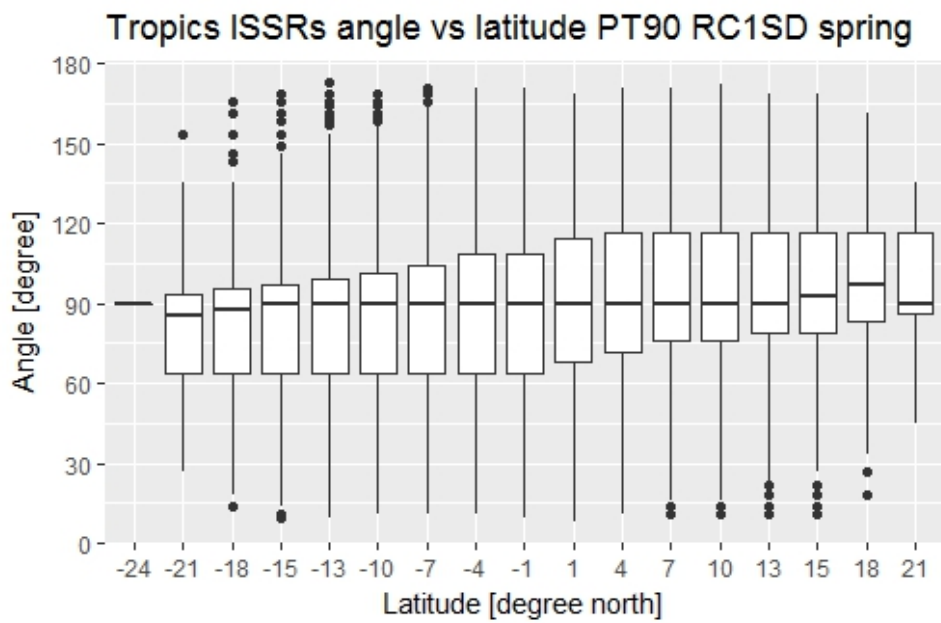


Figure 7.13: CFR Direction boxplot in horizontal plane Tropics spring

### 7.2.2. Direction of CFRs in the Vertical Plane

In this section presents the study of the CFRs' direction in the vertical plane, as explained in Section 7.1.2, the vertical plane is defined as the plane that is perpendicular to the Earth surface as well as the definition of the CFRs' direction presented in Section 7.2. The purpose of this section is to study the pattern of CFRs when they are only considered as connected within their own vertical plane and mainly focused on whether the CFRs are horizontal, vertical or tilted.

As for a horizontal CFR, the best way to avoid further flying through it is by shifting to a higher or lower flight level. Both vertical CFR and tilted CFR are more difficult to avoid compare to the horizontal one. Simply shifting the flight level cannot avoid keep flying through the CFRs. Therefore, further analyzing including combining their pattern with the CFR pattern observed in the horizontal plane are required.

#### NH Mid-latitude Regions

First, the CFRs' direction in the vertical plane within the NH mid-latitude regions are studied. Figure 7.15 and 7.16 presents the boxplots of the distribution of the CFRs' direction at different altitude for spring and winter. Generally, they are showing a very similar pattern centered around  $90^\circ$ , and in winter the CFRs are more tilted than spring. The kernel density plot of the direction for different seasons are presented in Figure 7.14, B.28, B.29 and B.30. Similar to the CFRs in the horizontal plane, the largest peak is at  $90^\circ$  with a density of more than 0.25, and the rest of the CFRs discovered within the vertical plane in the NH mid-latitude are tilted. There are four CFRs directions also appears a lot in the vertical plane, and coincidentally, the values of the rest four peaks are also similar to the direction of CFRs in the horizontal plane which are again  $45^\circ$ ,  $65^\circ$ ,  $115^\circ$  and  $135^\circ$ . This is probably due to the definition of the direction and the structure of the grids therefore, there is a higher chance for certain combination of grids to be considered as having a direction of  $45^\circ$  and  $135^\circ$ .

The distribution of CFR's direction within the vertical plane in summer and autumn are very similar to that in spring and the Figure for summer and autumn can be found in Appendix, Figure B.31 and B.32. The PDF of CFR's direction within the vertical plane in summer, autumn and winter are very similar to that in spring and the Figure for the three other seasons can be found in Appendix, Figure B.28, B.29 and B.30.

#### Tropics

Next, the CFRs' direction within the vertical plane in the tropics regions are studied. Figure 7.19 and 7.20, present the boxplots of the distribution of CFRs' direction at different latitudes for the spring and summer. Compare to the CFRs in the NH mid-latitude regions, the direction are more concentrated at  $90^\circ$  in spring. In summer, CFRs are more tilted than the CFRs in spring especially in the SH tropical regions. Their kernel density plot of spring and summer are presented in Figure 7.17 and 7.18. Again, like all the other kernel density plot, the peaks are at  $45^\circ$ ,  $65^\circ$ ,  $90^\circ$ ,  $115^\circ$  and  $135^\circ$ , compared to CFRs in the Tropics regions there are more  $90^\circ$  CFRs discovered, which are the horizontal CFRs. In spring, the density of the peak at the direction of  $90^\circ$  is around 0.3. The density of the peak at the direction of  $90^\circ$  in summer is more than 0.45. Therefore, in spring, more CFRs discovered in the vertical plane are likely to be tilted.

The boxplots of the distribution of CFRs' direction for autumn and winter have a very similar pattern to that in spring and the plots can be found in Appendix, Figure B.35 and B.36. The PDF of CFR's direction within the vertical plane in autumn and winter are very similar to that in summer and the Figure for the autumn and winter can be found in Appendix, Figure B.33 and B.34.

Mid-lat vertical ISSRs angle density RC1SD PT90 spring

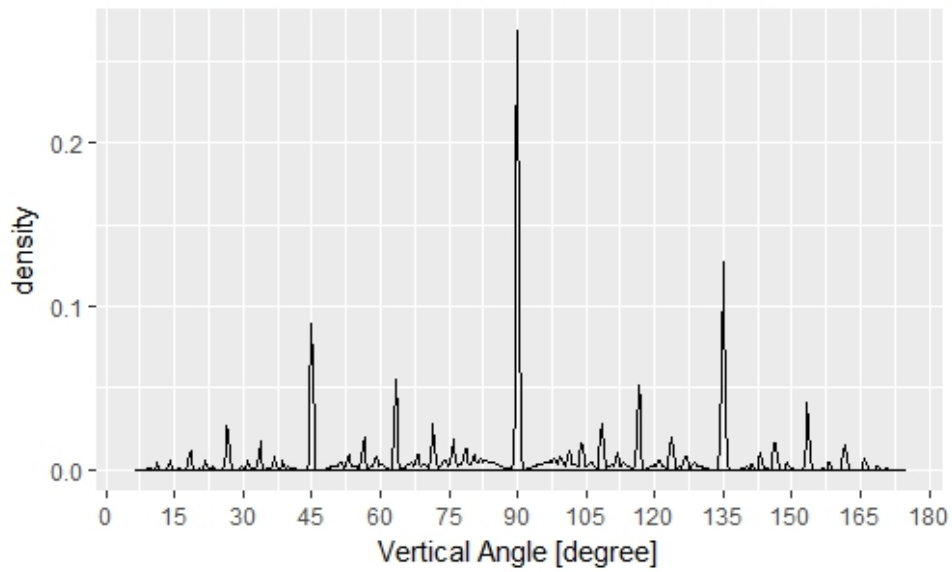


Figure 7.14: PDF of CFRs' Direction in vertical plane NH mid-latitude spring

Midlati vertical ISSRs angle vs lat PT90 RC1SD spring

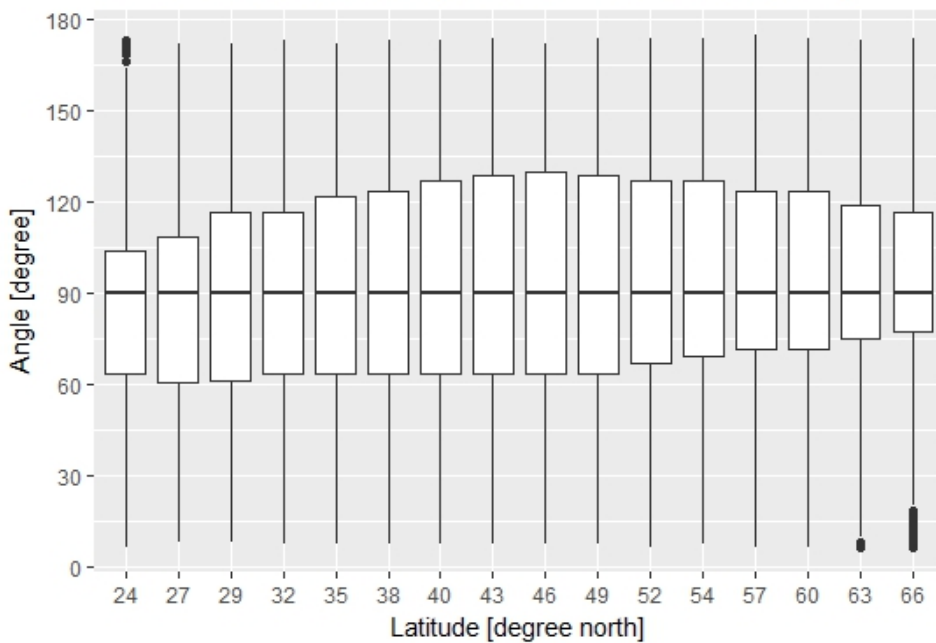


Figure 7.15: CFR Direction boxplot in vertical plane NH mid-latitude spring

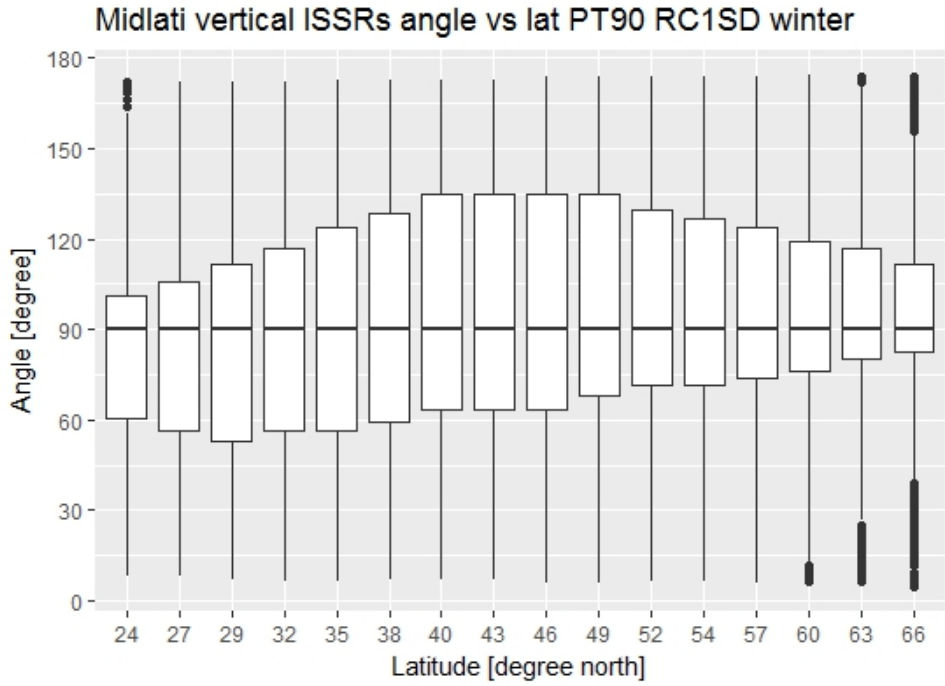


Figure 7.16: CFR Direction boxplot in vertical plane NH midlatitude winter

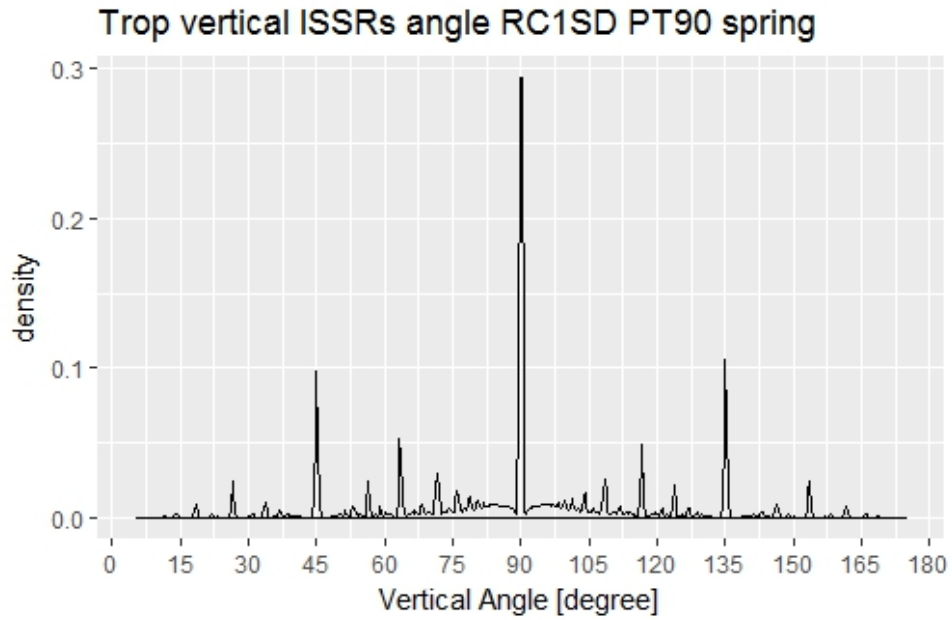


Figure 7.17: PDF of CFRs' Direction in vertical plane Tropics spring

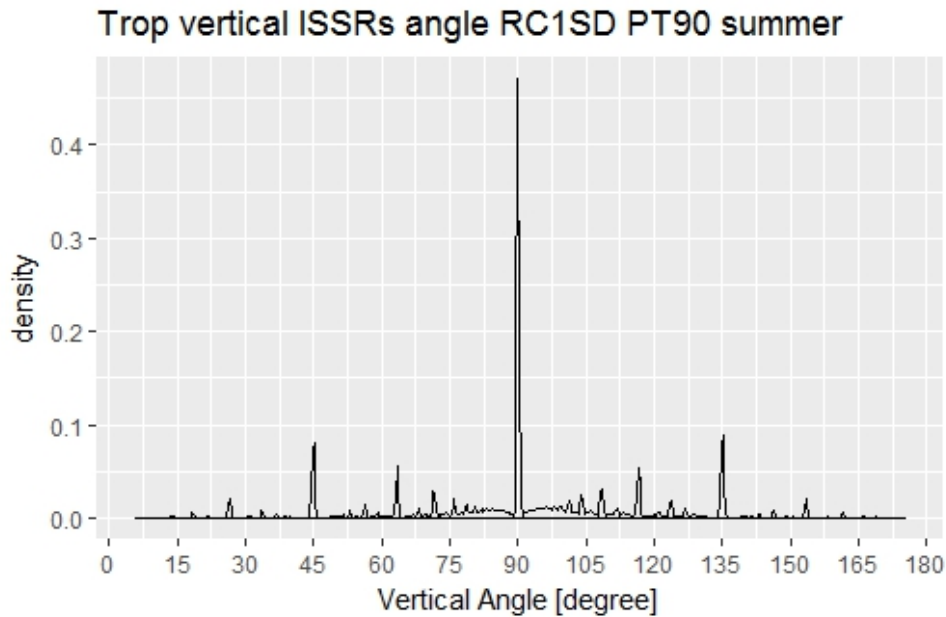


Figure 7.18: PDF of CFRs' Direction in vertical plane Tropics summer

### 7.2.3. Discussion

In the horizontal plane, as the PT is set to 90% which is a rather high value, the CFRs generally have stretch factor around 1 and 1.4. This indicates other than the dominant single grid CFRs, another typical shape of the CFR is when the length is six times of its width. For CFRs in both NH mid-latitude regions and Tropics, more than 20% of the CFRs are in the west-east direction due the general west-east direction air movement above these regions. Other than that, tilted CFRs with  $45^\circ$ ,  $65^\circ$ ,  $115^\circ$  and  $135^\circ$  also appears quite frequently following the atmospheric circulation pattern.

In the vertical plane, due to the height of grids defined in the EMAC is much smaller than their length, each grid have a origin stretch factor from around 7 to 26 depends on their geometric position. Therefore, the overall simulated CFRs' stretch factor in the vertical plane are much larger than that in the horizontal plane with a peak value around 11. And the CFRs in the tropics tend to have a higher stretch factor than the CFRs in the NH mid-latitude regions. Around 40% of the CFRs have a direction of  $90^\circ$  which means these CFRs are horizontal in their vertical plane. Compares to the CFRs in the horizontal plane, the CFRs within the vertical plane are less likely to be tilted which makes them easier to avoid. As most of them are in the horizontal direction, by shifting the flight level up or down a bit can avoid the aircraft from keeping flying in the CFRs.

Overall, according to the simulation results, if an aircraft is flying through a CFR, in order to avoid forming more contrails, it is more recommend to shift the flight level a bit. If that is not an option (in case it is in the way of other aircraft's flight route), then one has to slightly shift route within the horizontal plane at the same flight level, than it is better to shift slightly in the north-south direction or in the direction that's perpendicular to the atmospheric circulation pattern, as in the horizontal plane, the CFRs' direction is probably influenced by the atmospheric circulation pattern.

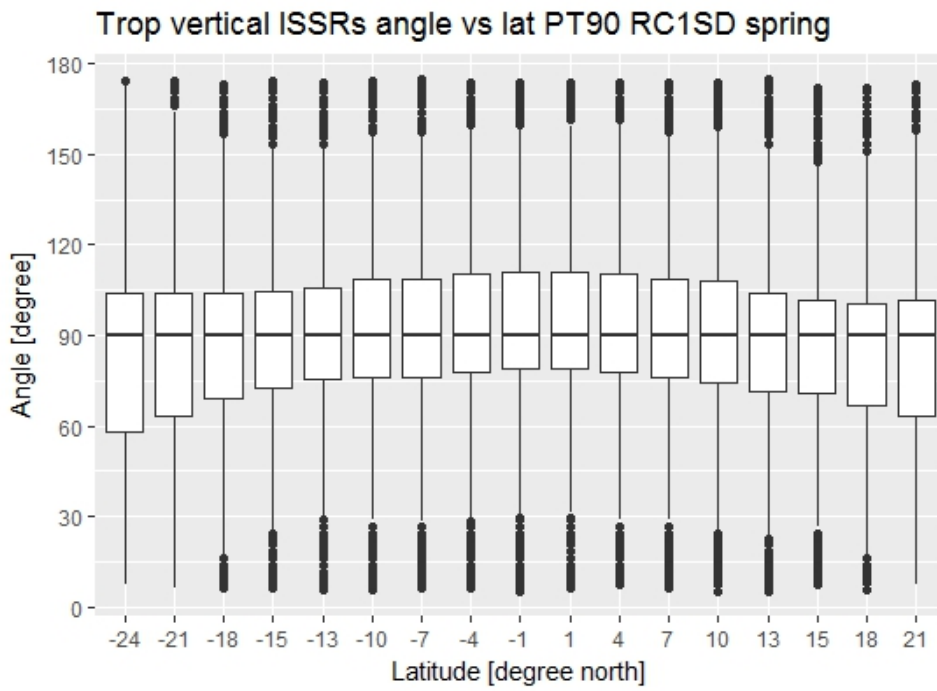


Figure 7.19: CFR direction boxplot in vertical plane Tropics spring

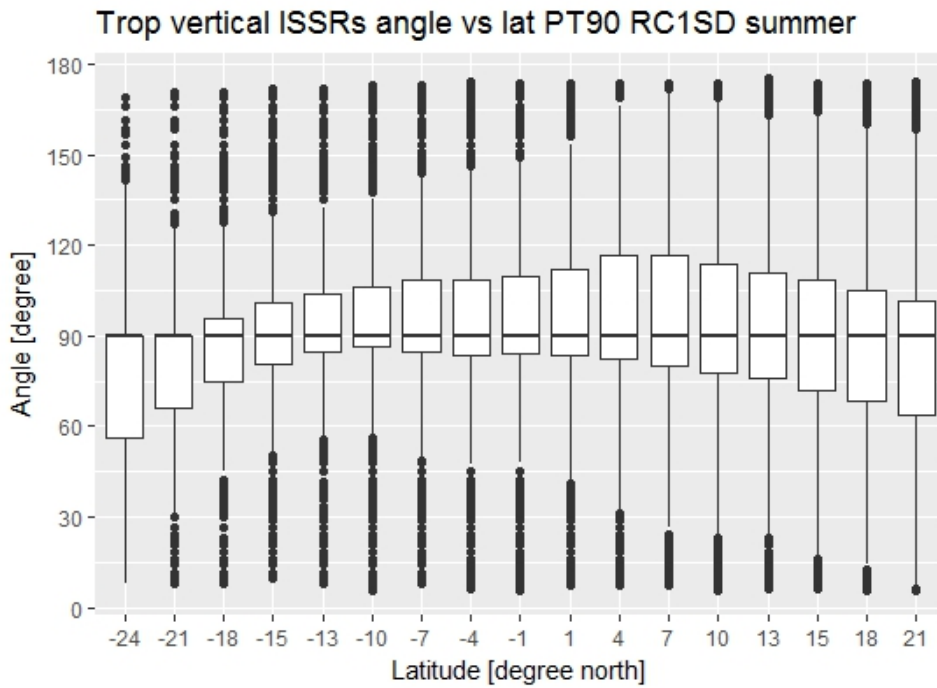
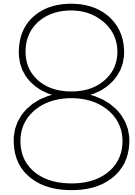


Figure 7.20: CFR direction boxplot in vertical plane Tropics summer



# Trends of Contrail Formation Regions (CFRs) and Climate Impact

Other than the analysis of the characterizations of the CFRs, the trend of the distribution of the CFRs are also analyzed in order to see how the climate changes are affecting the distribution of CFRs. This Chapter presents the study of the trend of the CFRs characterisation including the zonal mean coverage length, meridional mean coverage length in both NH midlatitude regions and tropics as well as a 117 years trend of the global and regional coverage length of CFRs in both meridional and vertical directions.

## 8.1. Trend of Zonal and Meridional Mean of CFRs

For each season, a past and future intercomparison of the 30 years mean value is performed for both zonal mean and meridional mean CFR coverage length. The specific time spans selected are explained in Section 4.2. At each grid, 30 datum are available, each representing mean value of data simulated for that year. Each data is calculated by taking the average of the CFRs' coverage length of one season in that year. Each group of 30 data from the same season are used for further comparing the CFRs' trend. The Welch's t-test are performed on all the data compared and analysis in this Chapter. The null hypothesis for Welch's t-test is: The difference between the average value of the past 30 years' data and the future 30 years' data are zero. For both past and future data set, at each grid, the difference between the averaged values for the 30 year data from the past and 30 year data from the future are calculated and the statistical significance test is performed on each set of data.

In each plot, both the difference between past and future as well as their confidence level are presented, as the difference between past and future is represented by the colour of each grid while the confidence level is represented by the shape of each grid. When the probability for null hypothesis to be true is low ( $p - value < 0.5$ ) which also indicate the confidence level of there are difference between the past and future average is higher than 95%, then the grid is represented by a "•", otherwise, if the confidence level is lower than 95%, then the grid is represented by a "+".

### 8.1.1. Meridional Mean of CFRs Coverage Trend

First, the trend of meridional mean of CFRs coverage are studied separately for both NH midlatitude regions and Tropics. As explained in Section 6.1, the meridional mean coverage length is calculated along each longitude circle. Due to the largely different distribution of CFRs in the NH midlatitude

regions and tropics at different pressure altitude, these two regions are analyzed separately so their difference are not averaged out.

### NH midlatitude regions

As presented in Section 6.1.1, in the NH midlatitude regions, the CFRs are mostly appeared at pressure altitude between 400 hPa to 200 hPa with a maximum ratio of CFRs' coverage around 10%. Figure 8.1, 8.2, 8.3 and 8.4 present the trend of meridional mean coverage length within the NH midlatitude regions, from each of these figure, a very obvious dividing line can be notices at the pressure altitude around 200 hPa. Above the dividing line, overall there is an addition 1% of CFRs' coverage ratio added to the current CFRs' coverage ratio. One thing need to be noticed is that, at these regions, the current CFRs' coverage ratio is around 1%, so the addition 1% of CFRs' coverage actually doubled the ratio of the CFRs' coverage at those regions. Then maximum increase of the CFRs' coverage ratio is around 2%. On the other hand, under the dividing line, in contrast, there is a decrease of around 1% of the CFRs coverage per unit.

When correlating the regions that are simulated to have an increase of the ratio of CFR coverage with the regions that currently have a higher density of the CFRs, the increase of CFRs coverage ratio mostly covered the regions that are currently highly covered by CFRs. The decrease of CFRs coverage ratio are mostly discovered in the regions that currently do not have a high coverage of CFRs. This actually indicates the CFRs currently with a higher density will shift up. Since the CFRs mostly appeared under the tropopause, according to the simulation results, the shifting upward of CFRs also suggest that the tropopause is slightly shifting up. This result also correspond with the assessment presented by Solomon et al. (2010), globally, the troposphere is warming up and the stratosphere is cooling down. Furthermore, according to Gettelman et al. (2010), they use different models to simulate the future trend of the tropopause and according to their simulation results, a shifting upward of the tropopause is also predicted.

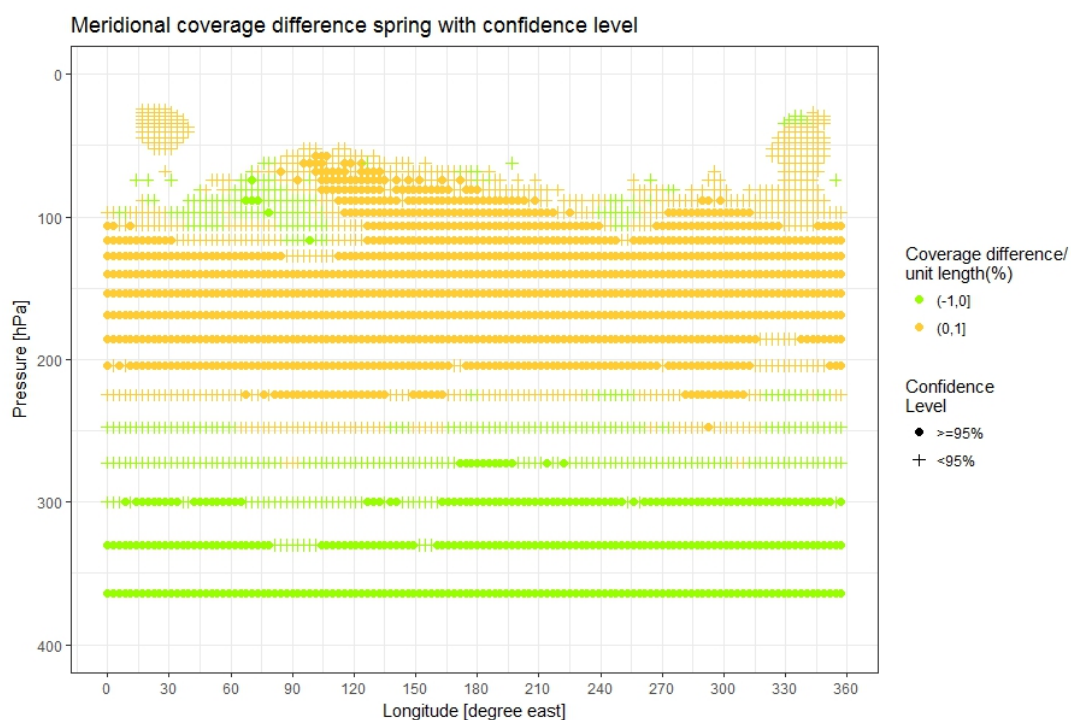


Figure 8.1: Meridional Mean of CFRs Coverage Difference in NH midlatitude Spring

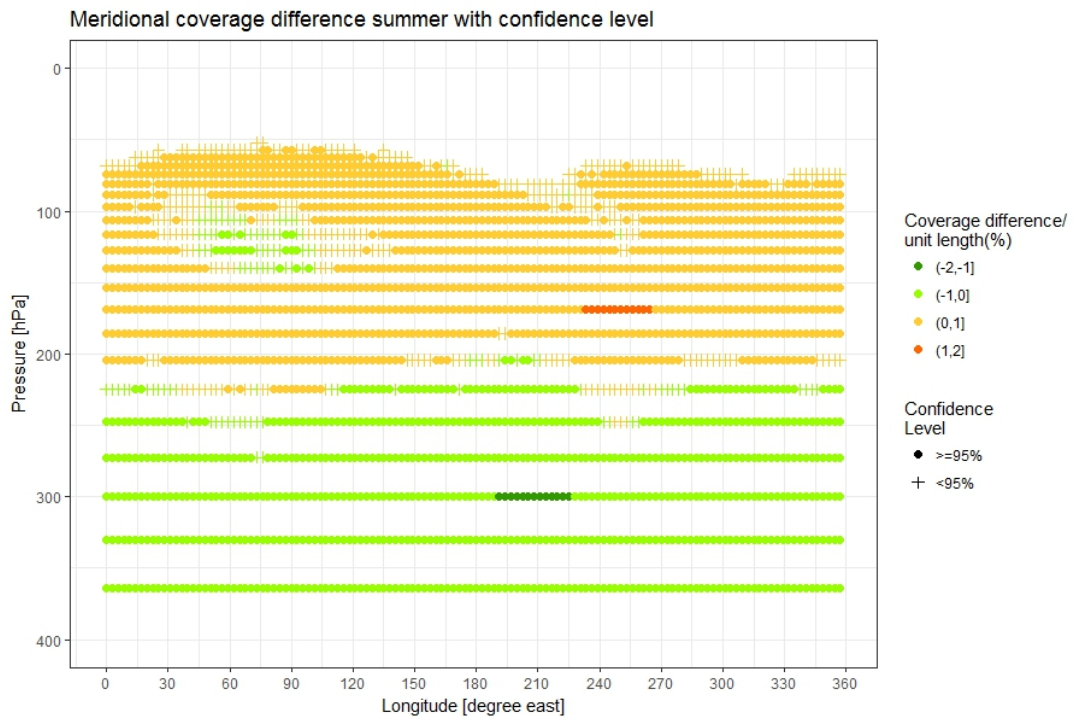


Figure 8.2: Meridional Mean of CFRs Coverage Difference in NH midlatitude Summer

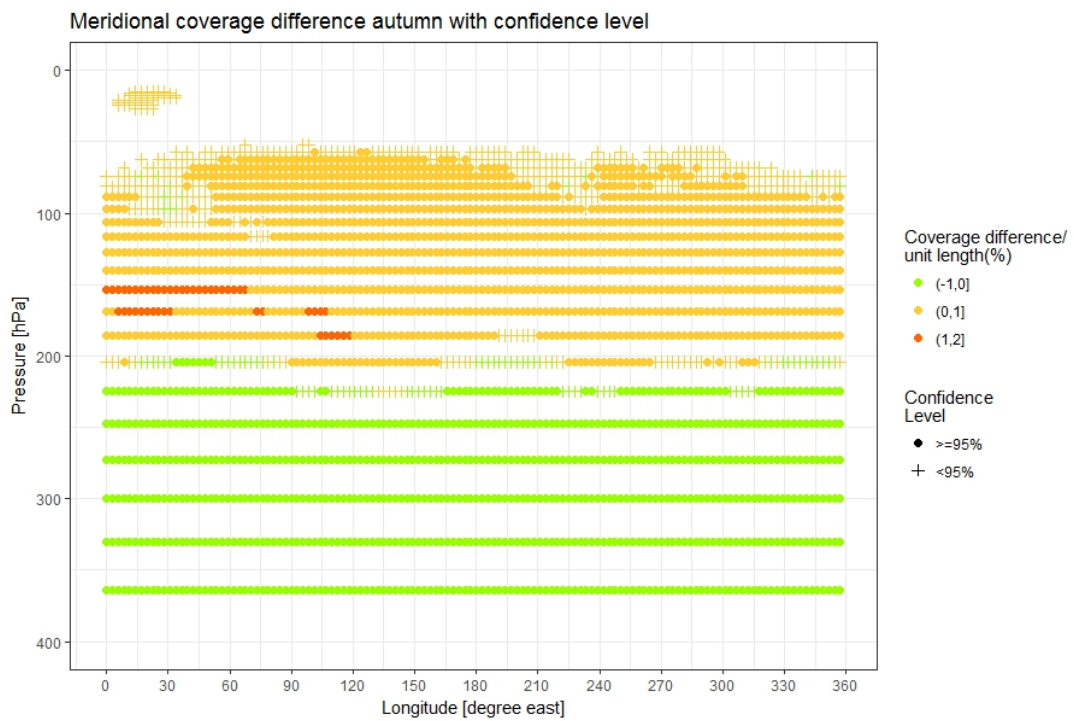


Figure 8.3: Meridional Mean of CFRs Coverage Difference in NH midlatitude Autumn

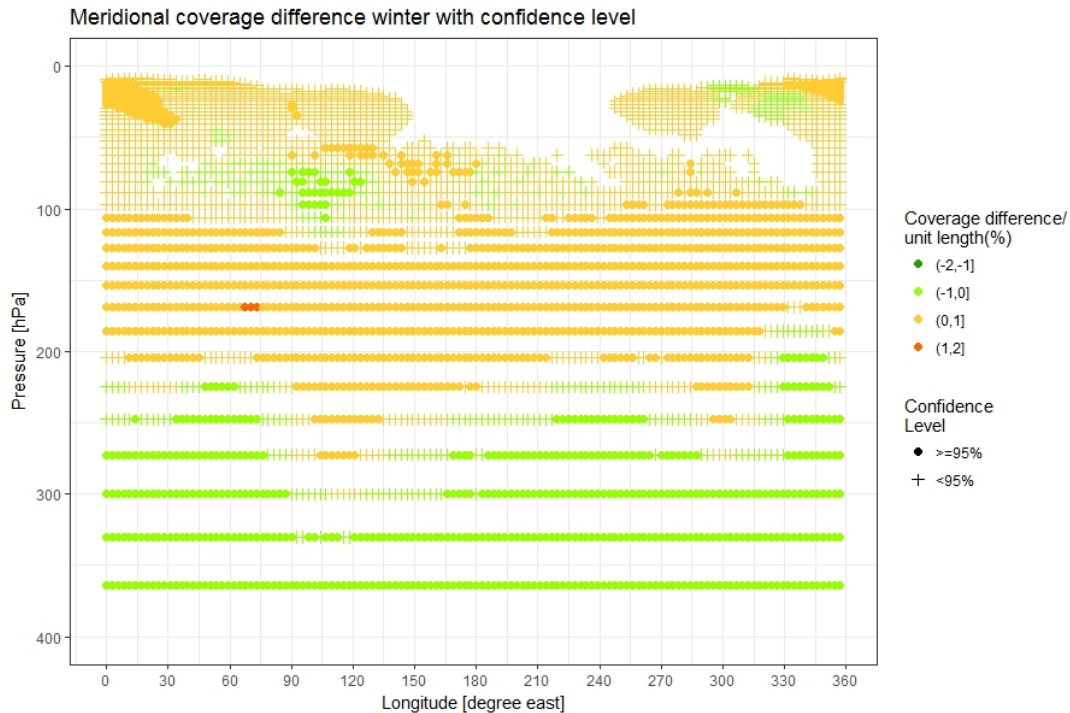


Figure 8.4: Meridional Mean of CFRs Coverage Difference in NH midlatitude Winter

## Tropics

In the tropics, as presented in Section 6.1.2, the regions with a high density of CFRs coverage mostly appear in the layer between the pressure altitude 150 hPa and 80 hPa, with the highest CFRs coverage ratio can reach more than 25%. Overall the CFRs have a much higher density in the tropics than in the NH midlatitude regions. The trend of the CFRs' coverage ratio in spring is presented in Figure 8.5. In spring, a very distinct dividing line is located at the pressure altitude around 80 hPa, an increase of about 3% extra CFRs' coverage within the regions above the dividing line. And under the dividing line, there is a generally a decrease of 1% CFRs' coverage ratio.

The trend of the CFRs' coverage ratio in summer, autumn and winter have a very pattern as the one presented in spring, and the plot for the rest three seasons can be found in Appendix, Figure C.1, C.2 and C.3

Again the trend here is suggesting a shifting upward of the CFRs, this is mainly due to the global warming as in the tropics region overall the temperate are considerably higher than the rest of the world. Therefore, in order to meet the requirements for contrails to be persistent, the temperature need to be lower than  $-273K$ . This is why currently most of the CFRs appeared in the regions higher than 150 hPa pressure altitude and in the future, due to the global warming, as the temperature increase globally, the atmosphere temperature where the temperature threshold of CFRs are met shifted upwards. As the CFRs are mostly located under the tropopause, this also correspond with the assessment that the tropopause is also shifting upward due to the global warming.

### 8.1.2. Zonal Mean CFRs Coverage Length Trend

The zonal mean of CFRs' coverage is calculated along each of the latitude circle and has a global coverage, it is more straight forward to distinguish the difference between the pressure altitude where CFRs appear the most in the tropics, midlatitude regions and polar regions. As discussed in Sec-

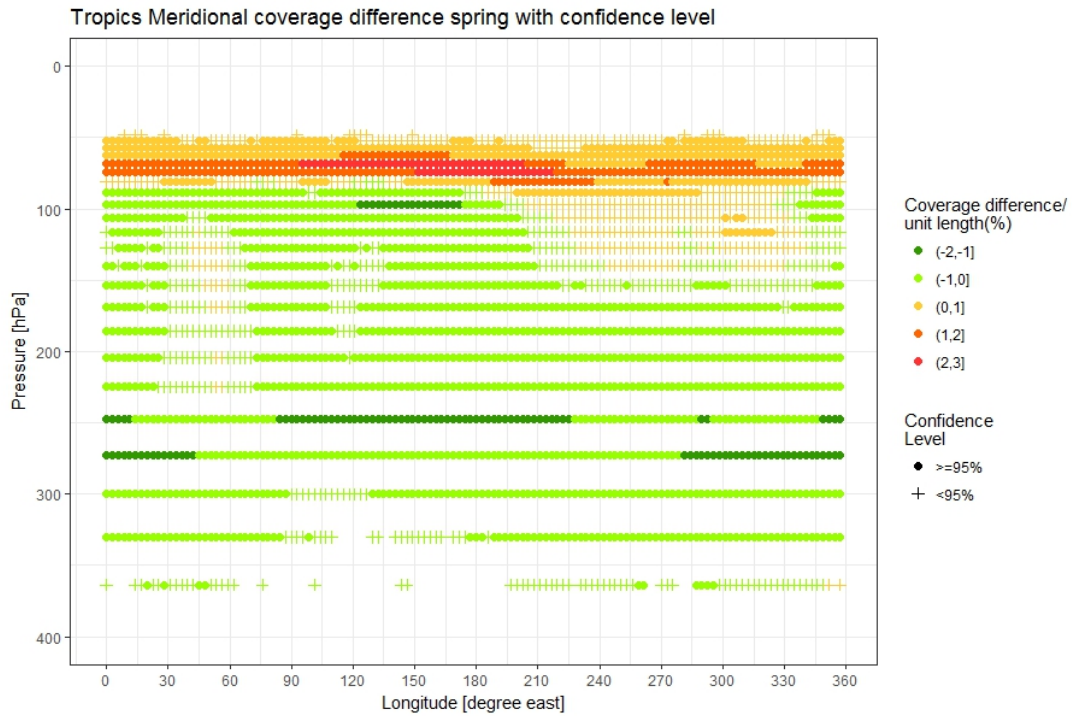


Figure 8.5: Meridional mean CFRs coverage difference in tropics spring

tion 6.3, in the tropics regions, CFRs appear the most at the pressure altitude around 100 hPa with the maximum coverage per unit length above 40%, and generally in the midlatitude regions and polar regions CFRs mostly appears in the regions below the regions with pressure altitude around 200 hPa. At these pressure altitude in the tropics, the atmosphere temperature is too high for contrails to persist.

The trend of the zonal mean CFRs coverage length for the four different seasons are presented in Figure 8.6, 8.7, 8.8 and 8.9. Coincide with the trend previously discovered in the meridional mean CFRs coverage, overall the CFRs are shifting upwards. The maximum of the increase of the CFRs coverage appears in the tropics at the pressure above 80 hPa with an extra 5% of CFRs coverage per unit length. In the midlatitude regions and polar regions, most of the increase take place above the regions where CFRs appear the most in the past. Other than that, above the polar regions, an increase of CFRs coverage in the stratosphere is always spotted. Since the seasons in the northern hemisphere is opposite to the seasons in the southern hemisphere, Figure 8.7 and Figure 8.9 present a pair of mirrored figures of the summer and winter trend in the opposite hemisphere.

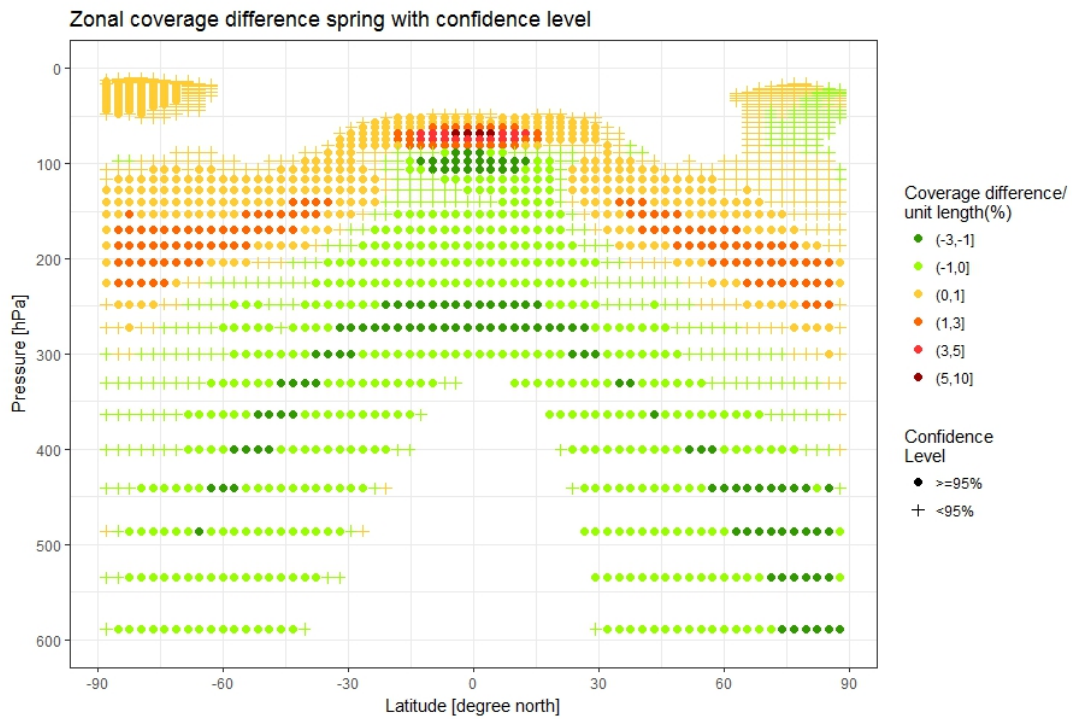


Figure 8.6: Zonal mean CFRs coverage length difference spring

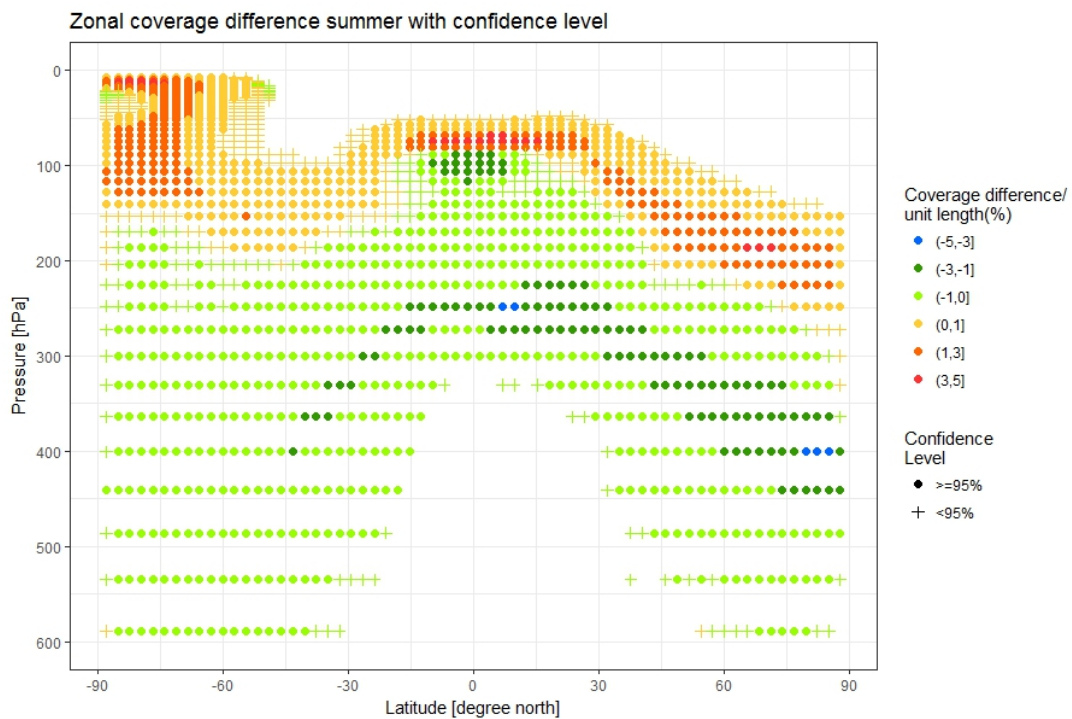


Figure 8.7: Zonal mean CFRs coverage length difference summer

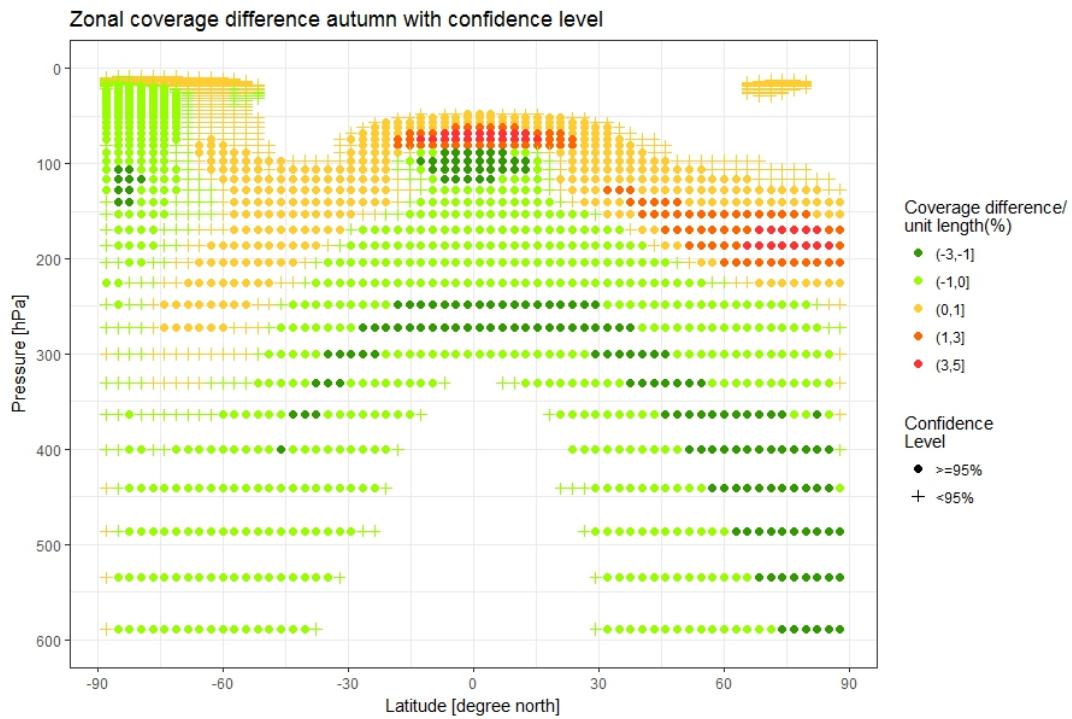


Figure 8.8: Zonal mean CFRs coverage length difference autumn

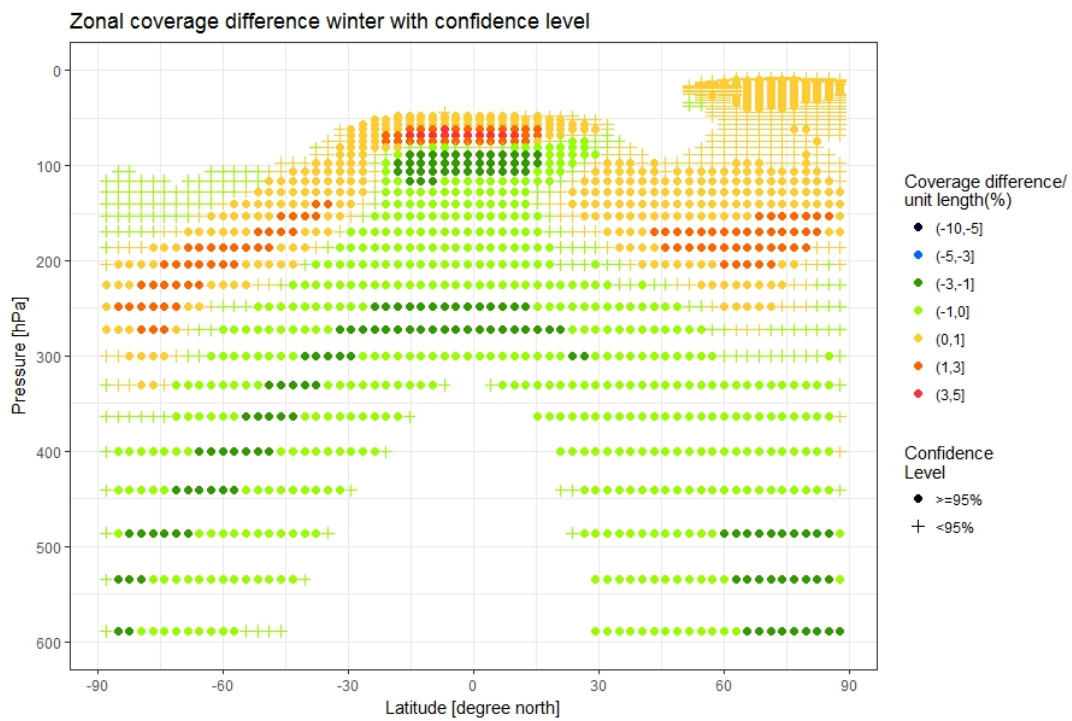


Figure 8.9: Zonal mean CFRs coverage length difference winter

## 8.2. Climate Impact on the Trend of CFRs

The analysis in the previous sections suggests that the overall trend of the CFRs coverage varied by their geographic locations. Depends on the location, the CFRs' coverage length might either increase or decrease. Furthermore, a general upward shifting trend of the CFRs, similar to the tropopause, is discovered. Therefore, in this section, the trend of the overall coverage of CFRs are presented by both the vertical extension of the CFRs globally and the meridional coverage length at a different height within both NH mid-latitude regions and Tropics. In this section, the datum simulated by EMAC submodel RC2-base-04 from the year 1983 to 2099 are analyzed to have a general overview of the CFRs' trend from the past to the future. In each figure presenting the trend of the CFRs coverage length and vertical extension, a trend line is given by a blue solid line and the grey area representing the 95% confidence level of the trend line.

### 8.2.1. Trend of the Global CFRs' Vertical Extension

This section presents the global vertical extension of CFRs from 1983 to 2099. For each year, the global vertical extension of CFRs is represented by the mean value of the CFRs' vertical extension calculated for every time step in that year. And the CFRs vertical extension of each time step is calculated by adding up all the vertical extension (km) of CFRs discovered globally at all latitude, longitude and altitude. The vertical extension is studied for the reasons that the thickness of the contrail actually can affect the net RF induced by that certain contrail as mention earlier in Chapter 2.4.

For the past 100 years, the Earth has been warming up gradually as shown in Figure 8.10 with a drastic increase in the global warming rate after 1980 mostly due to the anthropogenic influences (Brönnimann 2009; Hegerl et al. 2007). Other than the general increasing trend of the global temperature, an annual oscillation of the global temperature can also be observed due to different climate phenomena that might either have a global or regional impact on the climate (Christensen et al. 2013).

Since one dominant of the CFRs is the temperature, first, a comparison between the CFRs global vertical extension and the global land and ocean temperature anomalies between year 1983 and 2018 is presented. In Figure 8.11 is the global land and ocean temperature anomalies also from 1983 to 2018, the figure is produced by (Smith et al. 2008)<sup>1</sup>, where for each year, a global averaged temperature anomaly is calculated. From the figure, generally, a trend of the temperature anomalies increasing can be noticed which coincide with the current global warming situation. Furthermore, a slowing down of the increase rate can be noticed after 1998 which is probably due to the Interdecadal Pacific Oscillation (IPO) shifting from the positive (warm) phase to the negative (cool) phase (Dong and Dai 2015).

In Figure 8.12 is the trend of the CFRs global vertical extension from 1983 to the current year 2018. Generally, the annual mean CFRs' global vertical extension varied between 14900km and 15800km, where the maximum and the minimum only differ about 6%. For the covered 36 years, the trend of the CFRs' global vertical extension is not very noticeable yet.

In Figure 8.13, is the CFRs' global vertical extension from 1983 to 2099, a total of 117 years of simulation, other than a rather fluctuated trend with a difference sometimes larger than 10% between two consecutive years, a very obvious declining trend can be noticed this time. Approximately, the decrease of the global vertical extension is calculated to be around 5%, this is generally due to the global warming. Same declining trend of the global cloud coverage mostly those at middle and high levels is also discovered by Eastman et al. (2013). So overall the regions that are suitable for contrail to form and persist are getting smaller but since this is largely cause by the global warming and as

---

<sup>1</sup><https://www.ncdc.noaa.gov/monitoring-references/faq/anomalies.php>

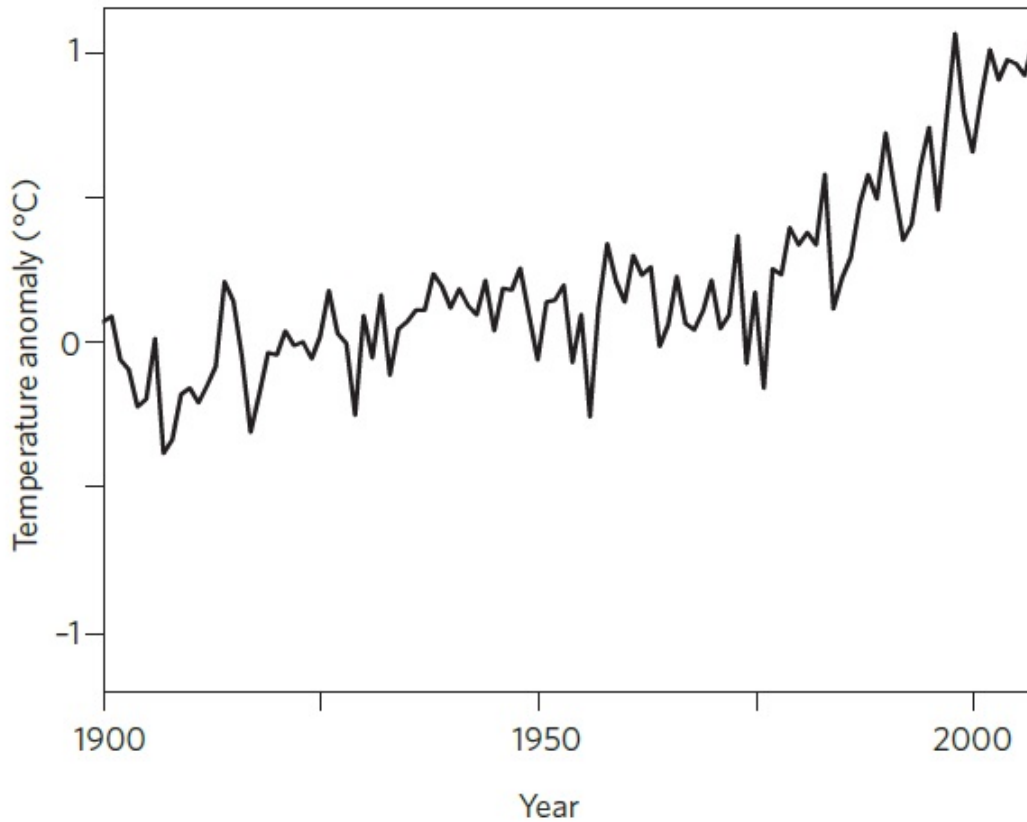


Figure 8.10: Annual mean surface air temperature averaged over the remaining land regions (Figure obtained from Stefan Brönnimann (2009))

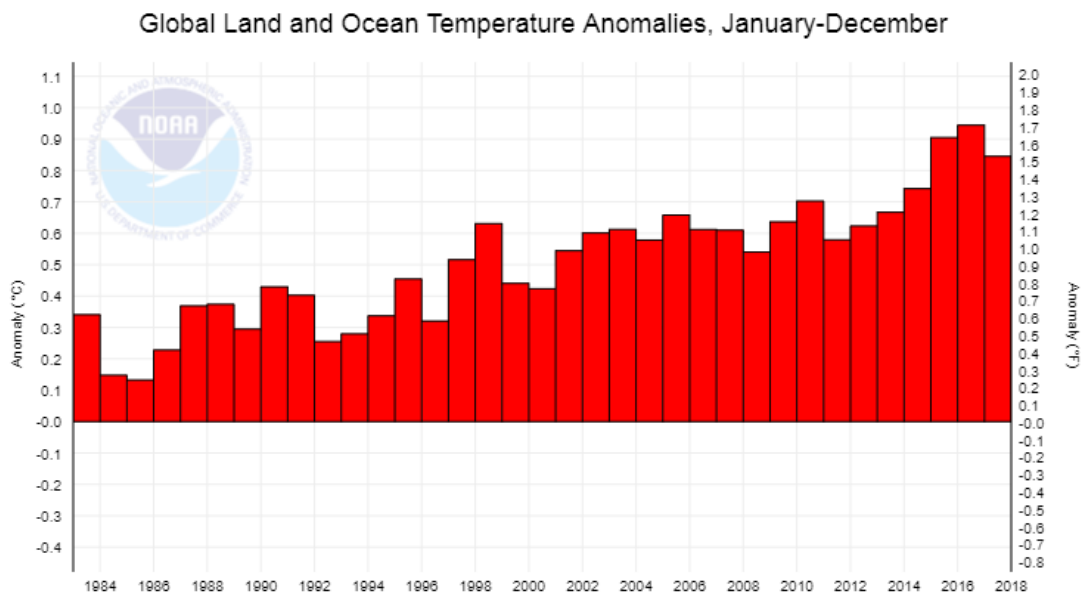


Figure 8.11: Trend of CFRs' global ocean and land temperature anomalies (figure obtained from NOAA National Centers for Environmental information, Climate at a Glance: Global Time Series, <https://www.ncdc.noaa.gov/cag/>, published July 2018, retrieved on August 4, 2018)

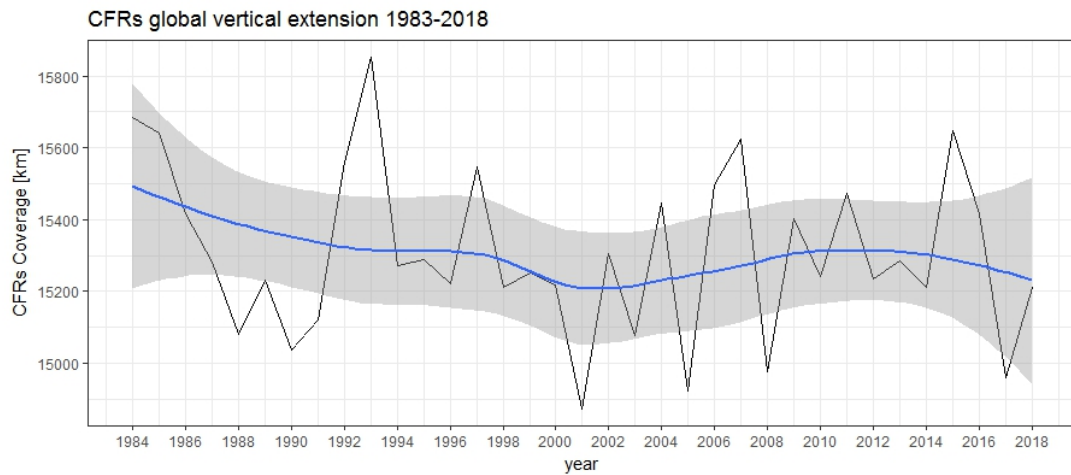


Figure 8.12: Trend of CFRs' global vertical extension 1983-2018

mentioned in Section 2.1, contrails contribute a lot to the global warming, it is still necessary to find ways to mitigate the formation of contrails.

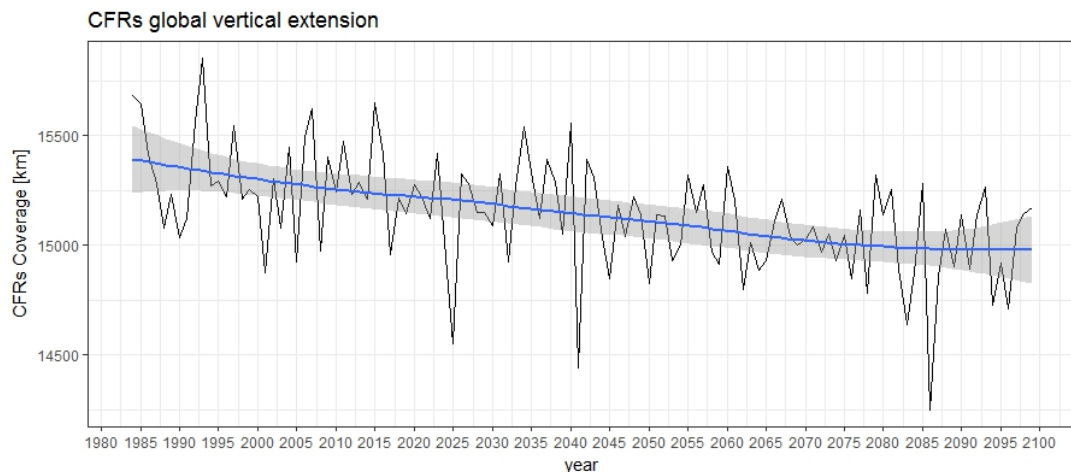


Figure 8.13: Trend of CFRs' global vertical extension

### 8.2.2. Trend of the CFRs' Meridional Mean Coverage Length

As demonstrated in Section 8.1.1, within different regions at different pressure altitude, the CFRs' coverage lengths are following different trend. Hence, according to the previous results, the trend of the CFRs meridional coverage length are simulated within NH mid-latitude and tropics separately for different pressure altitude: 75 hPa, 127 hPa and 250 hPa. The first two pressure altitude, 75 hPa and 127 hPa are selected based on the result from previous Section 8.1.2 that within different regions, the trend of the CFRs' coverage length are different. The third pressure altitude selected is within the common cruising altitude: 250 hPa (FL340). Since contrails are formed by the mixing of the aircraft exhaust air and the ambient atmosphere, the trend of CFRs' coverage length at the common cruising level can indicate the trend of contrails' coverage length if the common flight levels remain the same in the future.

In Figure 8.14 presents the CFRs meridional coverage length at pressure altitude 127 hPa within NH midlatitude. Figure 8.15 and 8.16 present the CFRs meridional coverage length within tropics at

the pressure altitude 127 hPa and 75 hPa. From the significant increasing trend of CFRs meridional coverage length presented in Figure 8.14 and 8.16, in the NH mid-latitude regions at 127 hPa and in the tropics at 75 hPa, the CFRs meridional coverage length in 2099 is doubled the amount in 1983 for both case. On the contrary, in the tropics at pressure altitude 127 hPa, as shown in Figure 8.15, the CFRs meridional coverage length have a decreasing trend. From 1983 to 2099, the CFRs meridional coverage length within this area decrease by 8%. Overall, these trend simulated are consistent with the results presented in Section 8.1.1.

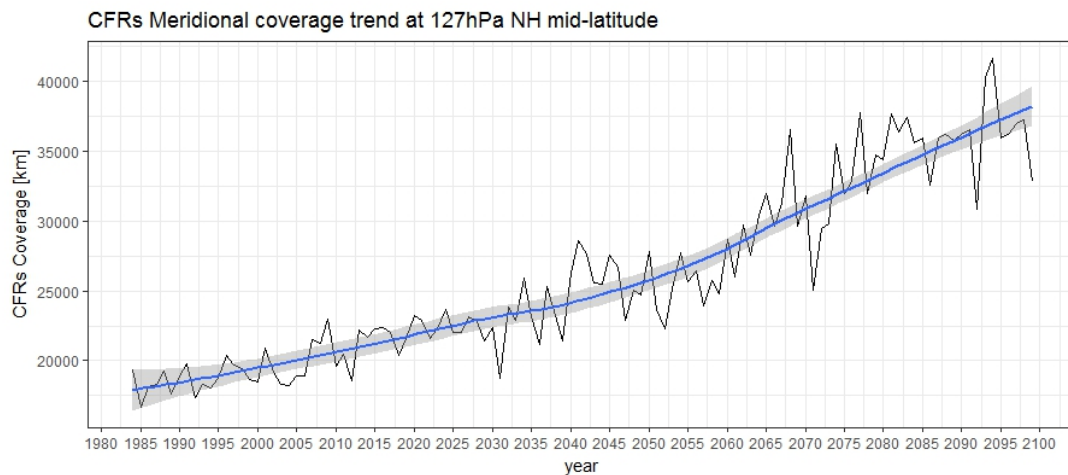


Figure 8.14: Trend of CFRs' meridional mean coverage length at 127hPa in the NH mid-latitude regions

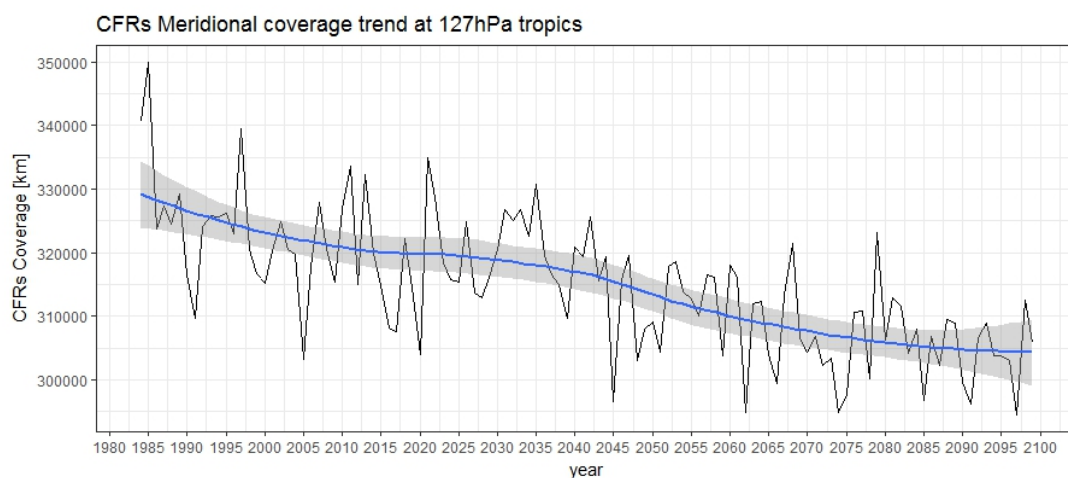


Figure 8.15: Trend of CFRs' Meridional Mean Coverage Length at 127hPa in the Tropics

In Figure 8.17 and 8.18 present the trend of the CFRs' yearly averaged meridional coverage length within mid-latitude regions and tropics at the pressure altitude around 250hPa. This pressure altitude correspond to flight level is around FL340, it is about 10km above mean sea level and is considered as the common cruising level. Since many aircraft fly at this altitude, the trend of the CFRs' meridional coverage length is studied to see the impact of climate change on the CFRs at these location. Both Figure 8.17 and 8.18 show a decreasing trend of the CFRs meridional coverage within both mid-latitude regions and tropics. In the mid-latitude regions at 250hPa, as presented in Figure 8.17, from 1980 to 2099, the yearly averaged CFRs meridional coverage length reduced about 8.7%. In the tropics as presented in Figure 8.18, the yearly averaged CFRs meridional coverage length reduced about 70.6% which is much larger than that in the mid-latitude regions. It can be seen that

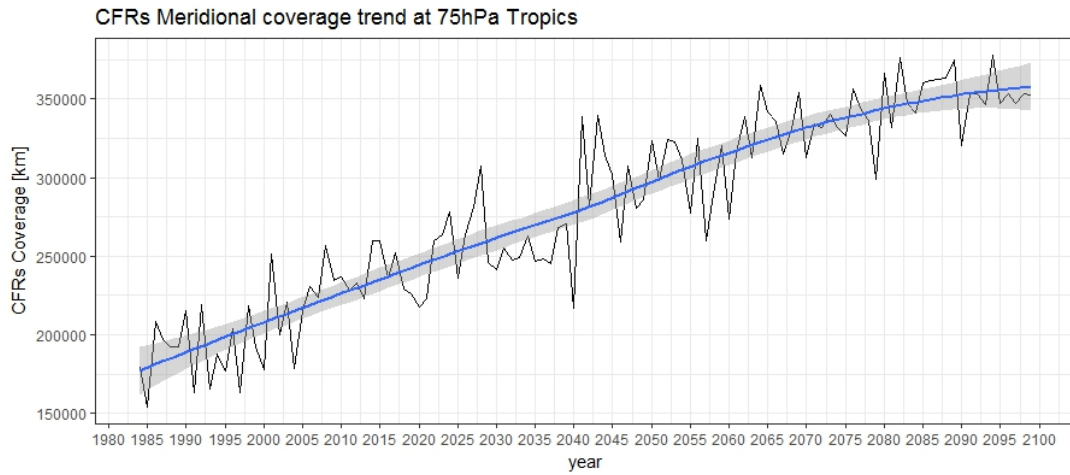


Figure 8.16: Trend of CFRs' Meridional Mean Coverage Length at 75hPa in the Tropics

the decreasing rate increases after round year 2040, this is most likely due to the global warming. It is possible that after year 2040, in the tropics the temperature in more regions are too warm for contrail to form and persist. So overall, the chance for contrails to form at these current common flight route will decrease especially in the tropics, however this is mostly due to the global warming.

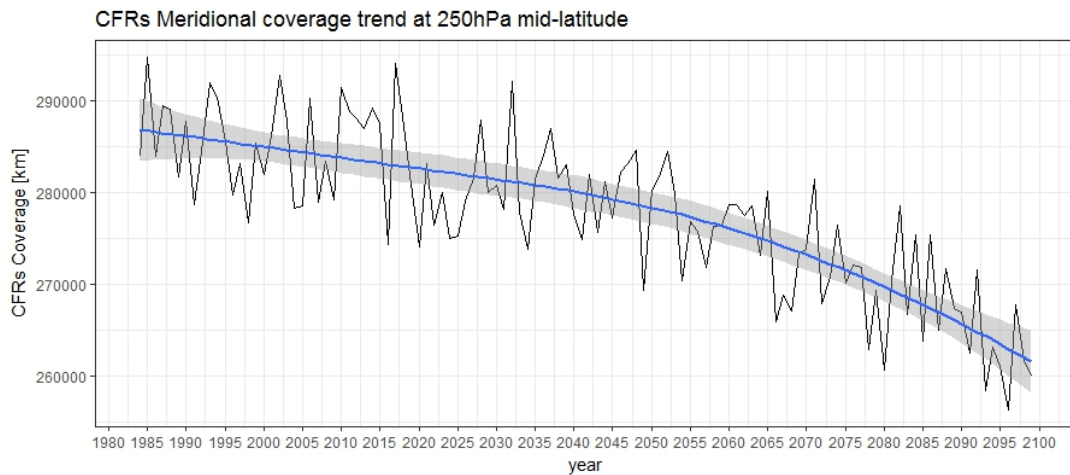


Figure 8.17: Trend of CFRs' meridional mean coverage length at 250hPa in the mid-latitude

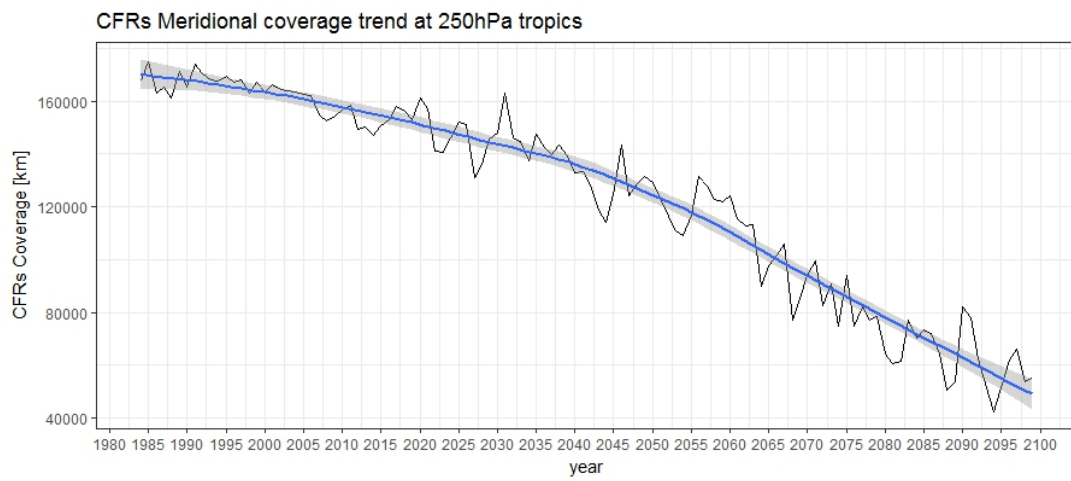


Figure 8.18: Trend of CFRs' meridional mean coverage length at 250hPa in the tropics

### 8.3. Discussion

From the past and future difference calculated for both CFRs' zonal mean coverage and CFRs' meridional mean coverage, a shifting upward of the trend of the distribution of CFRs can be noticed. This also corresponds with the upward shifting trend of the tropopause. Furthermore, at the current common cruising level, the CFRs' coverage length is simulated to have a decreasing trend, this indicates that if the common flight routes stay at the same flight level in the future, generally, less contrails will be formed. In this case, contrails will contribute less to the global warming in the future.

Globally, the regions that contrail can form and persist will decrease slightly. Depends on the location, the trend of the CFRs coverage length varied. Overall the distribution of CFRs are shifting upward, hence, it means less contrails can be formed at a lower pressure altitude and a higher chance for contrails to be formed and persistent at a higher pressure altitude. However, even with the decreasing of CFRs' coverage, it doesn't necessarily mean this can help slow down the global warming pace, since contrails can both heat up and cool down the atmosphere. The exact effect of the contrail depends on the time it persists as mentioned in Section 2.1 as well as its position, where a higher contrail tend to warm up the surrounding air and a lower contrail tend to cool down the atmosphere. Therefore, even with less CFRs' coverage length, the general up lifting of the CFRs can still contribute a lot to the global warming (A. Slingo and J. Slingo 1988). Furthermore, the decreasing trend of the CFRs is largely caused by the global warming itself as some regions are just too warm for contrails to form and persist.

Other than the seasonal variation of the CFRs' coverage length, a significant annual variation of the CFRs' coverage length can also be noticed from all the annual mean trend of the CFRs plotted. Since the global climate is dominated by the general global warming trend as well as multiple climate phenomena that can either have interannual or decadal impact on the regional or global climate (Christensen et al. 2013). As positive correlation between the temperature and the specific humidity is discovered globally (Dai 2006), for a year with higher temperature, the specific humidity is also going to be higher, leads to a hot and humid atmosphere condition that are not likely for contrail to form and persist. On the contrast, when the temperature is relative lower then the specific humidity is also going to be lower and lead to a cold and dry atmosphere condition which are more likely for contrails to form.

# Conclusions and Recommendations

## 9.1. Conclusions

As the global warming situation is getting more serious every day, it is crucial to slow it down in every possible aspect. Contrails induced RF contributes to about 30% of the aviation induced RF, therefore, it is very necessary to mitigate the amount of the contrails being formed. The purpose of this thesis is to analyze the characterisations and future trends of CFRs in order to help plan or change the flight route accordingly and hence mitigate the formation of contrails. The main objects are to analyze the characterisations of the CFRs including their coverage length and direction as well as to study their seasonality and trends. The CFRs are simulated by EMAC submodels RC1SD-base-10 and RC2-base-04.

Overall, the CFRs are generally appeared around the tropopause with a higher coverage length in the tropics than that in the mid-latitude regions. In the NH mid-latitude, the CFRs are distributed more dispersedly within the rather thick layer from 400hPa (FL235) to 200hPa (FL380), since it is unrealistic to totally avoid flying through this whole regions and the general size of the CFRs is smaller than that in the tropics, it is more realistic to change the flight path en route if the surrounding atmosphere is detected to be CFRs. Among the four seasons, the CFRs characterisation in spring and autumn are very similar due to their similar weather pattern. In winter, more CFRs appear at a lower and thicker layer compared to the CFRs appear in summer due to the temperature threshold for contrails to persist.

In the tropics, most of the CFRs appeared at pressure altitude around 180hPa to 80hPa. Furthermore, large CFRs appeared most frequently at the thin layer from 120hPa (FL475) to 80hPa (FL555). Currently, these layers are not among the common flight level, but in the future, it is still highly recommended to avoid flying through that regions. The current common cruising level is between FL340 and FL420, which correspond to 250hPa and 165hPa, in tropics, fewer CFRs are discovered within the lower level from 250hPa (FL340) to 200hPa (FL380) and are generally smaller than those discovered at a higher level. In the tropics, less seasonal variations of the CFRs' coverage length are spotted except for the regions above the tropical eastern Pacific ocean and the regions over the continents.

Within both NH mid-latitude regions and tropics, the CFRs generally have a stretch factor around 1 and 1.4, which indicates the general shape of the CFRs are dominant by the single grid non-stretched CFRs and the stretched CFRs that have a length six times its width. And the directions of the CFRs are dominated by a west-east direction mainly due to the Earth's rotation and the tilted CFRs mainly are

in the northwest-southeast (NW-SE) direction and southwest-northeast (SW-NE) direction following the prevailing wind pattern.

Generally, as most of the CFRs are detected to be horizontal within each of their vertical plane, when CFR is discovered en route, the best option is to change the flight level, by flying up or down one flight level can help avoid further flying through that CFR. And if changing the flight level is not an option, it is better to shift the flight route in the north-east direction, since the CFRs' direction is dominated by the west-east direction due to the earth rotation. And due to the influence of the prevailing wind pattern on the CFRs' direction, in the NH tropics, shifting the flight route in the northwest direction and in the SH tropics, shifting the flight route in the northeast direction also have a higher chance of avoiding further flying through that CFR.

Due to the global warming, as the atmosphere temperature at a lower altitude might be too high for contrails to form and persist, the regions with high density of CFRs will shift upward as well as a globally decreasing trend of the CFRs coverage length. However, since the CFRs will shift upward, if do not plan the flight route accordingly, more contrails will be formed at a higher altitude, compare to a contrail formed at a lower altitude, the contrail persist at a higher level is more likely to warm up the atmosphere which can contribute more to the global warming. Furthermore, at the current common cruising level, a general decreasing trend of the CFRs' coverage length in both NH mid-latitude regions and tropics is discovered. This indicates fewer contrails will be formed if the amount of flight and their flight routes remain the same in the future. At first glance, it might seem reassuring that a general decreasing trend of the CFRs coverage length is discovered, however, the fact that the general decreasing trend is mostly due to the global warming itself makes it less likely a good news. Additionally, with the amount of flight constantly increases every year, still more contrails might be formed in the future if no action were taken.

## 9.2. Recommendations

Based on the finding from this thesis, some recommendations are given as followed.

Since the direction of the CFRs largely depend on the prevailing wind pattern, For example, one can categorize the interested regions according to the prevailing wind pattern to have a better analysis of the direct influence of the prevailing wind pattern on the direction of CFRs.

More research can be performed on finding the relation between some specific seasonal wind pattern with the CFRs direction.

In stead of categorized the interested regions into tropics and NH mid-latitude regions, the interested regions can be categorized into more detailed and smaller regions based on the impact regions of different climate phenomena to help better understanding the effect of these climate phenomena on the CFRs direction in both vertical plane and horizontal plane. Therefore, can help better predict the CFRs' direction in the future based on the location and weather.

As contrails can both warm up and cool down the earth, and the exact impact depends largely on the time period when the contrail is formed and persist in the atmosphere. Further study can be performed on the difference between the CFRs distribution and characterisation during the day and during the night, as the contrail induced RF are different between day and night.

Since the season in the tropics is defined by a wet season and a dry season, when study the seasonal variation of the CFRs' characterisations in tropics, instead of four seasons, the datum can be categorized according to the wet and dry season to have a more reasonable analysis of the seasonal variations of the CFRs within tropics.

Simulation wise, reduce the size of the grid in both latitude and longitude direction, can enable

a better simulation result. When simulating the CFRs to calculate their directions, even the PT is set to high amount would not lead to many CFRs being neglected.



# A

## Appendix

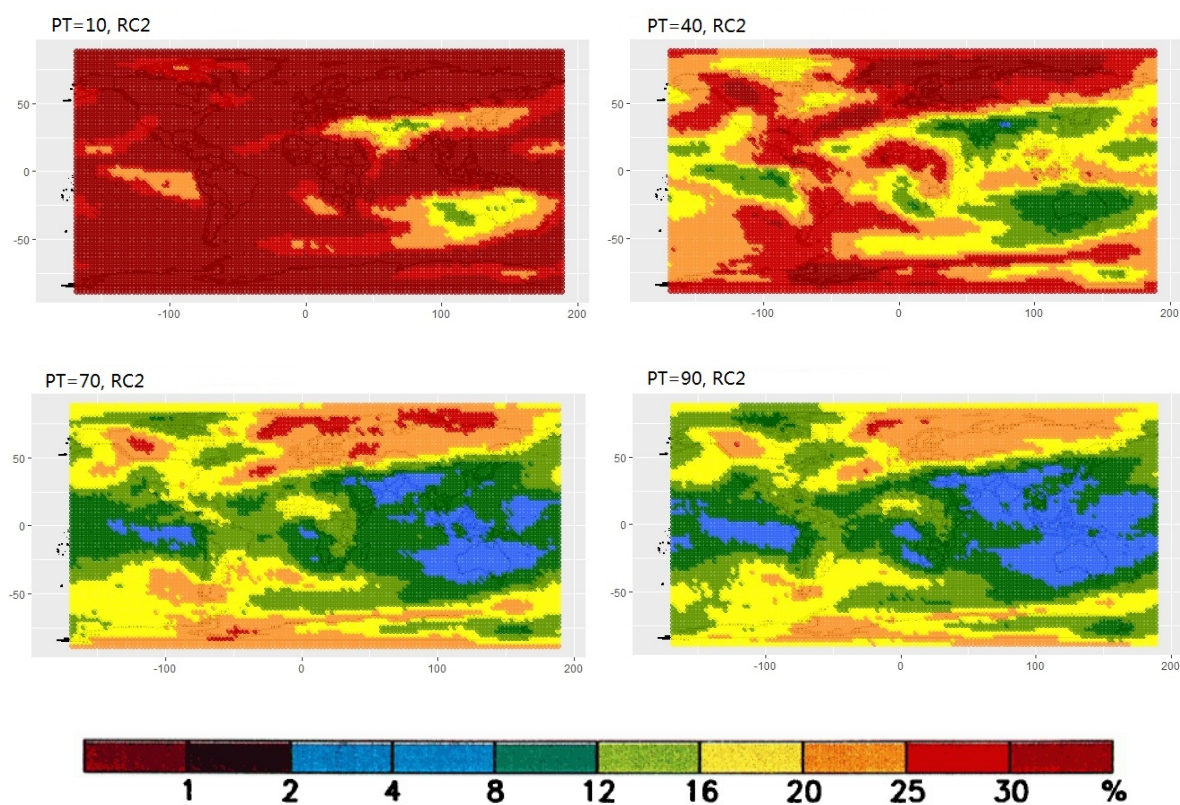


Figure A.1: CFR Frequency 200hPa RC2

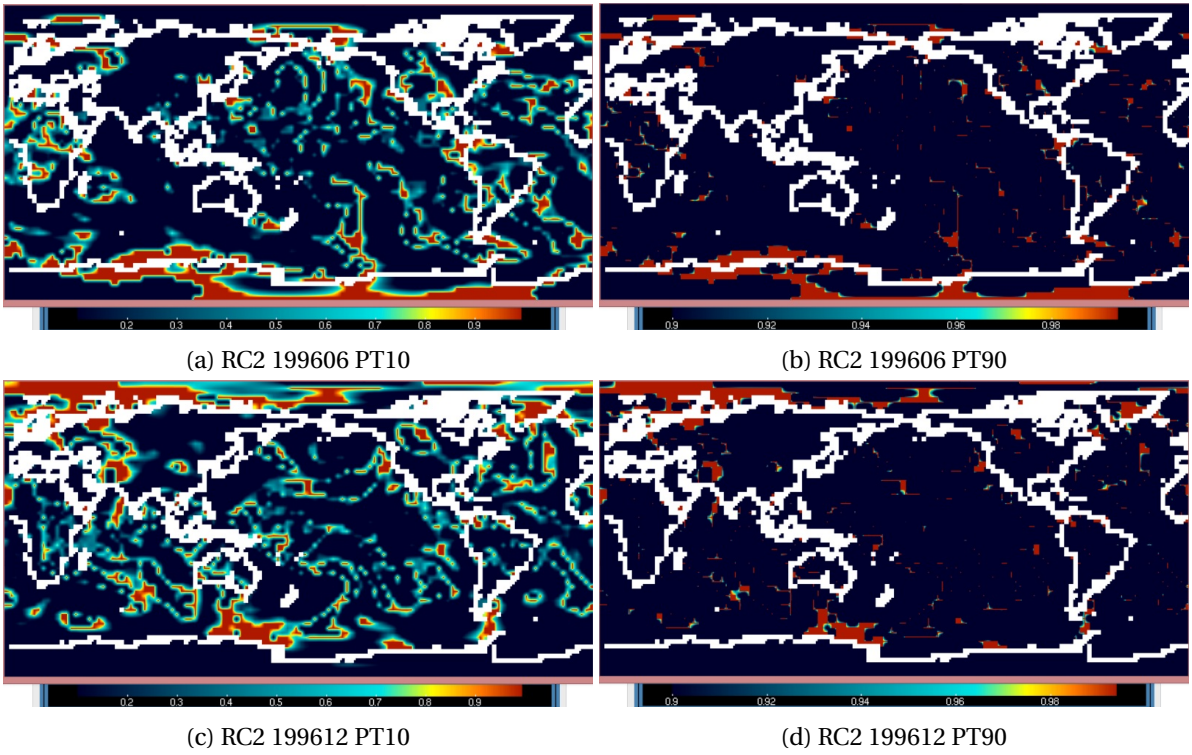


Figure A.2: RC2 PT10 and PT90 comparison of two different months in 1996

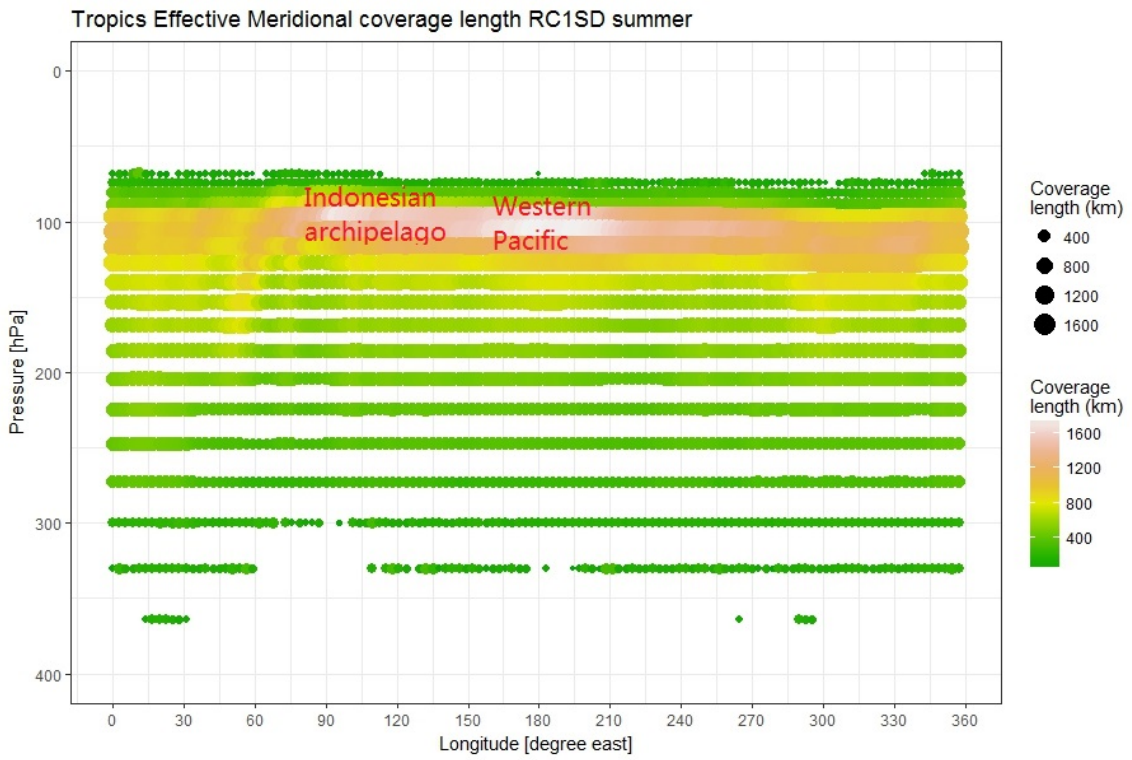


Figure A.3: Effective Meridional coverage length in Summer

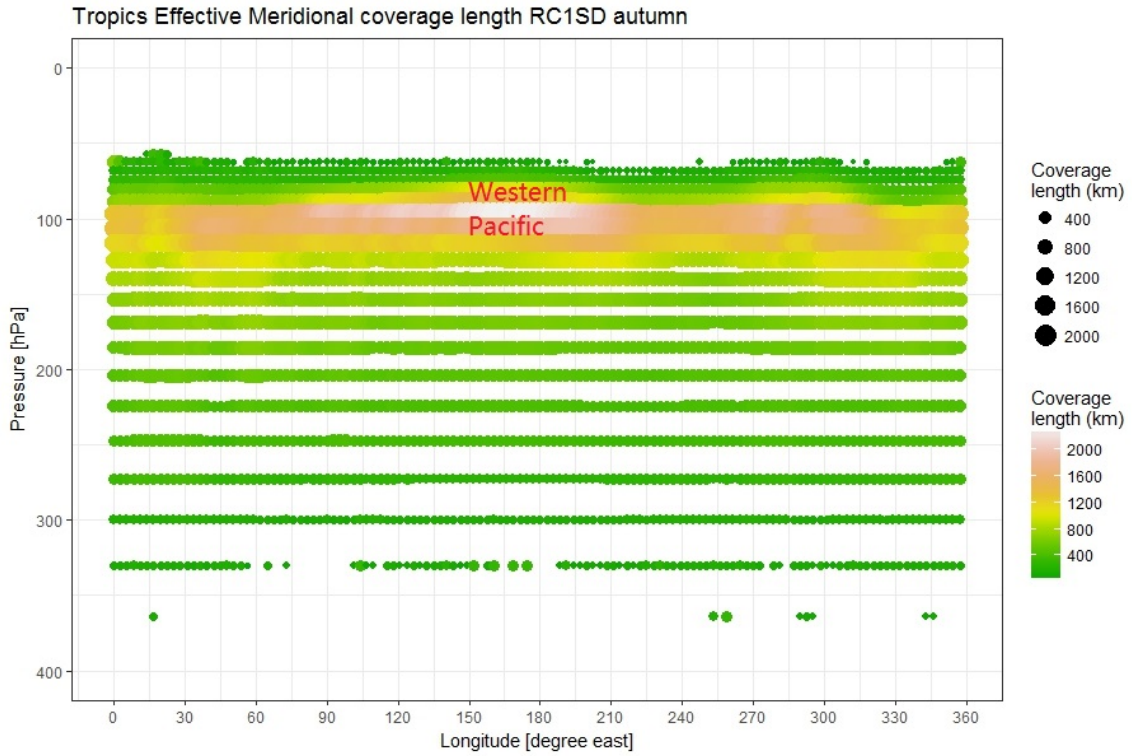


Figure A.4: Effective Meridional coverage length in Autumn

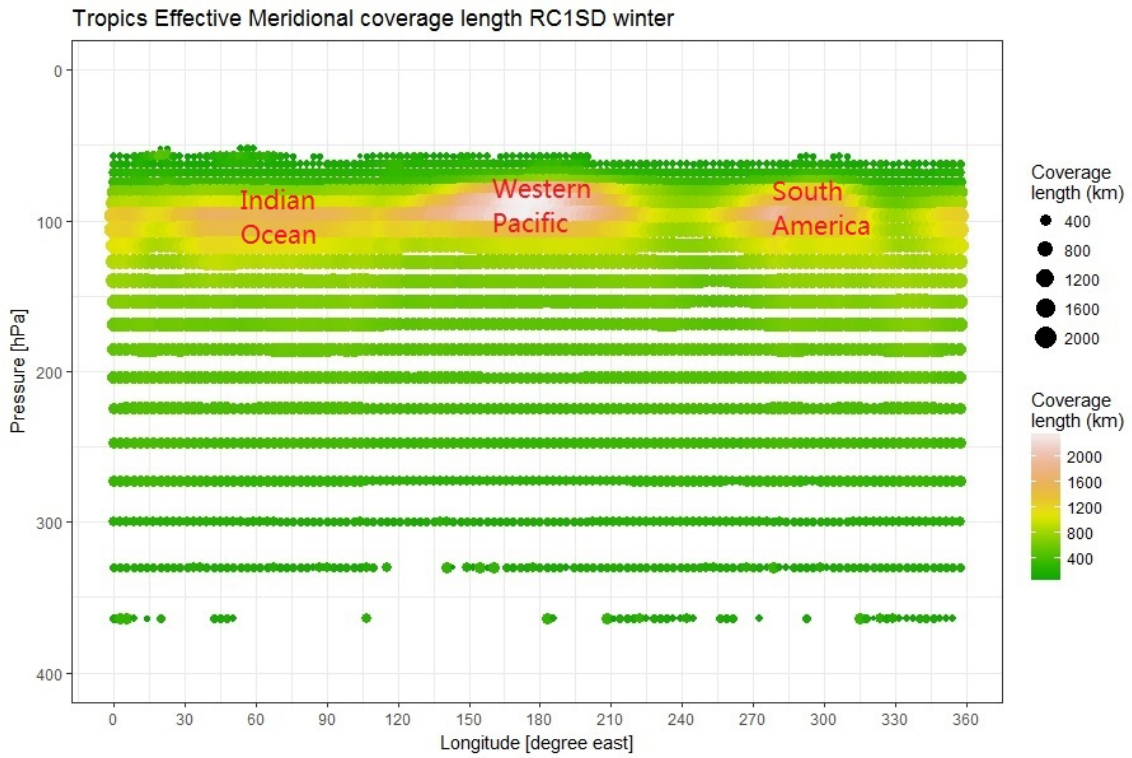


Figure A.5: Effective Meridional coverage length in Winter



# B

## Appendix

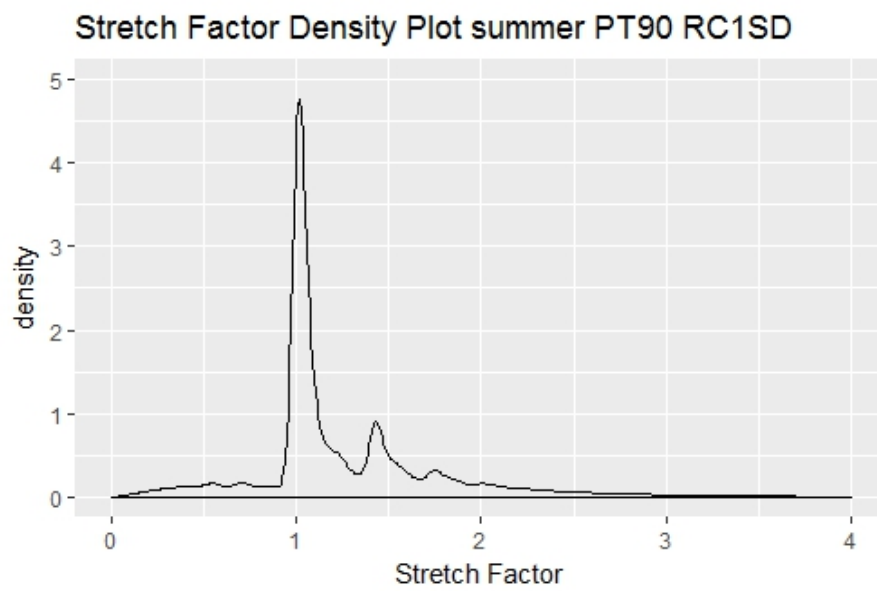


Figure B.1: PDF of CFRs' Stretch factor in horizontal plane NH mid-latitude summer

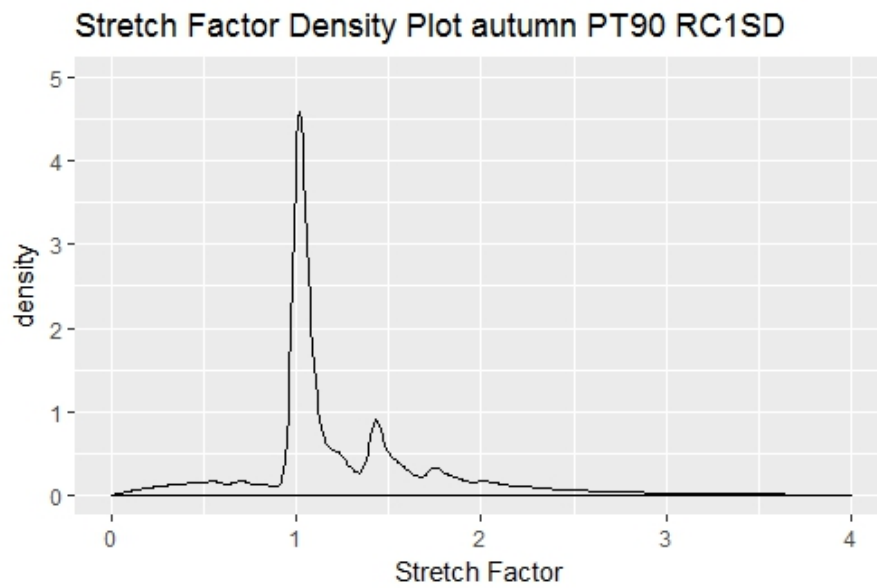


Figure B.2: PDF of CFRs' Stretch factor in horizontal plane NH mid-latitude autumn

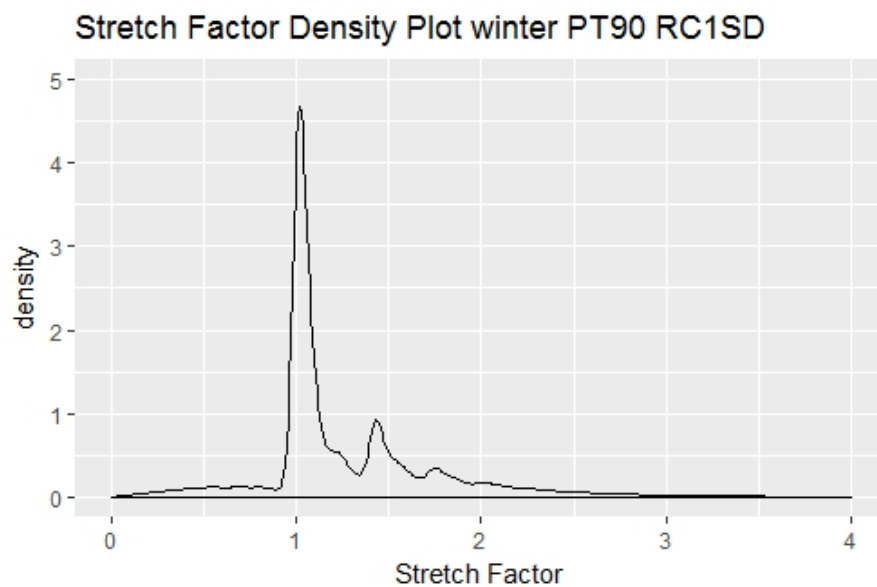


Figure B.3: PDF of CFRs' Stretch factor in horizontal plane NH mid-latitude winter

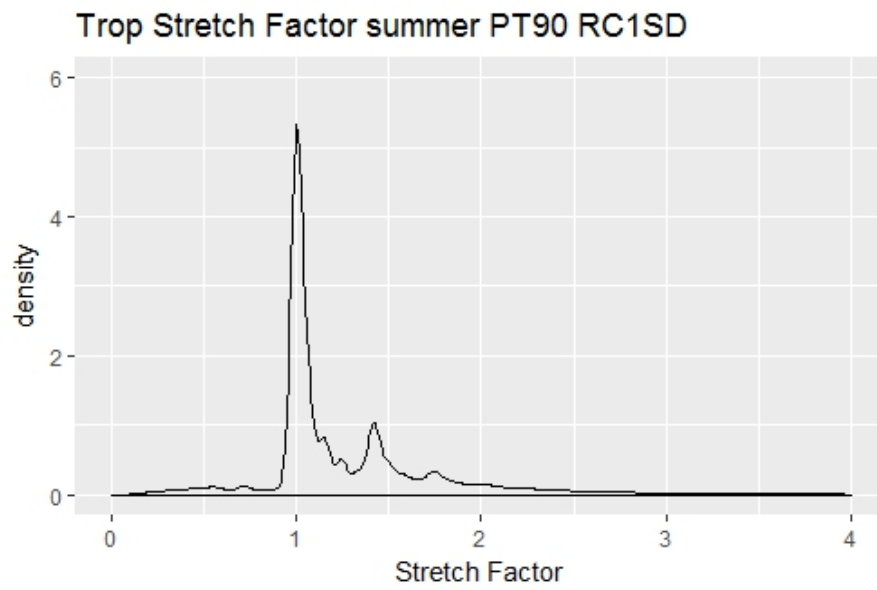


Figure B.4: PDF of CFRs' Stretch factor in horizontal plane Tropics summer

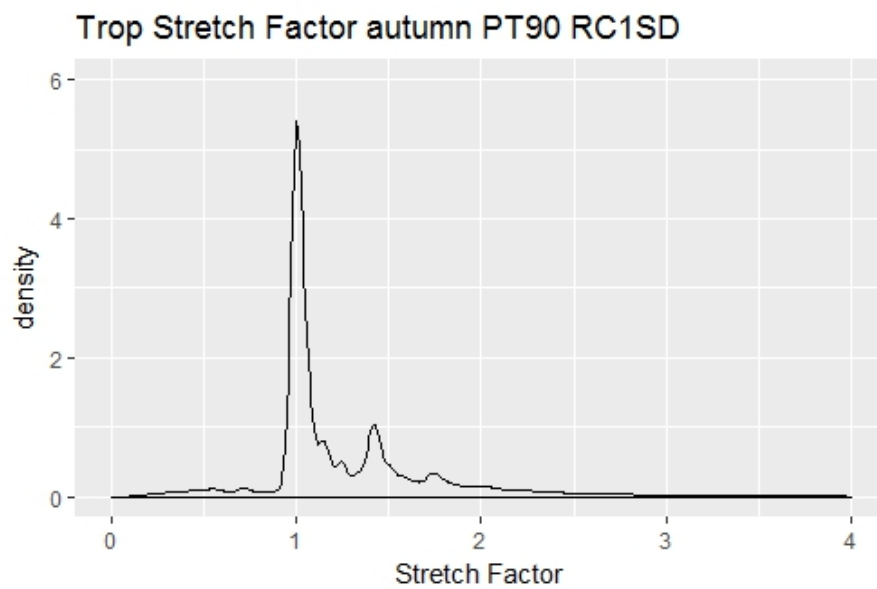


Figure B.5: PDF of CFRs' Stretch factor in horizontal plane Tropics autumn

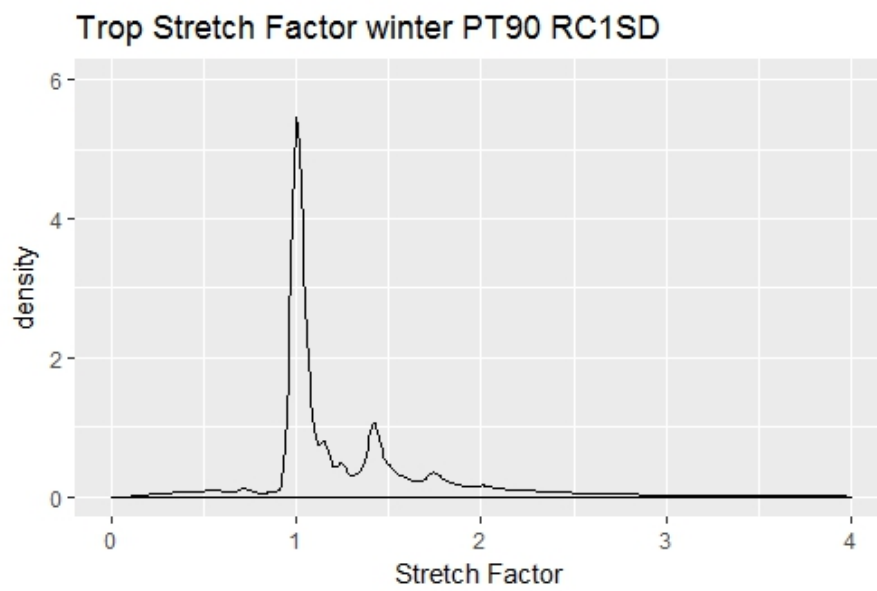


Figure B.6: PDF of CFRs' Stretch factor in horizontal plane Tropics winter

Table B.1: Grid Stretch factor in the vertical plane

level	ph(hpa)	height(km)	grid height (km)	1 grid stre_fac	2 grids stre_fac	2grid/1grid stre_fac
1.000	0.010	39.370	1.223	7.862	11.096	1.411
2.000	0.032	38.147	0.747	10.044	14.186	1.412
3.000	0.058	37.400	0.594	11.261	15.909	1.413
4.000	0.090	36.806	0.520	12.033	17.002	1.413
5.000	0.127	36.286	0.469	12.665	17.896	1.413
6.000	0.172	35.817	0.431	13.216	18.677	1.413
7.000	0.223	35.386	0.406	13.615	19.241	1.413
8.000	0.281	34.981	0.389	13.900	19.644	1.413
9.000	0.349	34.591	0.378	14.097	19.924	1.413
10.000	0.426	34.213	0.367	14.319	20.237	1.413
11.000	0.514	33.846	0.355	14.559	20.577	1.413
12.000	0.613	33.492	0.343	14.803	20.923	1.413
13.000	0.722	33.149	0.332	15.051	21.274	1.413
14.000	0.842	32.817	0.323	15.248	21.552	1.413
15.000	0.974	32.493	0.317	15.400	21.768	1.413
16.000	1.120	32.177	0.312	15.516	21.932	1.413
17.000	1.280	31.864	0.309	15.600	22.051	1.413
18.000	1.456	31.556	0.307	15.658	22.132	1.413
19.000	1.649	31.249	0.305	15.692	22.180	1.413
20.000	1.862	30.944	0.303	15.741	22.250	1.413
21.000	2.096	30.641	0.301	15.803	22.338	1.414
22.000	2.350	30.340	0.299	15.845	22.397	1.414
23.000	2.627	30.040	0.298	15.868	22.430	1.414
24.000	2.929	29.742	0.298	15.876	22.441	1.414
25.000	3.258	29.444	0.298	15.870	22.432	1.414
26.000	3.616	29.145	0.299	15.851	22.406	1.414
27.000	4.007	28.846	0.300	15.822	22.364	1.414
28.000	4.433	28.546	0.302	15.783	22.309	1.414
29.000	4.898	28.244	0.304	15.735	22.242	1.413
30.000	5.404	27.941	0.305	15.704	22.197	1.413
31.000	5.954	27.636	0.306	15.684	22.170	1.413
32.000	6.551	27.331	0.307	15.656	22.130	1.413
33.000	7.197	27.024	0.308	15.622	22.082	1.413
34.000	7.897	26.716	0.310	15.574	22.013	1.413
35.000	8.656	26.406	0.312	15.526	21.946	1.413
36.000	9.478	26.094	0.314	15.470	21.867	1.413
37.000	10.369	25.780	0.317	15.409	21.780	1.413
38.000	11.334	25.464	0.319	15.344	21.688	1.413
39.000	12.380	25.144	0.322	15.274	21.589	1.413
40.000	13.514	24.822	0.325	15.201	21.485	1.413
41.000	14.742	24.497	0.329	15.124	21.377	1.413
42.000	16.074	24.168	0.332	15.045	21.265	1.413
43.000	17.516	23.836	0.336	14.963	21.149	1.413
44.000	19.080	23.501	0.339	14.881	21.033	1.413
45.000	20.773	23.161	0.343	14.798	20.915	1.413

Table B.1: Grid Stretch factor in the vertical plane

level	ph(hpa)	height(km)	grid height (km)	1 grid stre_fac	2 grids stre_fac	2grid/1grid stre_fac
46.000	22.608	22.818	0.347	14.712	20.794	1.413
47.000	24.595	22.471	0.352	14.624	20.669	1.413
48.000	26.748	22.119	0.356	14.533	20.540	1.413
49.000	29.082	21.763	0.361	14.439	20.408	1.413
50.000	31.611	21.402	0.367	14.321	20.240	1.413
51.000	34.362	21.036	0.374	14.180	20.041	1.413
52.000	37.364	20.662	0.381	14.046	19.852	1.413
53.000	40.640	20.281	0.389	13.907	19.655	1.413
54.000	44.217	19.892	0.398	13.753	19.437	1.413
55.000	48.134	19.494	0.386	13.960	19.729	1.413
56.000	52.200	19.109	0.438	13.111	18.529	1.413
57.000	57.143	18.671	0.427	13.276	18.762	1.413
58.000	62.322	18.244	0.437	13.115	18.533	1.413
59.000	68.017	17.807	0.447	12.972	18.331	1.413
60.000	74.268	17.360	0.456	12.844	18.150	1.413
61.000	81.115	16.904	0.466	12.704	17.952	1.413
62.000	88.634	16.438	0.478	12.544	17.725	1.413
63.000	96.923	15.960	0.491	12.377	17.490	1.413
64.000	106.080	15.468	0.505	12.211	17.254	1.413
65.000	116.207	14.964	0.519	12.039	17.011	1.413
66.000	127.428	14.444	0.534	11.869	16.771	1.413
67.000	139.874	13.910	0.549	11.711	16.547	1.413
68.000	153.665	13.361	0.563	11.568	16.345	1.413
69.000	168.923	12.799	0.575	11.442	16.165	1.413
70.000	185.769	12.224	0.588	11.317	15.989	1.413
71.000	204.369	11.636	0.596	11.244	15.885	1.413
72.000	224.722	11.040	0.618	11.039	15.595	1.413
73.000	247.547	10.422	0.625	10.975	15.505	1.413
74.000	272.513	9.797	0.637	10.875	15.363	1.413
75.000	300.003	9.160	0.649	10.770	15.215	1.413
76.000	330.299	8.511	0.662	10.665	15.066	1.413
77.000	363.704	7.848	0.675	10.562	14.920	1.413
78.000	400.531	7.173	0.688	10.461	14.777	1.413
79.000	441.126	6.485	0.701	10.368	14.646	1.413
80.000	485.814	5.784	0.713	10.277	14.517	1.413
81.000	534.998	5.070	0.726	10.190	14.394	1.413
82.000	589.091	4.344	0.737	10.111	14.281	1.412
83.000	648.492	3.607	0.749	10.031	14.168	1.412
84.000	713.725	2.858	0.752	10.013	14.142	1.412
85.000	784.442	2.106	0.718	10.246	14.473	1.413
86.000	857.150	1.388	0.592	11.282	15.940	1.413
87.000	921.085	0.797	0.408	13.578	19.189	1.413
88.000	967.381	0.389	0.241	17.641	24.937	1.414
89.000	995.653	0.147	0.147	22.564	31.902	1.414

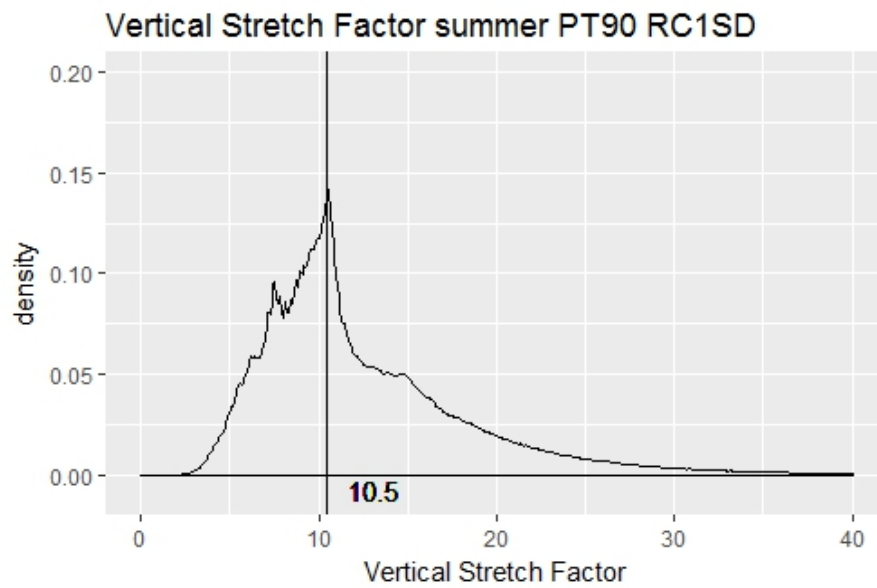


Figure B.7: PDF of CFRs' Stretch factor in vertical plane NH mid-latitude summer

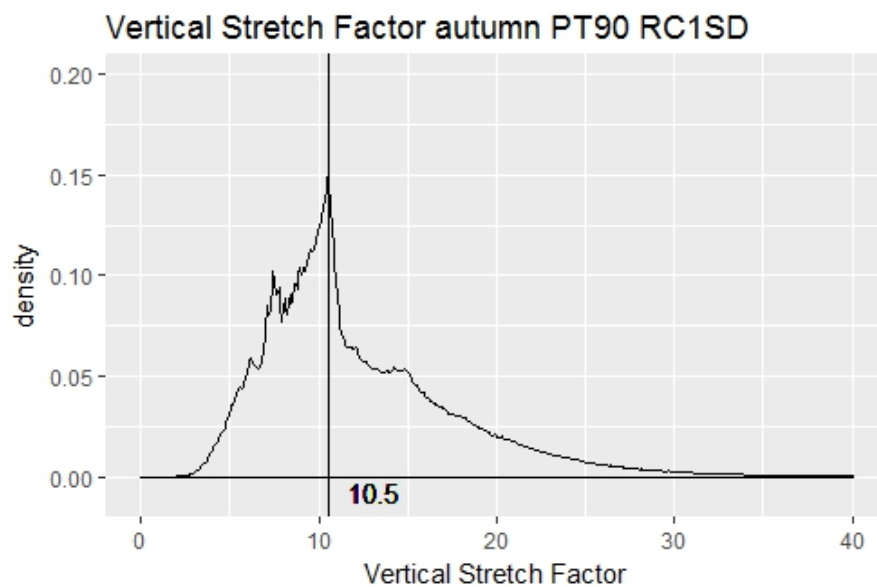


Figure B.8: PDF of CFRs' Stretch factor in vertical plane NH mid-latitude autumn

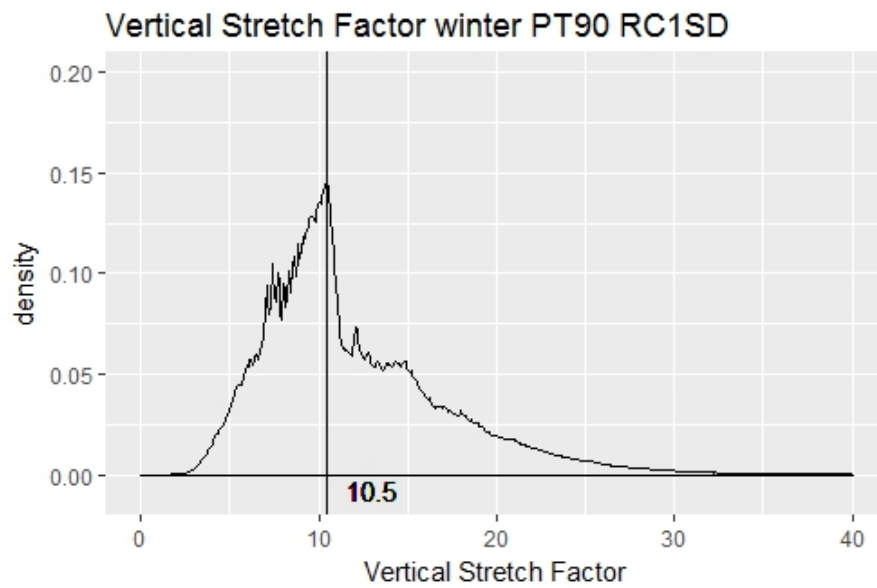


Figure B.9: PDF of CFRs' Stretch factor in vertical plane NH mid-latitude winter

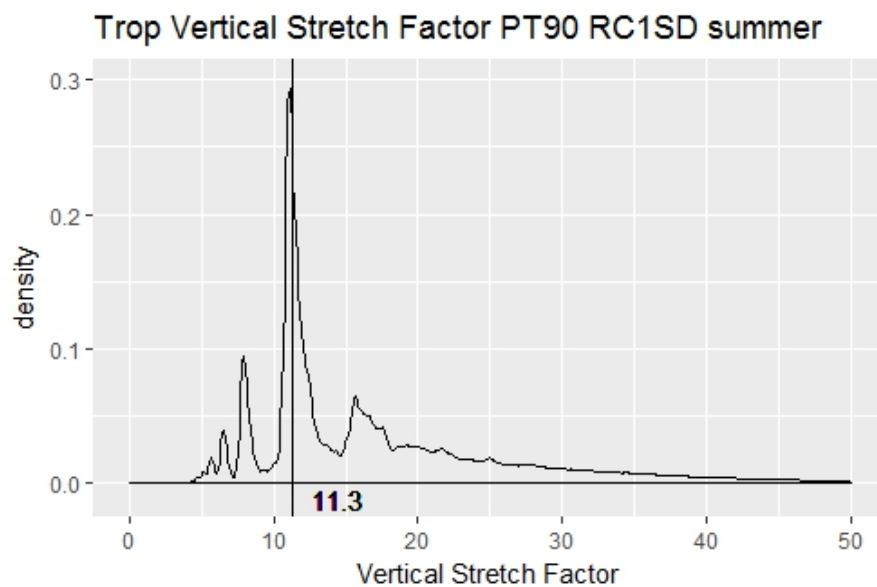


Figure B.10: PDF of CFRs' Stretch factor in vertical plane Tropics summer

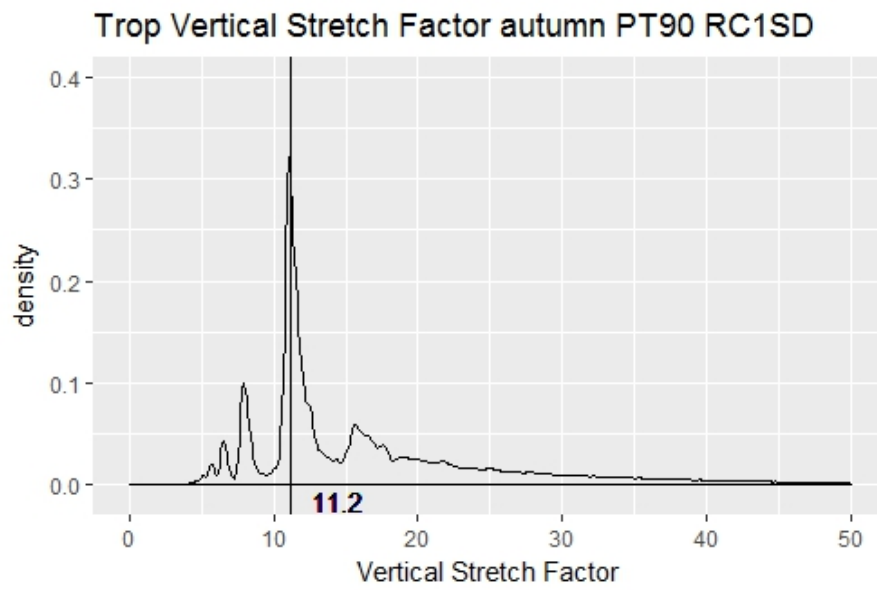


Figure B.11: PDF of CFRs' Stretch factor in vertical plane Tropics autumn

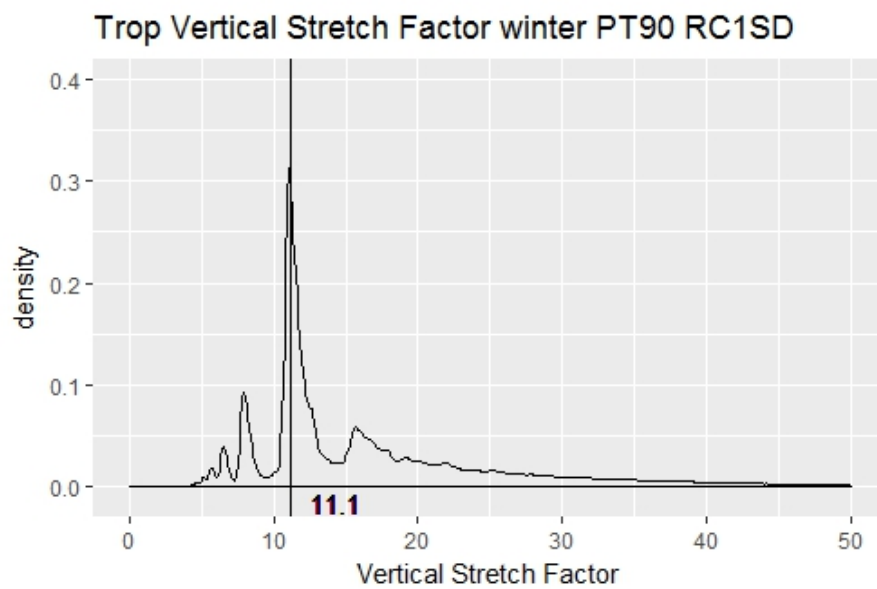


Figure B.12: PDF of CFRs' Stretch factor in vertical plane Tropics winter

Mid-lat ISSRs angle density RC1SD PT90 autumn

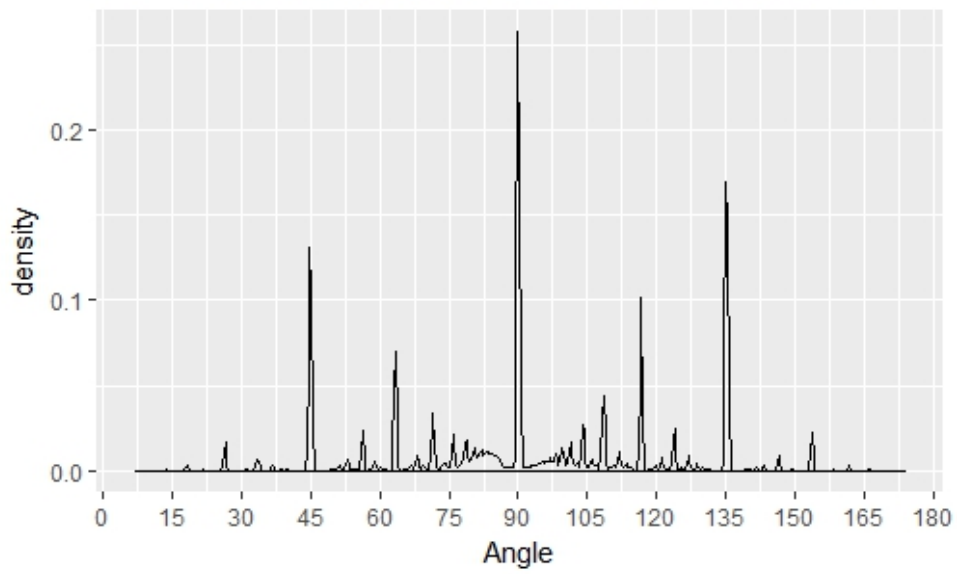


Figure B.13: Direction in horizontal plane NH midlatitude autumn

Mid-lat ISSRs angle density RC1SD PT90 winter

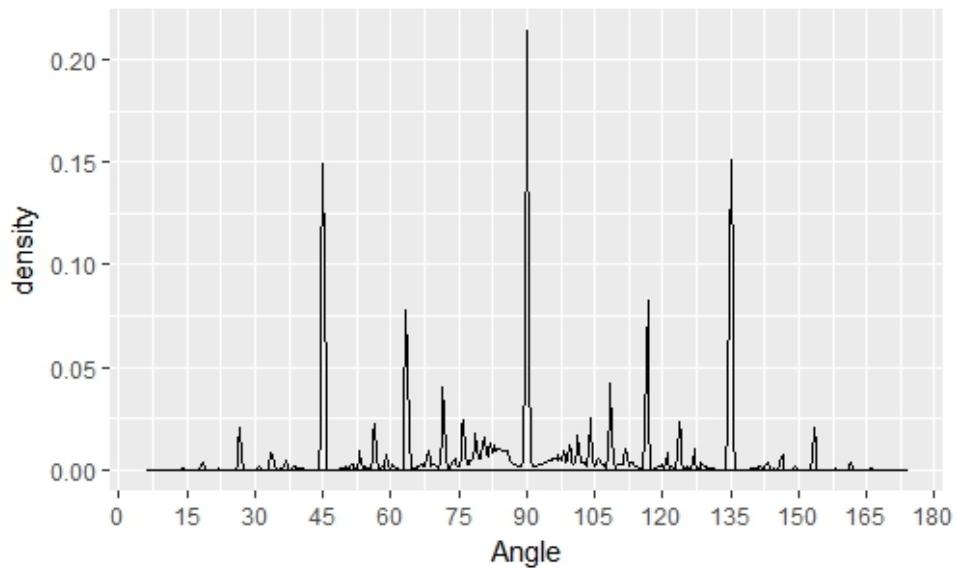


Figure B.14: Direction in horizontal plane NH midlatitude winter

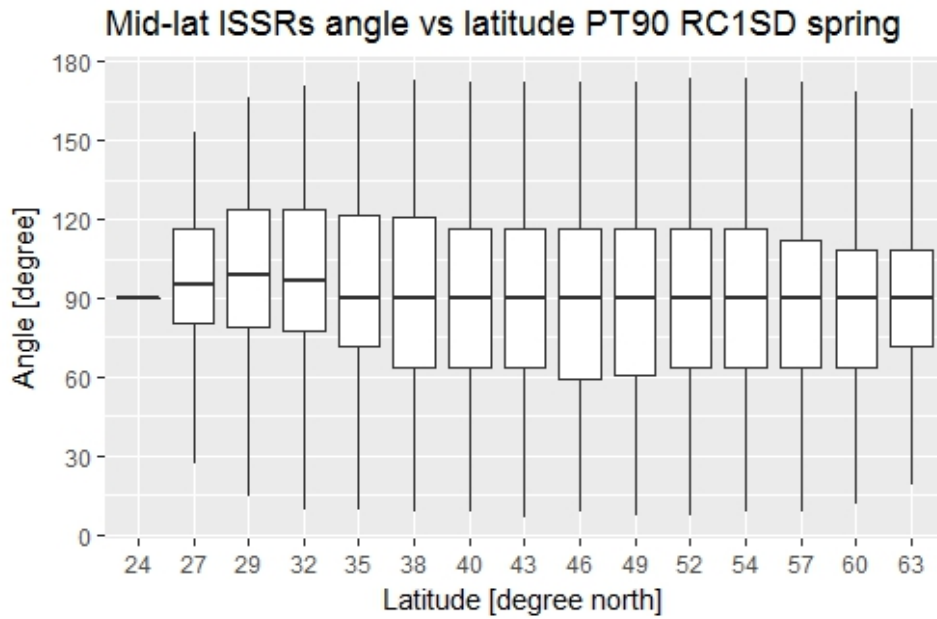


Figure B.15: CFR Direction boxplot in horizontal plane NH mid-latitude spring

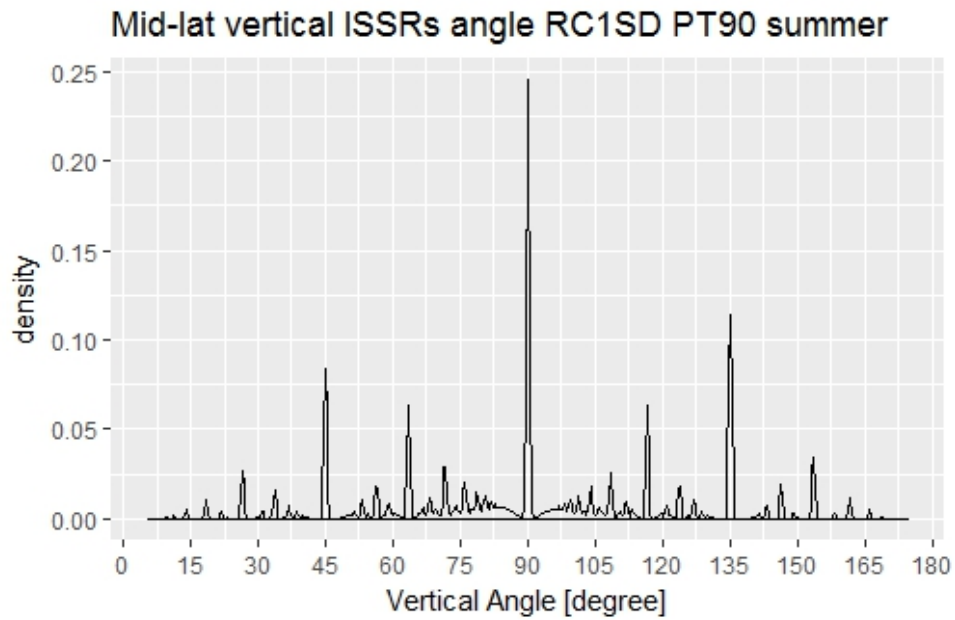


Figure B.16: CFR Direction boxplot in horizontal plane NH midlatitude summer

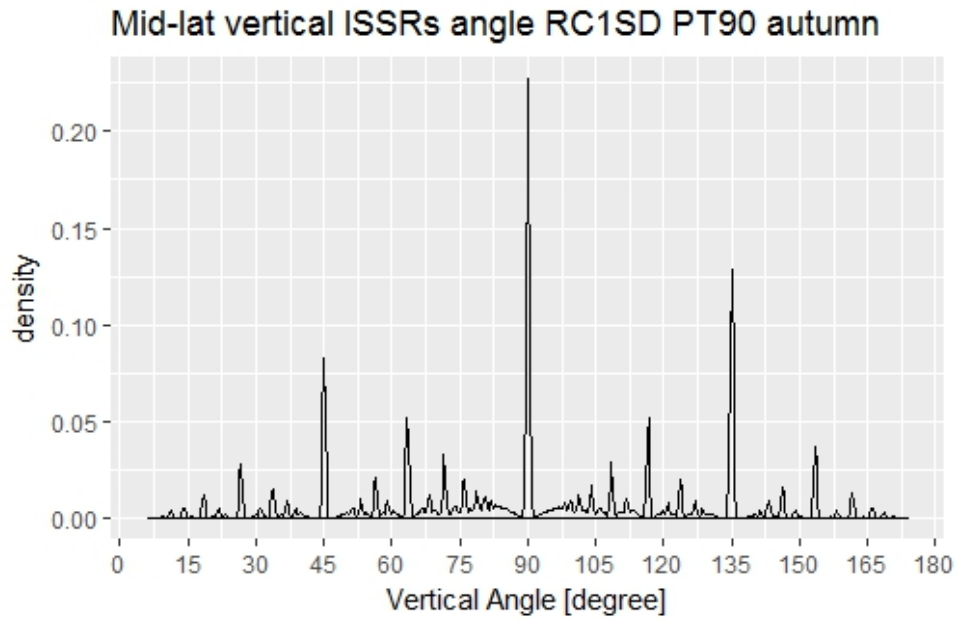


Figure B.17: CFR Direction boxplot in horizontal plane NH midlatitude autumn

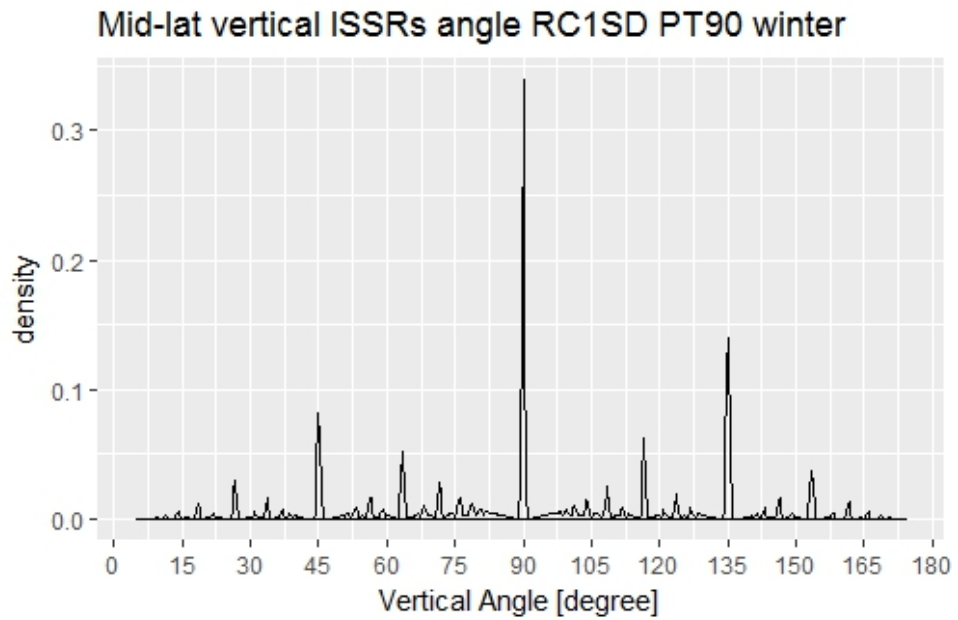


Figure B.18: CFR Direction boxplot in horizontal plane NH midlatitude winter

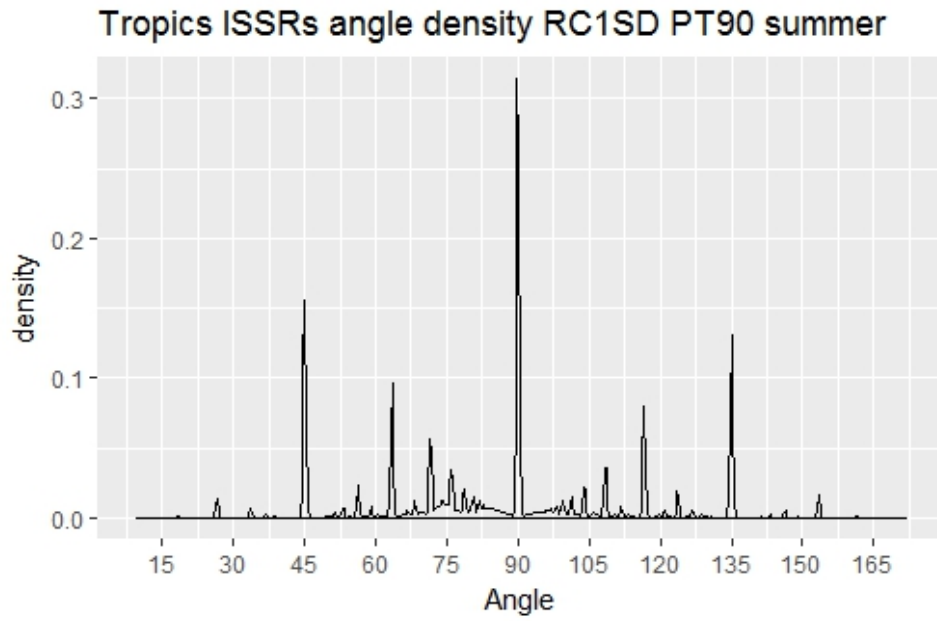


Figure B.19: PDF of CFRs' Direction in horizontal plane Tropics summer

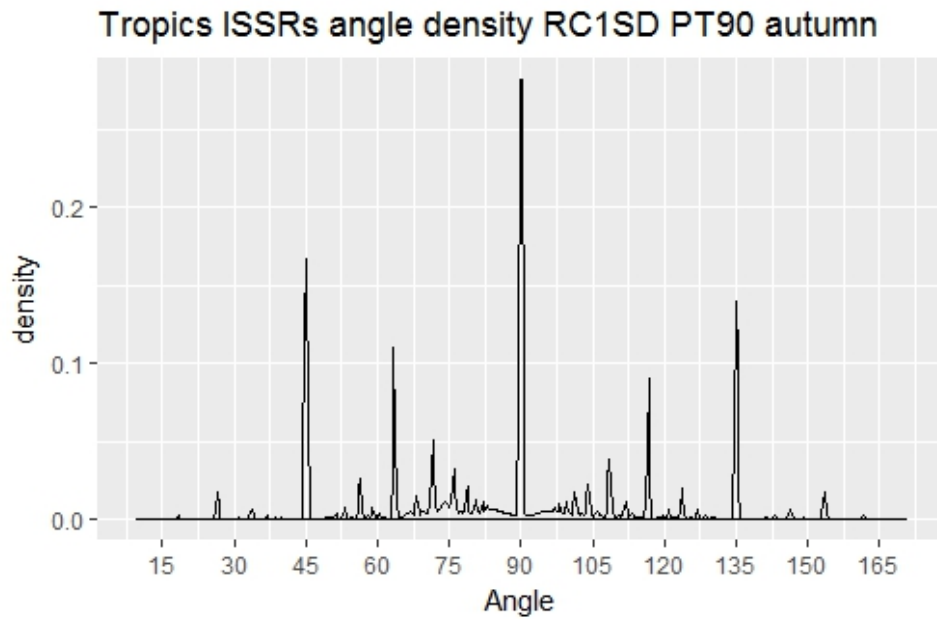


Figure B.20: PDF of CFRs' Direction in horizontal plane Tropics autumn

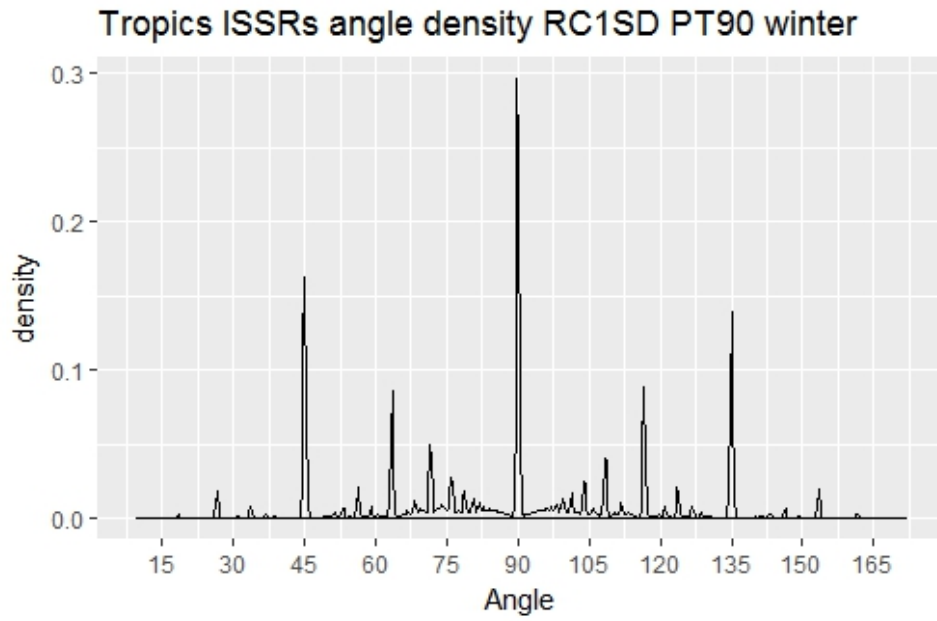


Figure B.21: PDF of CFRs' Direction in horizontal plane Tropics winter

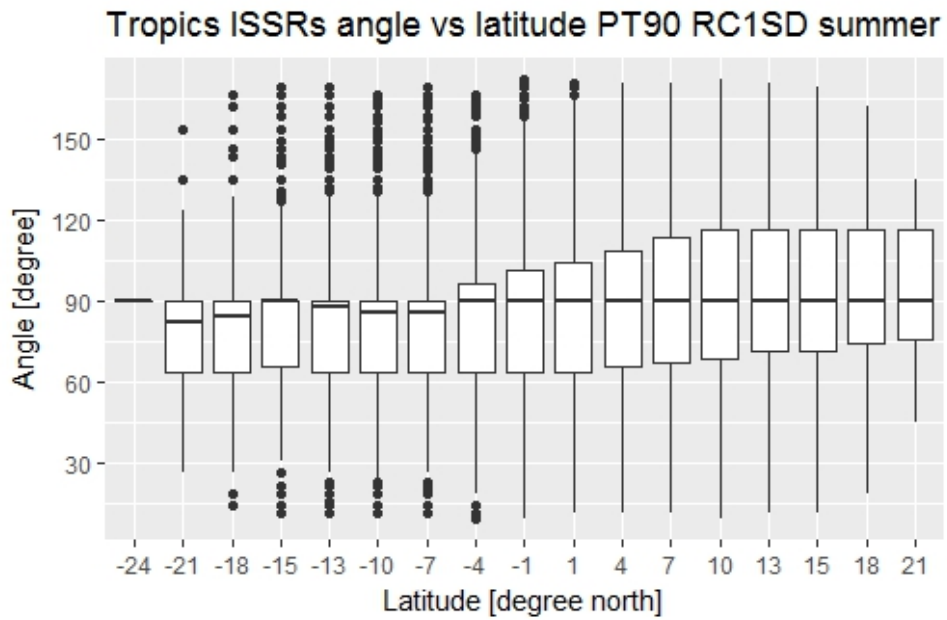


Figure B.22: CFR Direction boxplot in horizontal plane Tropics summer

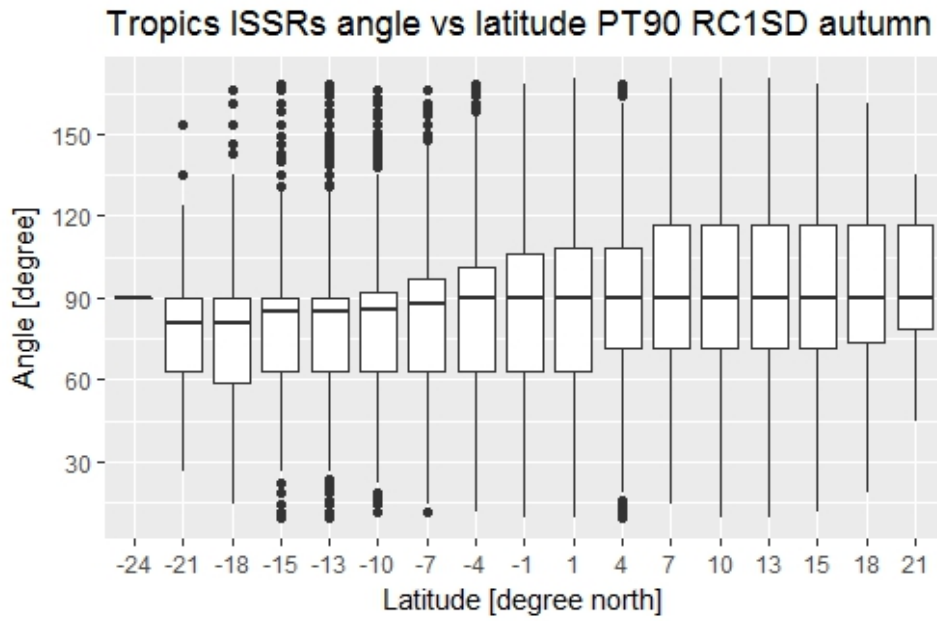


Figure B.23: CFR Direction boxplot in horizontal plane Tropics autumn

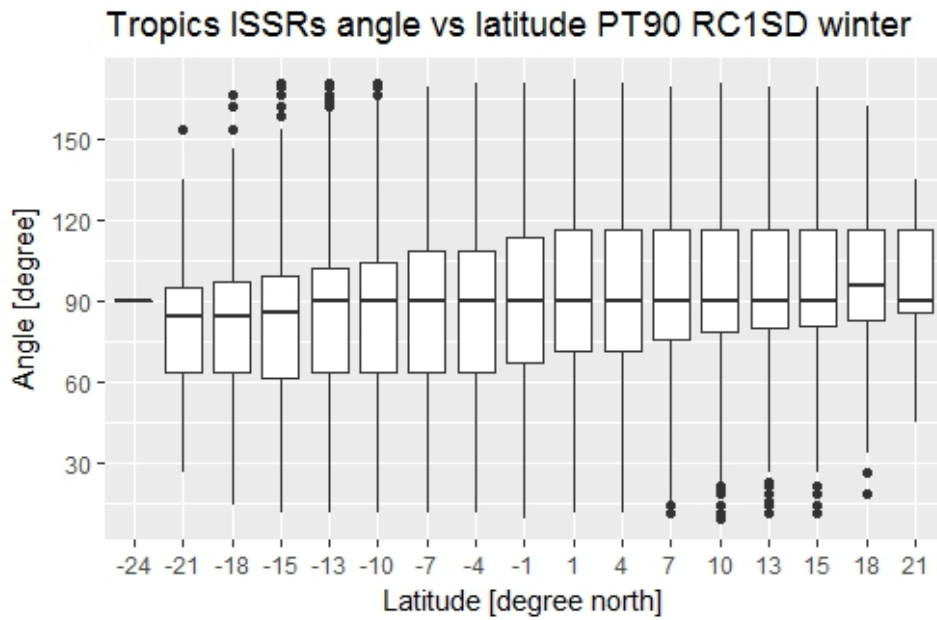


Figure B.24: CFR Direction boxplot in horizontal plane Tropics winter

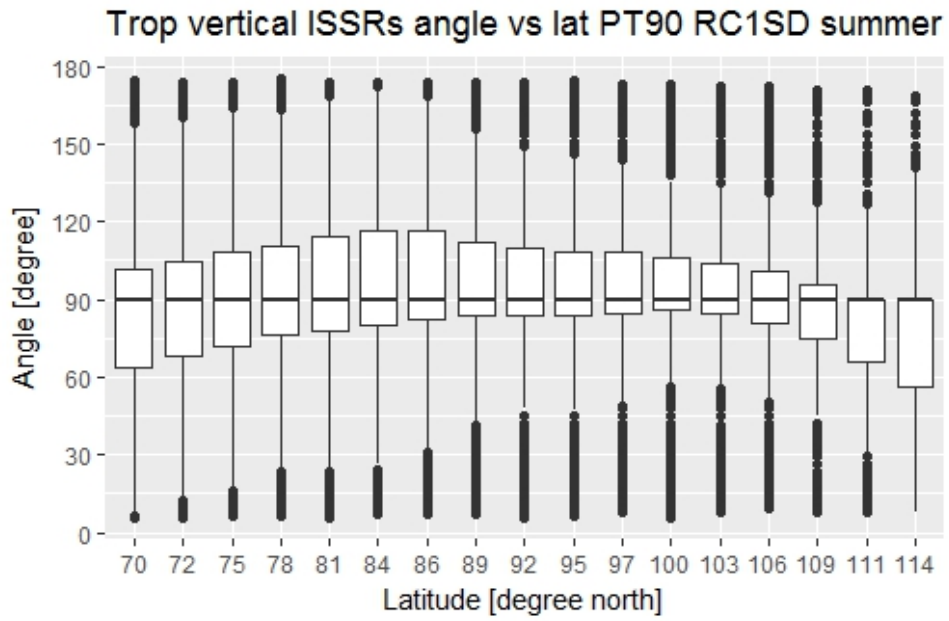


Figure B.25: CFR Direction boxplot in horizontal plane Tropics summer

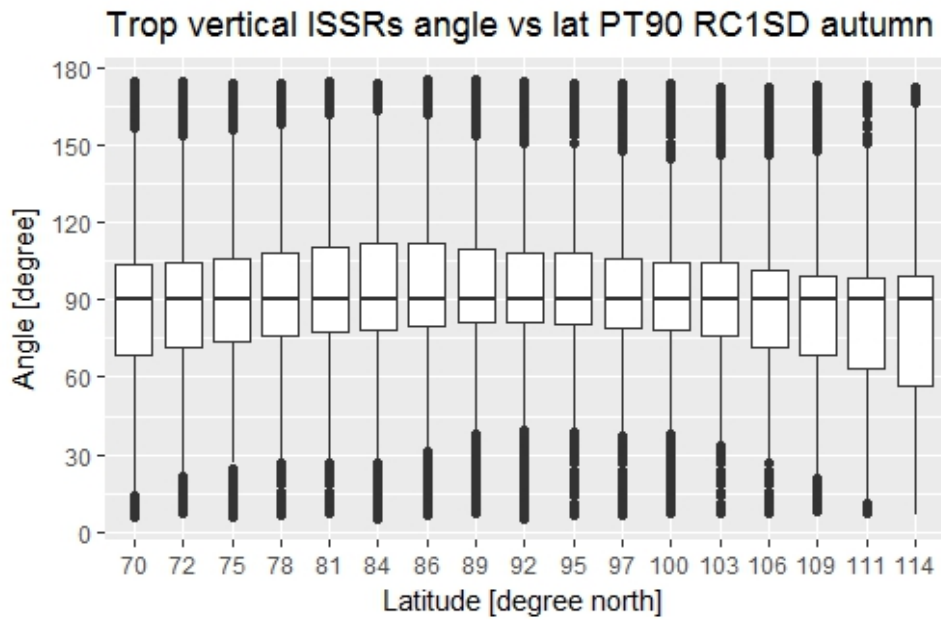


Figure B.26: CFR Direction boxplot in horizontal plane Tropics autumn

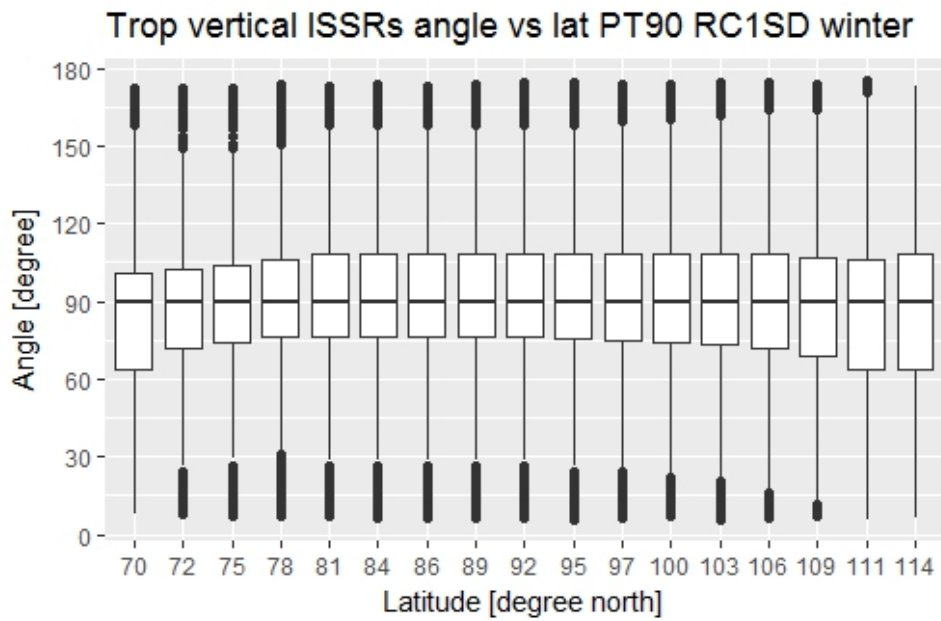


Figure B.27: CFR Direction boxplot in horizontal plane Tropics winter

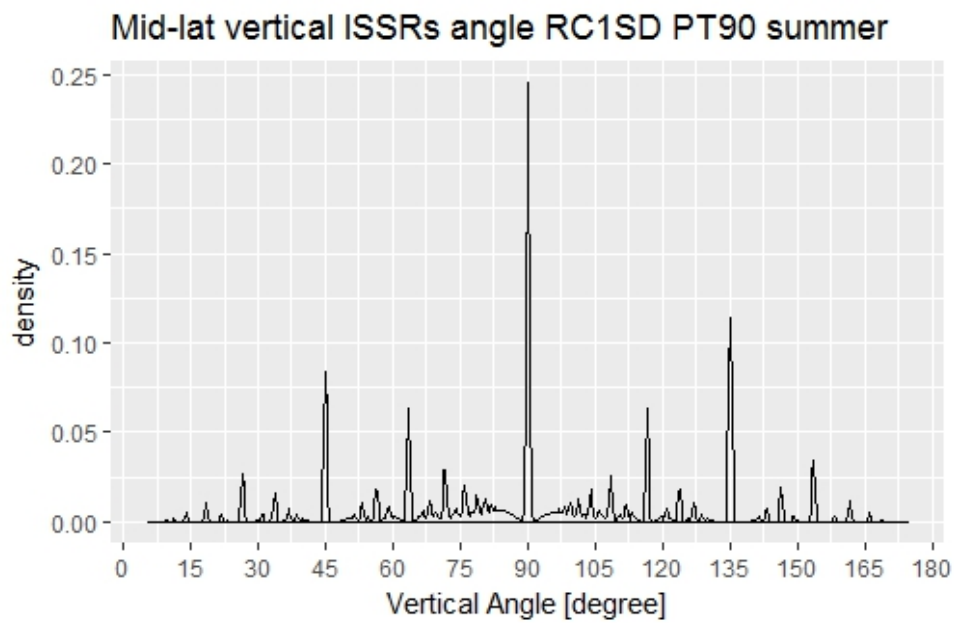


Figure B.28: PDF of CFRs' Direction in vertical plane NH mid-latitude summer

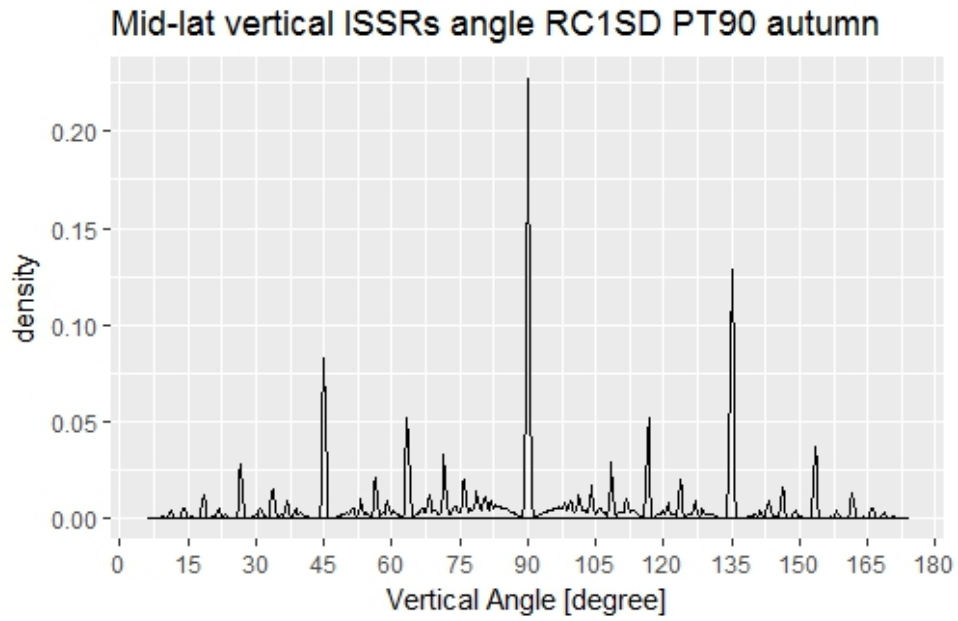


Figure B.29: PDF of CFRs' Direction in vertical plane NH mid-latitude autumn

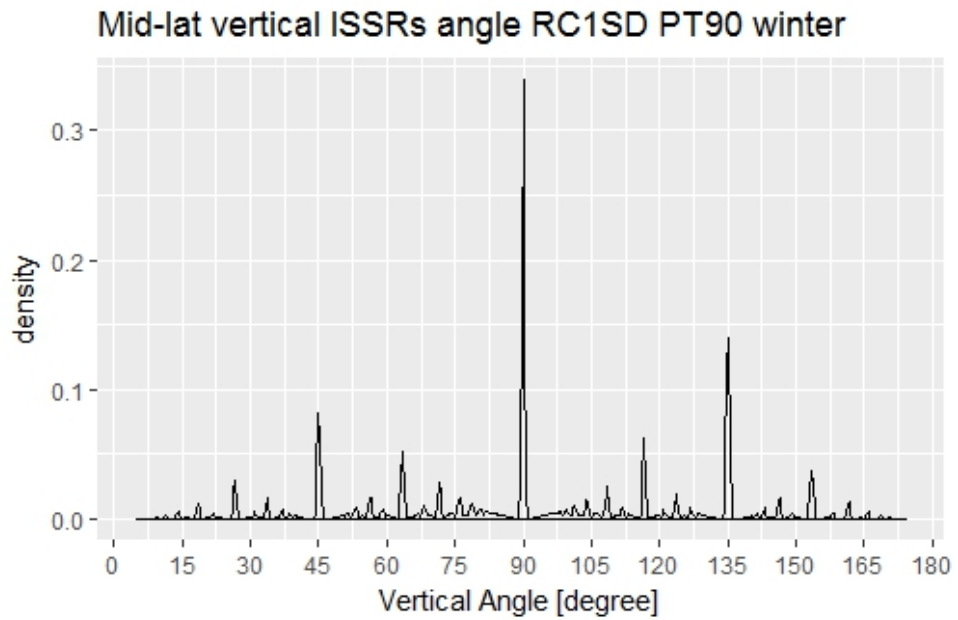


Figure B.30: PDF of CFRs' Direction in vertical plane NH mid-latitude winter

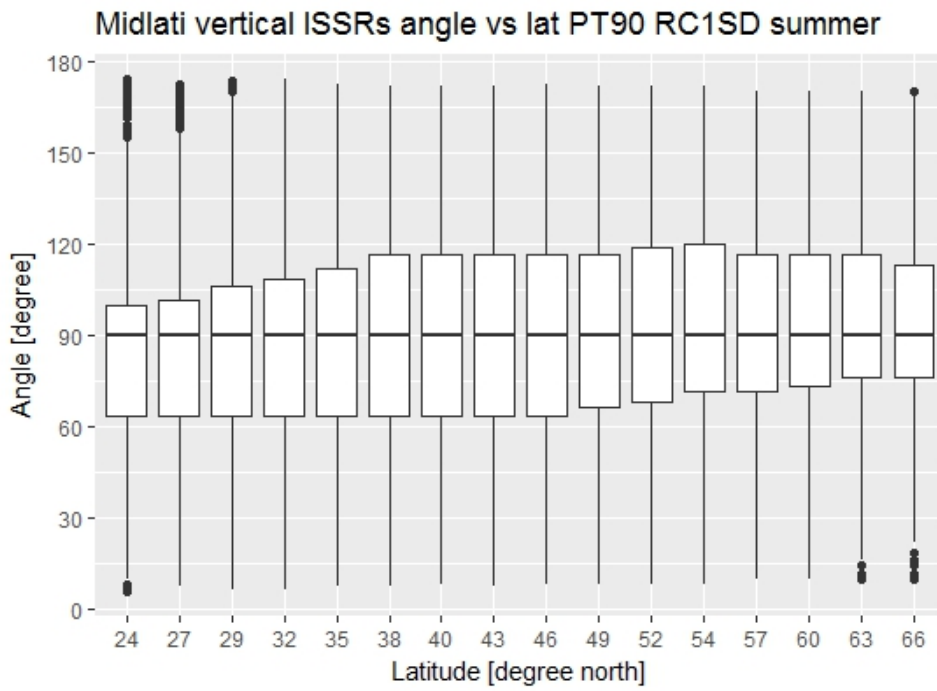


Figure B.31: CFR Direction boxplot in vertical plane NH midlatitude summer

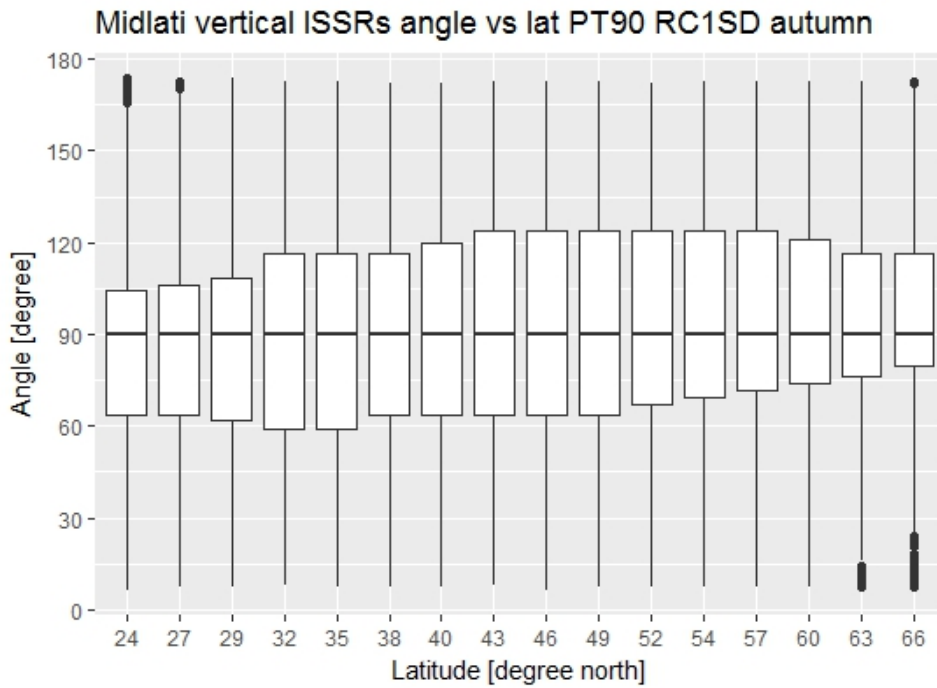


Figure B.32: CFR Direction boxplot in vertical plane NH midlatitude autumn

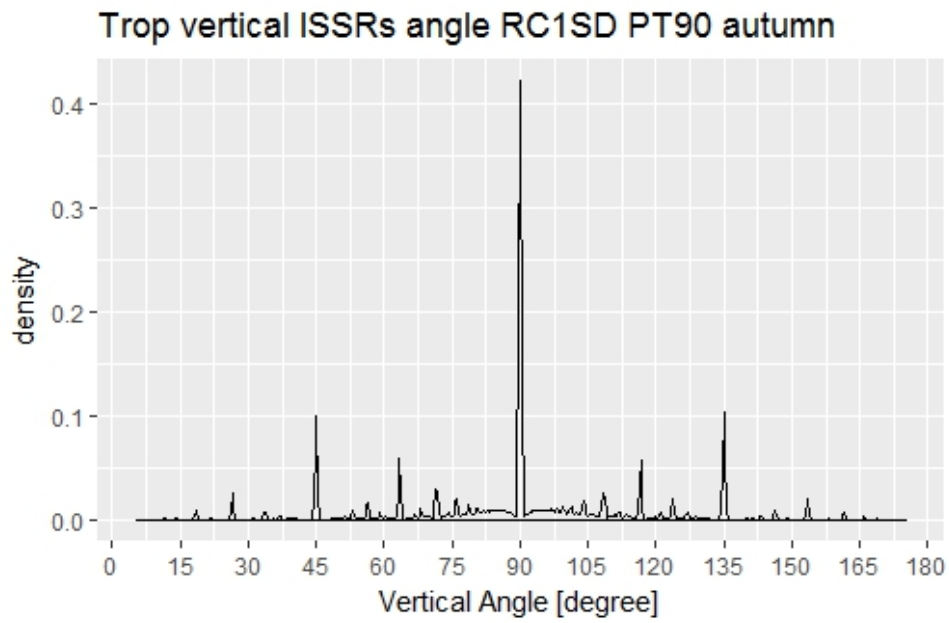


Figure B.33: PDF of CFRs' Direction in vertical plane Tropics autumn

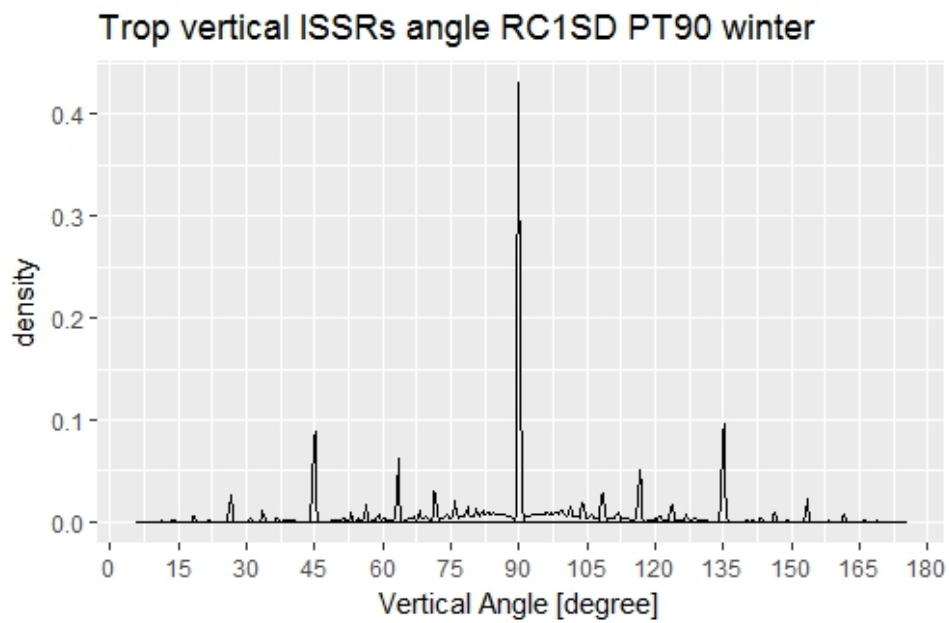


Figure B.34: PDF of CFRs' Direction in vertical plane Tropics winter

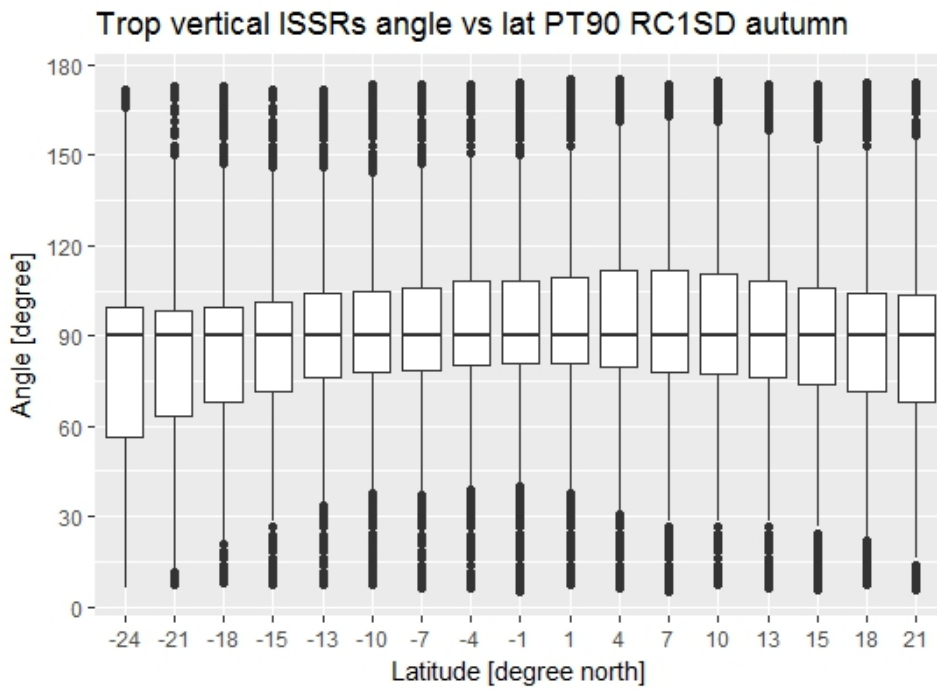


Figure B.35: CFR direction boxplot in vertical plane Tropics autumn

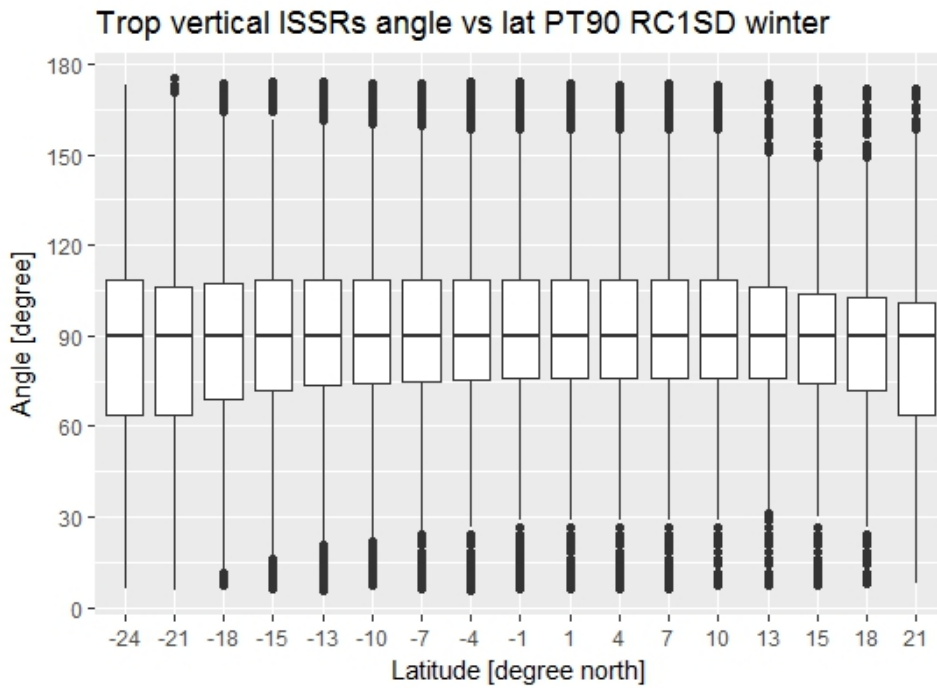


Figure B.36: CFR direction boxplot in vertical plane Tropics winter



# C

## Appendix

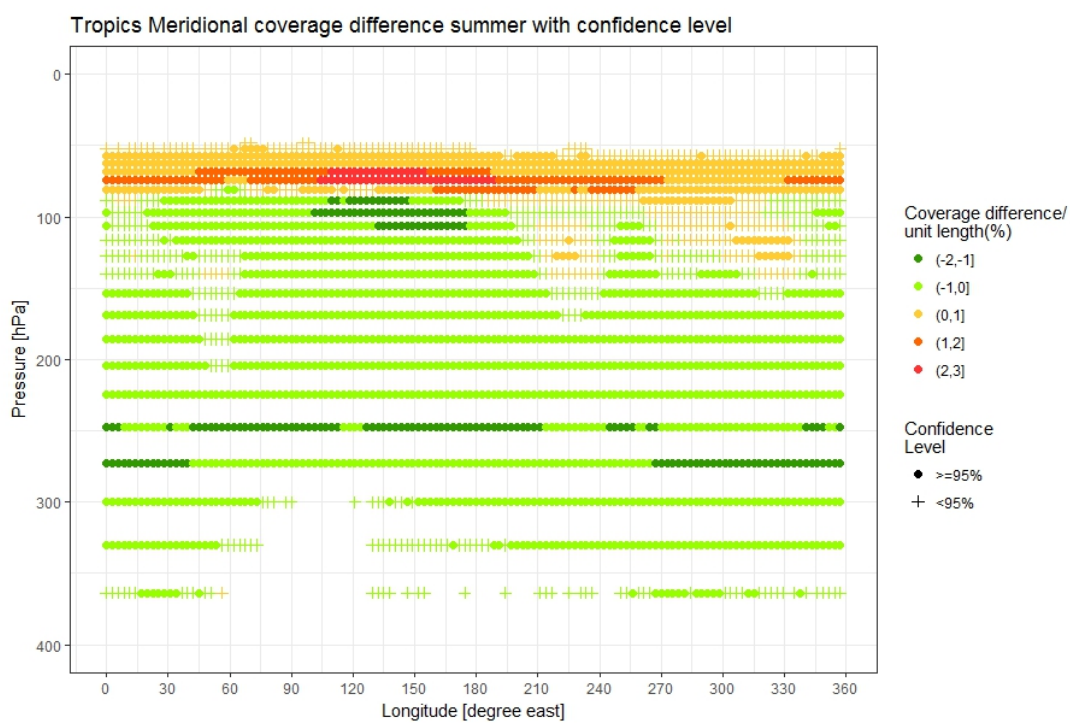


Figure C.1: Meridional mean CFRs coverage length difference in tropics summer

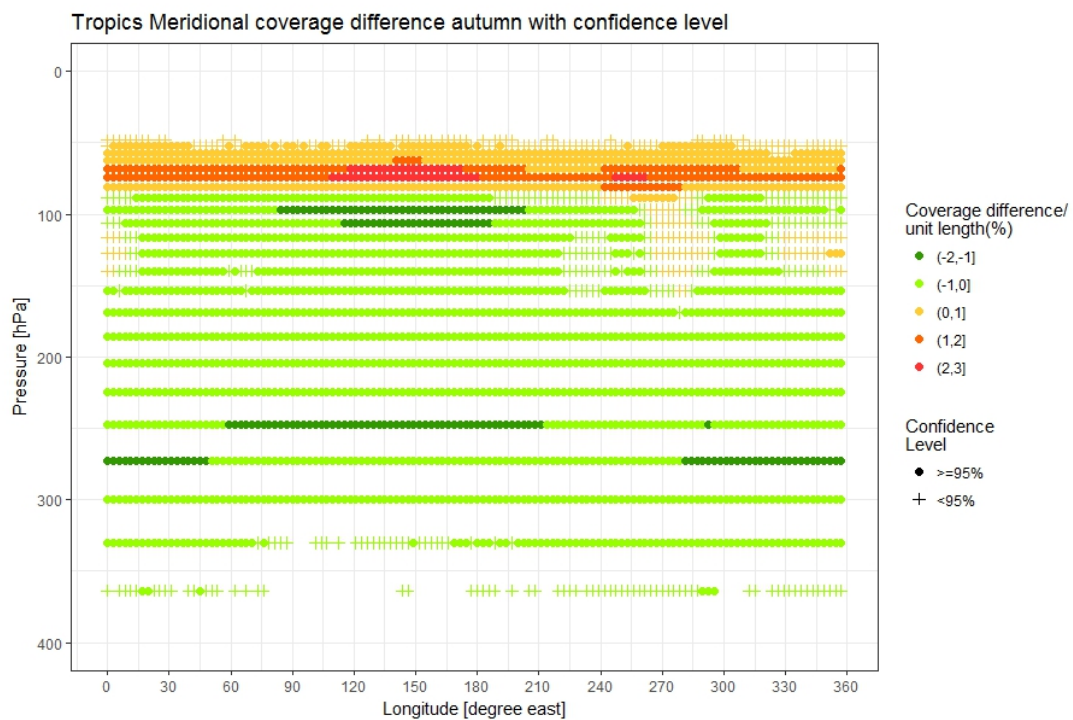


Figure C.2: Meridional mean CFRs coverage length difference in tropics autumn

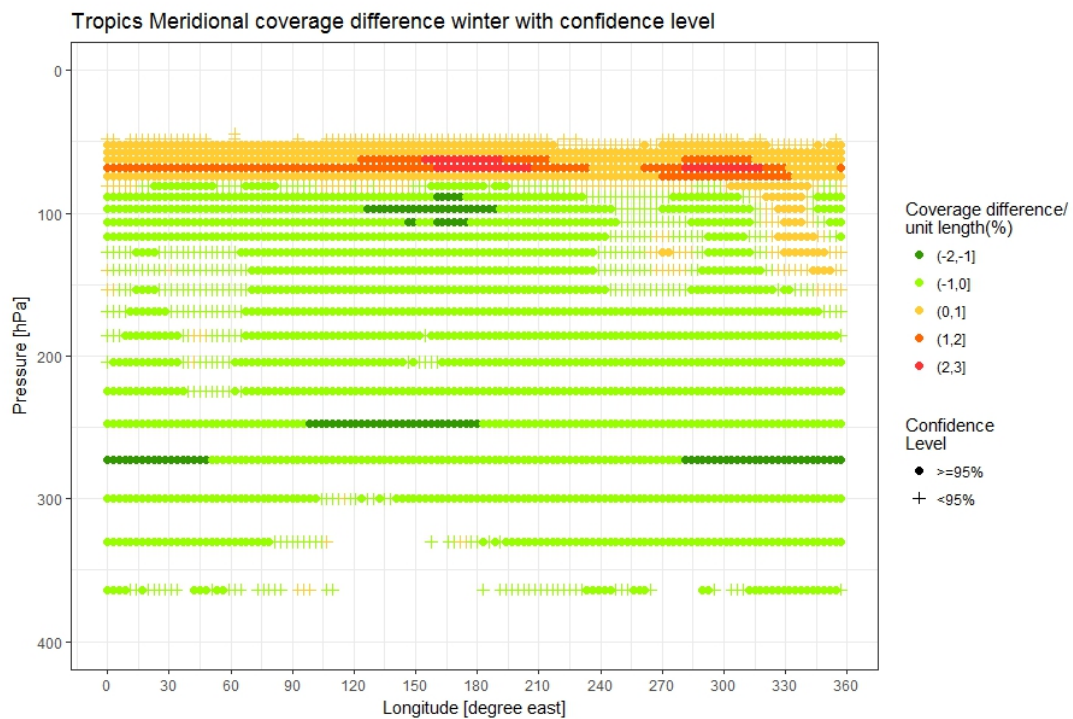


Figure C.3: Meridional mean CFRs coverage length difference in tropics winter

# Bibliography

- Appleman, Herbert (1953). "The formation of exhaust condensation trails by jet aircraft". In: *Bulletin of the American Meteorological Society*, pp. 14–20.
- Avila, Denis and Lance Sherry (2016). "Method for analysis of Ice Super Saturated Regions (ISSR) in the US airspace". In: *Integrated Communications Navigation and Surveillance (ICNS), 2016*. IEEE, 10B2–1.
- Brönnimann, Stefan (2009). "Early twentieth-century warming". In: *Nature Geoscience* 2.11, p. 735.
- Burkhardt, Ulrike et al. (2008). "Contrail cirrus supporting areas in model and observations". In: *Geophysical Research Letters* 35.16.
- Christensen, Jens Hesselbjerg et al. (2013). "Climate phenomena and their relevance for future regional climate change". In:
- Dai, Aiguo (2006). "Recent climatology, variability, and trends in global surface humidity". In: *Journal of Climate* 19.15, pp. 3589–3606.
- Dee, Dick P et al. (2011). "The ERA-Interim reanalysis: Configuration and performance of the data assimilation system". In: *Quarterly Journal of the royal meteorological society* 137.656, pp. 553–597.
- Dima, Ioana M and John M Wallace (2003). "On the seasonality of the Hadley cell". In: *Journal of the atmospheric sciences* 60.12, pp. 1522–1527.
- Dong, Bo and Aiguo Dai (2015). "The influence of the interdecadal Pacific oscillation on temperature and precipitation over the globe". In: *Climate dynamics* 45.9-10, pp. 2667–2681.
- Eastman, Ryan and Stephen G Warren (2013). "A 39-yr survey of cloud changes from land stations worldwide 1971–2009: Long-term trends, relation to aerosols, and expansion of the tropical belt". In: *Journal of Climate* 26.4, pp. 1286–1303.
- Forecast, Global Market (2015). *Flying by Numbers 2015–2034*.
- Gottelman, Andrew et al. (2010). "Multimodel assessment of the upper troposphere and lower stratosphere: Tropics and global trends". In: *Journal of Geophysical Research: Atmospheres* 115.D3.
- Gierens, Klaus (2007). "Are fuel additives a viable contrail mitigation option?" In: *Atmospheric Environment* 41.21, pp. 4548–4552.
- Gierens, Klaus, Ling Lim, and Kostas Eleftheratos (2008). "A review of various strategies for contrail avoidance". In: *The Open Atmospheric Science Journal* 2, pp. 1–7.
- Gierens, Klaus and Margarita Vázquez-Navarro (2017). "Statistical analysis of contrail lifetimes from a satellite perspective". In: *Meteorologische Zeitschrift*.
- Haglund, Fredrik (2008). "Potential of lowering the contrail formation of aircraft exhausts by engine re-design". In: *Aerospace Science and Technology* 12.6, pp. 490–497.
- Haywood, James M et al. (2009). "A case study of the radiative forcing of persistent contrails evolving into contrail-induced cirrus". In: *Journal of Geophysical Research: Atmospheres* 114.D24.
- Hegerl, Gabriele C et al. (2007). "Understanding and attributing climate change". In:
- Hoinka, Klaus P (1998). "Statistics of the global tropopause pressure". In: *Monthly Weather Review* 126.12, pp. 3303–3325.
- Jöckel, P et al. (2015). "Earth System Chemistry Integrated Modelling (ESCiMo) with the Modular Earth Submodel System (MESSy, version 2.51)." In: *Geoscientific Model Development Discussions* 8.10.

- Lee, David S, David W Fahey, et al. (2009). “Aviation and global climate change in the 21st century”. In: *Atmospheric Environment* 43.22, pp. 3520–3537.
- Lee, David S, Giovanni Pitari, et al. (2010). “Transport impacts on atmosphere and climate: Aviation”. In: *Atmospheric Environment* 44.37, pp. 4678–4734.
- Mannstein, Hermann, Peter Spichtinger, and Klaus Gierens (2005). “A note on how to avoid contrail cirrus”. In: *Transportation Research Part D: Transport and Environment* 10.5, pp. 421–426.
- Marenco, Alain et al. (1998). “Measurement of ozone and water vapor by Airbus in-service aircraft: The MOZAIC airborne program, An overview”. In: *Journal of Geophysical Research: Atmospheres* 103.D19, pp. 25631–25642.
- Mason, Simon et al. (2015). “Accessing and using climate data and information in fragile, data-poor states”. In: *International Institute for Sustainable Development: Winnipeg, MB, Canada*.
- Meerkötter, R et al. (1999). “Radiative forcing by contrails”. In: *Annales Geophysicae*. Vol. 17. 8. Springer, pp. 1080–1094.
- Miyakoda, K, RF Strickler, and J Chludzinski (1978). “Initialization with the data assimilation method”. In: *Tellus* 30.1, pp. 32–54.
- Pauluis, Olivier, Arnaud Czaja, and Robert Korty (2008). “The global atmospheric circulation on moist isentropes”. In: *Science* 321.5892, pp. 1075–1078.
- Peixoto, JoséP and Abraham H Oort (1996). “The climatology of relative humidity in the atmosphere”. In: *Journal of climate* 9.12, pp. 3443–3463.
- Ponater, Michael, Susanne Marquart, and Robert Sausen (2002). “Contrails in a comprehensive global climate model: Parameterization and radiative forcing results”. In: *Journal of Geophysical Research: Atmospheres* 107.D13, ACL–2.
- Schmidt, Ernst (1941). “Die entstehung von eisnebel aus den auspuffgasen von flugmotoren”. In: *Schriften der Deutschen Akademie der Luftfahrtforschung, Verlag R. Oldenbourg, München, Heft 44* 5.44, pp. 1–15.
- Schumann, Ulrich (1996). “On conditions for contrail formation from aircraft exhausts”. In: *Meteorologische Zeitschrift* 5, pp. 4–23.
- (2012). *Atmospheric physics: Background-Methods-Trends*. Vol. 1. Springer-Verlag Berlin Heidelberg.
- Schumann, Ulrich and Andrew J Heymsfield (2017). “On the life cycle of individual contrails and contrail cirrus”. In: *Meteorological Monographs* 58, pp. 3–1.
- Slingo, A and JM Slingo (1988). “The response of a general circulation model to cloud longwave radiative forcing. I: Introduction and initial experiments”. In: *Quarterly Journal of the Royal Meteorological Society* 114.482, pp. 1027–1062.
- Smith, Thomas M et al. (2008). “Improvements to NOAA’s historical merged land–ocean surface temperature analysis (1880–2006)”. In: *Journal of Climate* 21.10, pp. 2283–2296.
- Solomon, Susan (2007). *Climate change 2007-the physical science basis: Working group I contribution to the fourth assessment report of the IPCC*. Vol. 4. Cambridge University Press.
- Solomon, Susan et al. (2010). “Contributions of stratospheric water vapor to decadal changes in the rate of global warming”. In: *Science* 327.5970, pp. 1219–1223.
- Spichtinger, Peter and Klaus Gierens (2004). “Ice-supersaturated Regions”. In: *Deutsches Zentrum fuer Luft- und Raumfahrt. Forschungsberichte* 2004, p. 211.
- Spichtinger, Peter, Klaus Gierens, and William Read (2003). “The global distribution of ice-supersaturated regions as seen by the Microwave Limb Sounder”. In: *Quarterly Journal of the Royal Meteorological Society* 129.595, pp. 3391–3410.
- Stocker, Thomas (2014). *Climate change 2013: the physical science basis: Working Group I contribution to the Fifth assessment report of the Intergovernmental Panel on Climate Change*. Cambridge University Press.

- Stuber, Nicola et al. (2006). "The importance of the diurnal and annual cycle of air traffic for contrail radiative forcing". In: *Nature* 441.7095, p. 864.
- Stuefer, Martin and G Wendler (2004). "Contrail studies and forecasts in the subarctic atmosphere above Fairbanks, Alaska". In: *Proceedings (electronic version) 11th Conference on Aviation, Range, and Aerospace, Hyannis P.* Vol. 8.
- Welch, Bernard L (1947). "The generalization of student's' problem when several different population variances are involved". In: *Biometrika* 34.1/2, pp. 28–35.
- Wexler, Harry (1959). "Seasonal and other temperature changes in the Antarctic atmosphere". In: *Quarterly Journal of the Royal Meteorological Society* 85.365, pp. 196–208.